REGULATION OF CARDIAC MUSCLE CONTRACTION

EFFECT OF TROPOMYOSIN ISOFORM EXPRESSION AND CARDIOMYOPATHY MUTATIONS IN TROPOMYOSIN AND TROPONIN

By

Sabrina Eida Boussouf

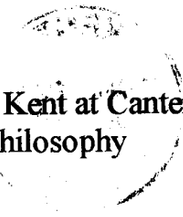

A thesis submitted to the University of Kent at Canterbury for the degree of Doctor of Philosophy

Faculty of Science, Technology and Medical Studies

Department of Biosciences

2004

DECLARATION

No part of this thesis has been submitted in support of an application for any degree qualification of the University of Kent or any other University or Institute of learning

Bourouf 15/9/2004

ABSTRACT

Regulation of the acto-myosin interaction is mediated by the Ca^{2+}-induced changes in the properties of the thin filament proteins tropomyosin and troponin. Two major tropomyosin isoforms, α and β, are expressed in striated muscle with larger amounts of β expressed in slow-contracting skeletal muscle and slower beating hearts of big mammals. The regulatory properties of α and β tropomyosin were defined in terms of the three-state model of regulation. The Ca^{2+}-dependent regulation of the thin filament was identical for α and β in the presence of skeletal troponin proteins. However, β tropomyosin-containing thin filaments were more Ca^{2+} sensitive in the presence of cardiac troponin. The thermal stability of the two isoforms was also examined using Differential Scanning Calorimetry. β tropomyosin was significantly less thermostable than α tropomyosin as it is partially unfolded at 37 °C when free in solution. In the presence of actin, both α and β tropomyosin stability is increased. However, β tropomyosin unfolding starts at 40 °C, a temperature the body can reach. These findings provide an explanation for the low level of β tropomyosin expression in the heart and the fact that it is predominantly found associated with α tropomyosin as a heterodimer.

Familial Hypertrophy Cardiomyopathy (FHC) is an autosomal dominant disease, which causes sudden death of young and healthy individuals. The effect of FHC mutations expressed in tropomyosin and troponin proteins on the regulatory process was investigated. Two mutations in α tropomyosin (D175N and E180G), and three mutations in trponin (G203S and K206Q in TnI, L29E in TnC) were examined. Both D175N and E180G increased the Ca^{2+} sensitivity of the system when associated with cardiac troponin. Also, both mutations decreased the local stability of tropomyosin when free in solution. In the presence of actin, D175N tropomyosin thermal stability was indistinguishable from wild type. No detectable changes in the regulatory function of the thin filament were observed with troponin mutations G203S in troponin I and L29E in troponin C. However, K206Q mutation in troponin I caused an increase in the Ca^{2+} sensitivity interestingly only when troponin I was phosphorylated.

To my Parents, Sandra, Salah & Mounia

Acknowledgements

I would like to express my deep gratitude to my supervisor Professor Mike Geeves for offering me the chance to work in his lab and for continuous guidance and support.

I would like to thank all the members of the Geeves lab past and present especially Richard, Dave, Dan, Maqsood, Marieke, Sue, Christine and Miklos for their help and for providing the lovely atmosphere. I am very thankful to Nancy Adamek for her protein preparations and technical support and to Dr Arthur Coulton and Tim Martin for proof reading my chapters. Special thanks to Dr Robin Maytum for his supervision and guidance. I am thankful to Dr Richard Williamson and Dr Mark Howard for allowing me to use their computer facilities. I would also like to express my very special thanks to all my friends especially Sam, Amel, Merzaka and Eric for continuous support, my wonderful parents and my lovely sister Sandra and brother Salah for their love.

In addition, I would like to thank our collaborators and all those who contributed to this work. Dr Robin Maytum for the cloning of the α Tm gene both WT and carrying the cardiomyopathy mutations. Dr Kornelia Jaquet and Anja Schmidtmann at the University of Bochum in Germany for expressing the cardiac troponin proteins and producing the troponin cardiomyopathy mutants. Finally, Professor Dmitrii Levitsky and Elena Kremneva at Russian Academy of Sciences (Moscow) for performing the DSC measurements.

Last but not least, as I am very grateful to the British Heart Foundation for financial support and to the Biosciences Department at the University of Kent for providing all the facilities.

TABLE OF CONTENT

Chapter 1: Introduction

Chapter 2: Materials and Methods

Chapter 3: Techniques and Analytical Procedures

Chapter 4: Bacterially expressed tropomyosin isoforms

Chapter 5: Study of FHC mutations expressed in tropomyosin

Chapter 6: Study of FHC mutations expressed in troponin

Chapter 7: Summary and General Discussion

Appendix

LIST OF FIGURES

LIST OF TABLES

CHAPTER 1

INTRODUCTION

Motility is an indispensable feature in living organisms. It occurs in all eukaryotic cells and ultimately results in active transport through membranes, cell division, the beating of flagella and cilia and the contraction of muscles. Muscle is the most understood motility system. Over the decades, a combination of functional and structural studies provided insights into the molecular mechanisms controlling muscle contraction and its regulation. Understanding these processes will have implications in not only understanding muscle function in health and disease but also energy transduction for force and motion production in both muscle and non-muscle cells.

The importance of studying the proteins which regulate muscle contraction is reflected by the potential development of therapeutic target drugs that can alter the contractile properties of the heart in a desired way. The characterisation of these proteins has also allowed their use as biochemical markers for the diagnosis of several heart injuries.

The results presented in this thesis have been obtained using both skeletal and cardiac proteins, the structure and function of which are described in this chapter.

1 Muscle structure and proteins

1.1 General structure of striated muscle

Both skeletal and cardiac muscles have a striated appearance when viewed under the light microscope. Skeletal muscle consists of a bundle of long muscle fibres (also referred to as muscle cells) each consisting of a number of myofibrils (Figure 1.1a). The fibre striations arise from the presence of repeating units named sarcomeres which can be seen on an electron micrograph of longitudinal section of a myofibril (Figure 1.2a). Figure 1.2b is a schematic representation of a sarcomere structure. It consists of alternating dark and light bands, the A and I bands respectively. The A band makes up the thick filament (150 Å in thickness) whereas the I band makes up the thin filament (90 Å in thickness), the proteins that constitute these two filaments will be discussed in details in section 1.2. A cross-section through a muscle fibre reveals the hexagonal arrangement of the two filaments with one thick filament being surrounded by six thin filaments (Figure 1.1b). At the centre of each I band is found a Z line. Two

successive Z lines form the boundaries of one sarcomere unit. The region of the A band where there is no overlap with the I band is named the H zone.

The cardiac and skeletal sarcomeric structures are very similar except for the existence of different protein isoforms. However, the general anatomy and the nature of the stimulation signal for contraction are different between the two types of muscle. Cardiac muscle cells are smaller in diameter and length as compared to their skeletal counterparts. Also, skeletal muscle cells are innervated whereas the action potential that triggers the heartbeat is generated within the heart itself by pacemaker cells.

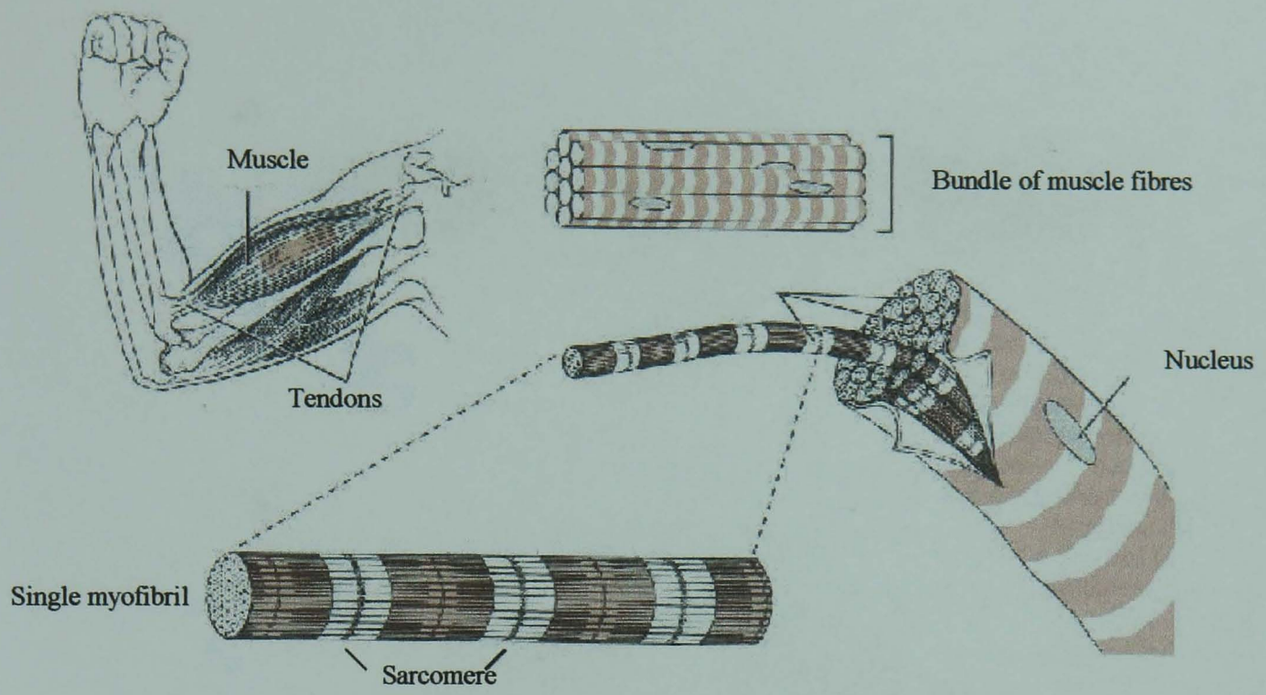

Figure 1.1a: Anatomy of skeletal muscle. Skeletal muscle is a bundle of fibres. Each fibre or muscle cell is made up of a bundle of myofibrils consisting of repeating sarcomere units (Mathews *et al*, 2000).

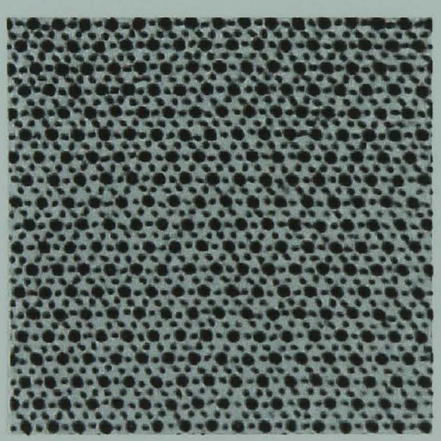

Figure 1.1b: Transverse section through filament lattice. The cross section shown was performed where the thick and thin filaments overlap. One thick filament is surrounded by six thin filaments (Stryer, 1996).

a)

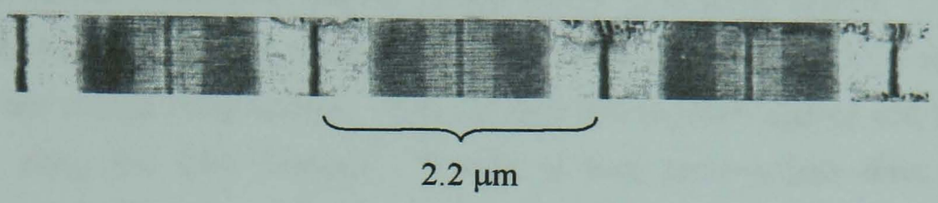

b)

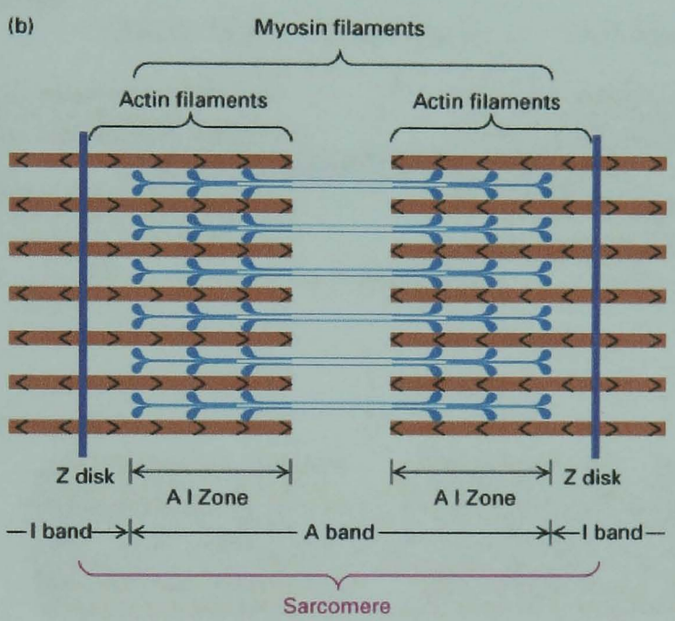

Figure 1.2: The sarcomere structure. (a) Electron micrograph of a myofibril showing the different bands which give the muscle its striated appearance. (b) Schematic representation of the sarcomere showing the thick (blue) and thin (red) filaments, the Z-lines which determine the sarcomere boundaries and the A and I bands (Lodish *et al*, 2001).

The sarcomere is the basic contractile unit. The thick and thin filaments slide over each other leading to shortening of the sarcomere length and resulting in muscle contraction. The sliding theory was first put forward by Huxley and Hanson (1954) as well as Huxley and Niedergerke (1954) when they demonstrated that the length of both thin and thick filaments remained constant during muscle contraction (Figure 1.3). The interaction between the two filaments is aided by heads projecting from the thick filament and named cross-bridges. Cross-bridges are regularly spaced and helically arranged along the thick filament. Details of how cross-bridges drive muscle contraction and on how the process is regulated are discussed in sections 2 and 3.

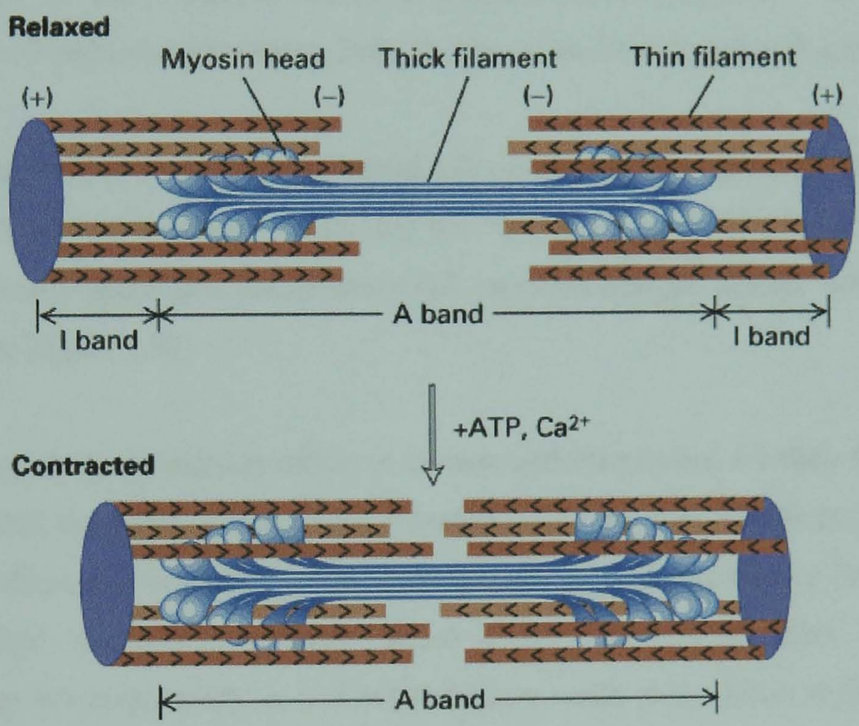

Figure 1.3: Sarcomere shortening by filament sliding. In the presence of both Ca^{2+} and ATP, the sarcomere undergoes contraction as a result of the sliding of the think and thick filaments past each other. The length of the two filaments remains unchanged. Actin is a polarised filament and both its barbed (+) and pointed (-) ends are shown in this figure (Lodish *et al*, 2001).

1.2 Muscle proteins

1.2.1 Myosin

The major protein component of the thick filament is myosin. Myosin is expressed in almost every vertebrate cell and to date 18 different classes have been reported in the literature (Sellers, 2000). Muscle myosin or myosin type II is made up of six polypeptide chains: two identical heavy chains (MHC) with a molecular weight of 220 kDa each and two pairs of light chains (about 20 kDa each) named the essential and regulatory light chains (ELC and RLC respectively). The C-terminal half of each myosin II heavy chain forms a long α-helical tail which associates with the α-helical tail of the second heavy chain, giving rise to a coiled coil rod-like tail structure. The N-terminal end of the molecule forms a globular head structure. A neck region, associated with the two light chains, links the two structural domains (Figure 1.4a).

Under physiological conditions the myosin II molecules aggregate and the coiled coil tails become packed together constituting the core of the thick filament structure. The globular myosin heads previously described as cross-bridges project out of the thick filament (see Figure 1.3).

Different muscle types express different myosin isoforms suited for their function. It is now clear that the MHC is the major determinant of the mechanical properties of the fibre (Schiaffino and Reggiani, 1996) and currently 8 MHC are known to be expressed in mammalian sarcomeric muscles (Weiss *et al*, 1999). Two MHC isoforms are expressed in the heart, MHC-α and MHC-β/slow while in the adult skeletal muscle 4 isoforms exist: slow MHC-I and fast MHC-IIA, IIX and IIB. The slow skeletal MHC-I has identical properties to the cardiac MHC-β/slow. The three remaining MHC proteins are developmental isoforms.

The myosin II molecule is susceptible to proteolytic digestion. At high salt concentration, chymotrypsin treatment cleaves the molecule into two segments 1) light meromyosin (LMM) which consists of a long coiled coil tail 2) heavy meromyosin (HMM) which consists of a coiled coil tail and the two globular myosin heads. A further digestion of the HMM molecule with papain yields two identical subfragment 1

molecules (S1) and a rod-like shaped subfragment 2 (S2) (Lowey *et al*, 1969) (Figure 1.4b). S1 is a 130 kDa fragment made up of 95 kDa heavy chain and one of each light chain molecule. S1 exhibits all the enzymatic activity of the myosin molecule (ATPase activity) and retains the ability to bind the thin filament. At low salt concentration, myosin molecules aggregate to form a filament. In this case only the neck region of the myosin molecule is accessible to proteolysis. Chymotrypsin treatment under these conditions yields S1 with only one light chain (the ELC chain) and a long coiled coil tail (see chapter 2, section 1.2.11).

The first S1 X-ray crystal structure from chicken was resolved by Rayment *et al* (1993a) (Figure 1.5). The myosin head region or the motor domain can be subdivided into three subdomains: 25K (N-terminal), 50K (middle) and 20K (C-terminal) domains which can be proteolytically separated. The 50K domain is further subdivided by a cleft into upper and lower 50K and comprises the actin-binding domain of the motor protein. The ATP binding pocket of the motor is located where the three subdomains come together (see structure). The 20K domain at the C-terminal end of S1 is a long α-helix that extends from the actin-binding site, binds the light chains and would normally be connected to the coiled coil tail of myosin. The RLC binds at the extreme C-terminal end of the 20K helix, whereas the ELC is found in the middle region of the helix. The two light chains share sequence and structural homology with the calmodulin protein. However, unlike calmodulin which contains four Ca^{2+}-binding motifs, RLC contains only one and ELC none.

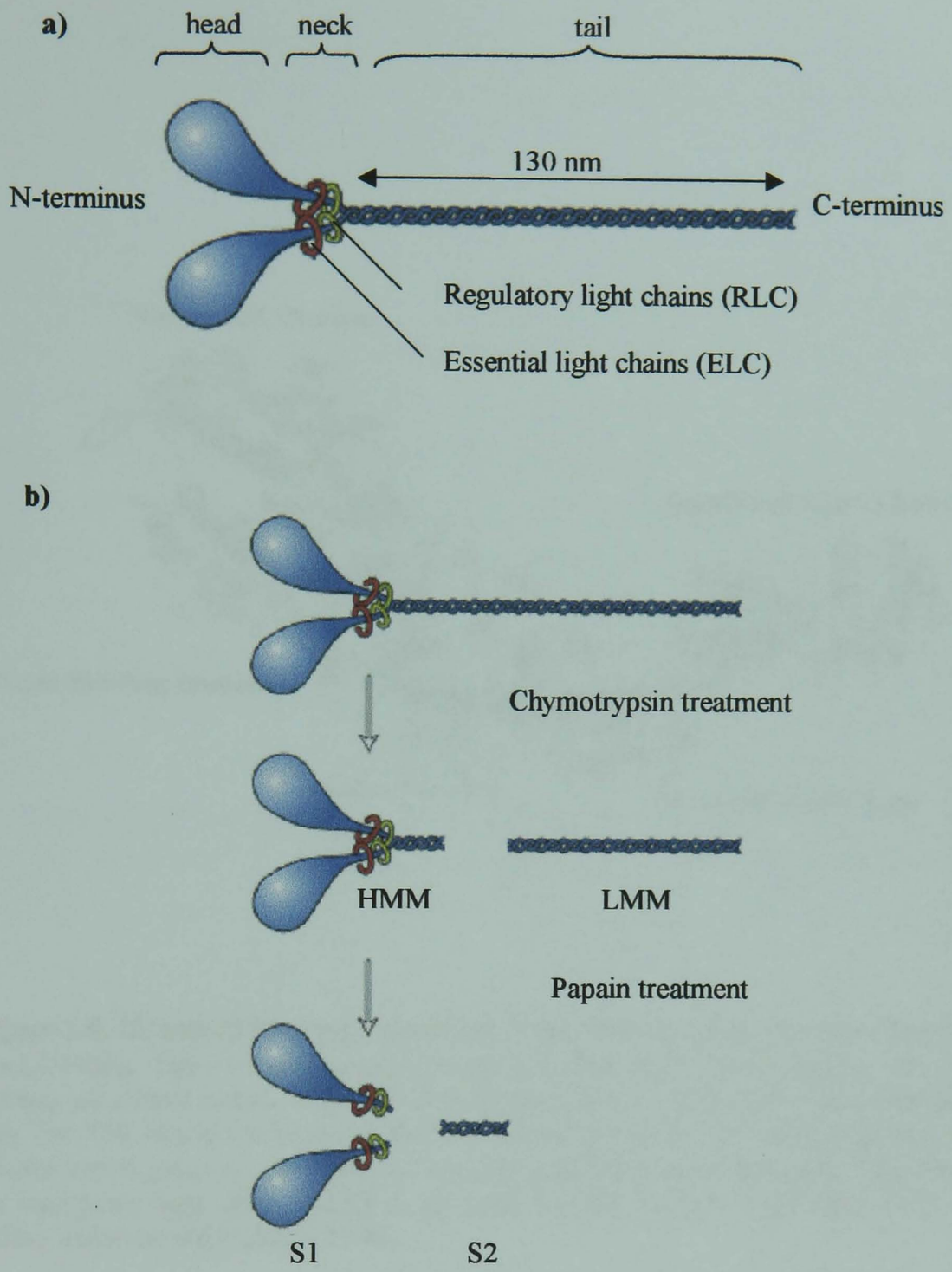

Figure 1.4: (a) Schematic representation of Myosin II structure. The protein is a dimer made up of two globular heads which comprise the ATPase active site functionning as a motor, a neck region where the light chains bind and long tail characterised by its coiled coil structure. **(b) Enzymatic cleavage of Myosin II.** Myosin II subfragments are produced by treatment with chymotrypsin to yield HMM (Heavy Meromyosin) and LMM (Light Meromyosin) and then with papain to yield S1 and S2 (myosin Subfragment 1 and 2). Both HMM and S1 retain the full ATPase activity of the molecule (Lodish *et al*, 2001).

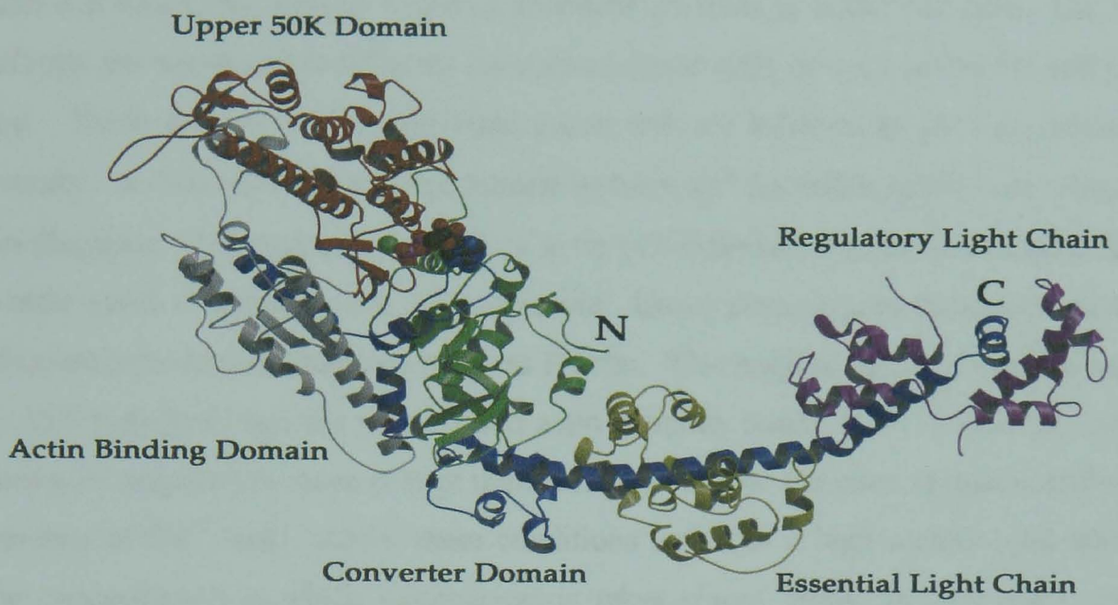

Figure 1.5: Myosin II S1 crystal structure from chicken skeletal muscle (Rayment *et al*, 1993a). The S1 head domain consists of both β-sheets and α-helices. The head domain are colour coded: the upper 50K domain in red and the lower 50K domain in grey, the 20K domain in blue and the 25K domain in green. The neck region, a long α-helix which extends from the head domain, binds two-calmodulin-like light chains: the regulatory light chain (RLC) in magenta and the essential light chain (ELC) in yellow (Geeves and Holmes, 1999)

1.2.2 Thin filament proteins

The thin filament is made up primarily of three types of proteins: actin, tropomyosin (Tm) and troponin (Tn) proteins (Figure 1.6).

1.2.2.1 Actin

Actin is a ubiquitous protein found in abundant amounts in eukaryotic cells. Different isoforms are expressed in different specialised tissue cells or even within the same cell type. These are encoded by different genes and are believed to provide functional diversity. α-Actin is the vertebrate muscle isoform and the major constituent of muscle thin filaments. The monomeric form of actin (43 kDa) has a globular structure called G-actin which is bound to one ATP molecule. Under physiological conditions, G-actin polymerises to form a filament known as F-actin. This polymerisation process is driven by ATP hydrolysis and the polymerised actin is tightly bound to ADP (Carlier, 1990). During its preparation, actin is kept unpolymerised at low salt concentrations and in the presence of Ca^{2+} ions. Under these conditions actin has a high critical concentration (the concentration at which polymerisation takes place), which in this case is about 0.1 mM. Polymerisation is achieved by increasing the salt concentration and by adding Mg^{2+} ions to displace the bound Ca^{2+} ions (Spudich and Watt, 1971). Under these conditions, the actin critical concentration goes down to about 0.1 μM. The rate at which actin polymerisation takes place is considerably faster than the rate at which ATP hydrolysis occurs. Also, the rate at which actin monomers are added at the barbed end of the filament is significantly higher than the rate at which they are added at the pointed end of the filament (F-actin is a polar molecule as all its monomeric units point in the same direction with respect to the filament axis (Figure 1.8)). On the other hand, the ATP hydrolysis rate is higher at the pointed end compared to the barbed end. Consequently, the pointed end of the filament will contain ADP-bound actin monomers whereas the barbed end will have ATP or ADP-Pi-bound actin monomers. The opposite is true for the disassembly of the filament. This process is known as treadmilling and is very dynamic in the case of cytoplasmic actin as compared to muscle actin (reviewed in Carlier, 1991 and Sheterline *et al*, 1995).

When using low actin concentrations (less than 1 μM), it is necessary to stabilise the filament with phalloidin, a fungal cyclic peptide that binds to polymerised actin and reduces the critical concentration by two orders of magnitude (Cooper, 1987).

The first X-ray structure of G-actin was determined by Kabsch *et al* (1990) (Figure 1.7). Actin could be crystallised in the monomeric G-form, which is suitable for X-ray studies, because it can bind to pancreatic DNase I (Deoxyribonuclease I) in a 1:1 complex overcoming the problems arising from its tendency to polymerise. This structure was followed by the publication of other G-actin structures in complex with profilin (Schutt *et al*, 1993) and gelsolin (McLaughlin *et al*, 1993). The most recent structure of G-actin bound to a probe that prevents its polymerisation was resolved by Graceffa and Dominguez (2003). All the G-actin atomic structures revealed the presence of two major domains of approximately the same size though referred to as small and large domains separated by a cleft where both the nucleotide and cation (Mg^{2+} or Ca^{2+}) reversibly bind. These two domains are further subdivided into two subdomains 1 and 2 located in the small domain, 3 and 4 located in the large domain. Both N and C termini of G-actin lie in subdomain 1 also where the most reactive Cys 374 is located.

A model for the actin polymer structure based on the detailed structure of the actin monomer combined with actin filament images obtained with electron microscopy and X-ray diffraction was put forward by Schroder *et al*, (1990); Lorenz *et al*, (1995). In this structure, the filament is shown as a long helix consisting of two linear strands of F-actin wrapped around each other (Figure 1.6). In the double-stranded actin filament the monomers are oriented in the same direction relative to the filament axis as seen with S1-decorated actin filaments which show and arrowhead-like appearance confirming the actin polarity (Flicker *et al*, 1991) (Figure 1.8). This is because opposite ends of the actin monomer are found at each end of the filament while the same actin monomer subdomains are exposed to the outside (subdomains 1 and 2 are exposed to the outside of the filament whereas subdomains 3 and 4 face the interior of the filament).

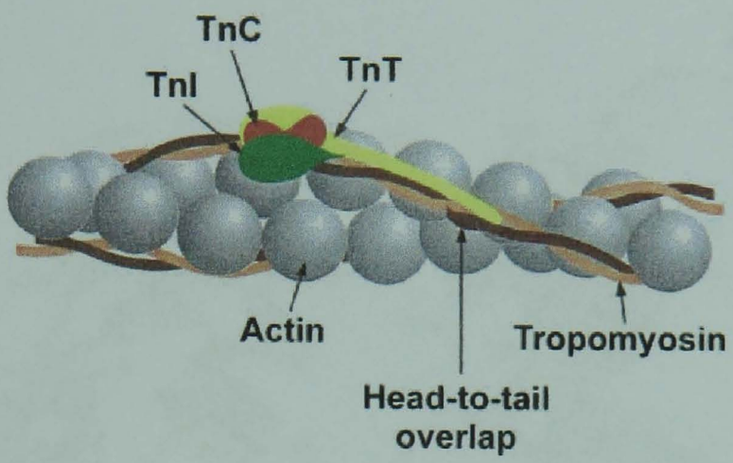

Figure 1.6: Schematic representation of the thin filament structure. The thin filament is made up of a double stranded actin filament to which binds tropomyosin (Tm) and the troponin (Tn) complex. Tm is an extended coiled-coil structure which wraps itself around the actin backbone. The Tn complex is made up of three subunits: the inhibitory subunit (TnI), the Ca^{2+}-binding subunit (TnC) and finally the Tm-binding subunit (TnT). The C-terminal end of one Tm overlap with the N-terminal end of the neighbouring Tm molecule. One Tm.Tn complex binds every seven actins (Gordon *et al*, 2000).

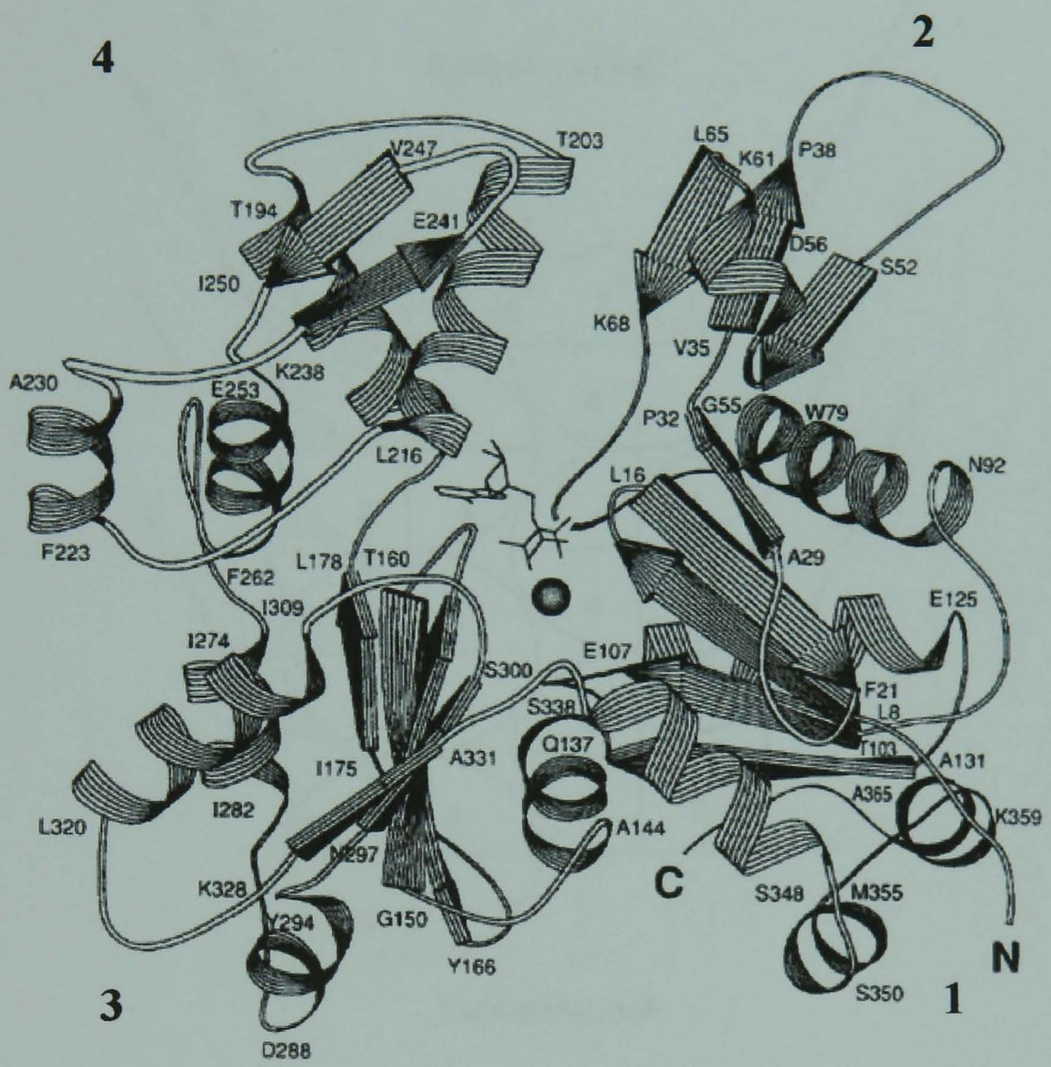

Figure 1.7: G-actin crystal structure. Monomeric actin is divided up into two major domains by a cleft where cation and nucleotide bind. Each domain is further divided into subdomains 1 and 2 (on the right), 3 and 4 (on the left). Both N- and C-termini are located in subdomain 1 (Kabsch *et al*, 1990)

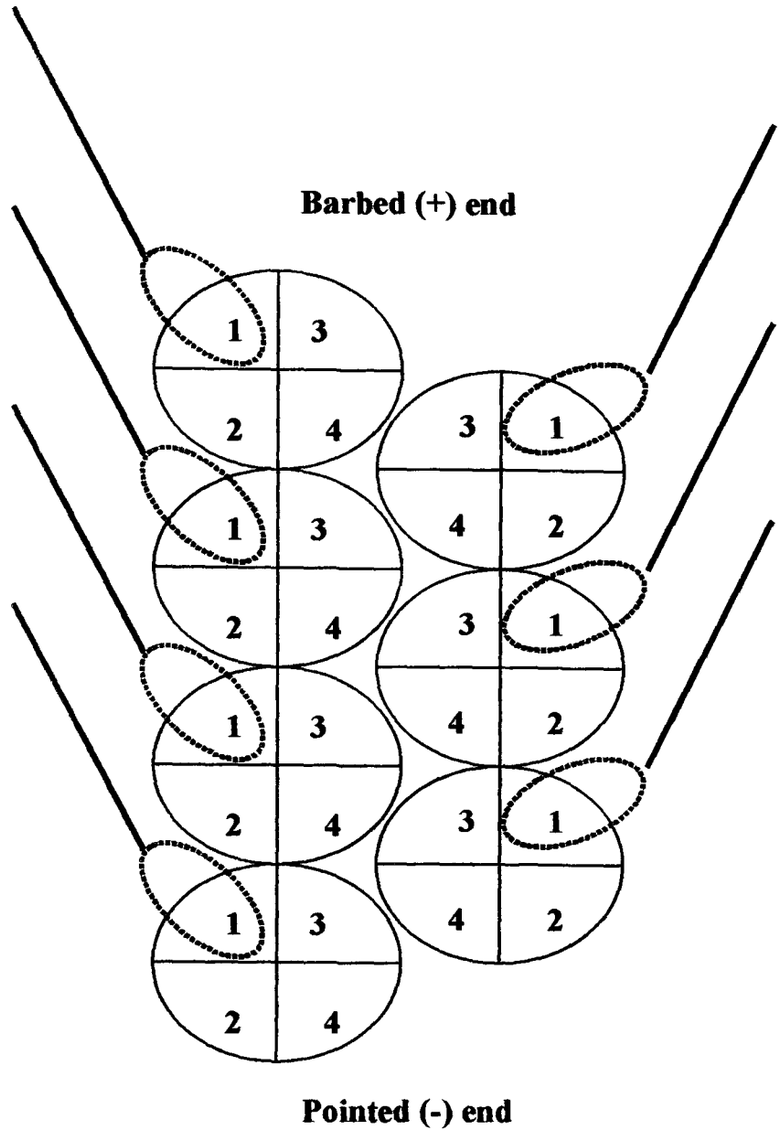

Figure 1.8: Schematic representation of the F-actin double helix. The F-actin is a polarised filament as shown by the pattern of myosin molecule (blue) binding forming an arrowhead-like appearance. The monomers are oriented such as all subdomains 1 and 3 point towards the barbed (+) end of the filament whereas all subdomains 2 and 4 point towards the pointed (-) end of the filament. Subdomain 1 and 2 always face the outside of the filament. Myosin binding site is mainly at subdomain 1 and at the interface between subdomains 1 and 3. Note that the myosin head and the actin monomers are not drawn to scale.

1.2.2.2 Tropomyosin

Tropomyosin (Tm) is present in most eukaryotic cell types associated with actin. It is an extended molecule made up of two α-helical chains which interact with each other giving rise to a coiled-coil structure (Philips *et al*, 1986) (Figure 1.9). This is made possible because of the characteristic repeating pattern of the heptad motif in which successive groups of seven amino acids (*a-b-c-d-e-f-g*) have hydrophobic residues in the first and fourth positions (*a* and *d* residues). These hydrophobic residues form a long hydrophobic strip along the sequence of each Tm helix stabilising the core of the coiled-coil structure. In the coiled-coil, residues *a* and *d* are non-polar and interact with one another. These hydrophobic residues are highly conserved in all Tm isoforms found in all types of eukaryotic cells. Residues *e* and *g* on the other hand tend to be either acidic or basic and can form either inter- or intra-chain salt bridges, further stabilising the coiled-coil (Figure 1.10) (Tobacman, 1996; Gordon *et al*, 2000; Perry, 2001). However, unlike most coiled-coils, Tm is characterised by the presence of alanine clusters in its sequence (Brown *et al*, 2001). These alanines are believed to bend the molecule and provide some sort of flexibility necessary for Tm to wrap around actin. Flexibility of Tm is also essential for its function as a key player in the Ca^{2+}-mediated regulation of muscle contraction in both skeletal and cardiac muscles. This aspect is discussed in great detail in section 3. Tm is also found in the cytoskeleton of non-muscle cells associated with actin involved in cell trafficking. However, the exact biological function of non-muscle Tm is not clear.

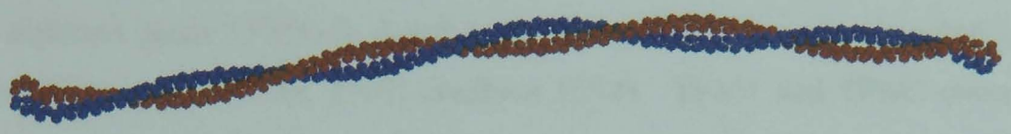

Figure 1.9: Tropomyosin structure. Tm is made up of two α-helices which interact with each other giving rise to a coiled-coil structure

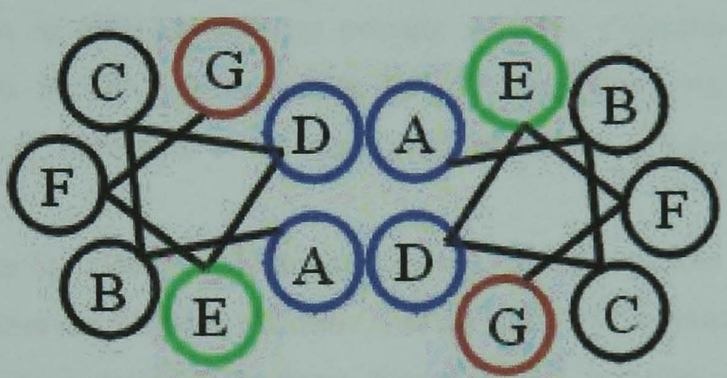

Figure 1.10: Cross-section of an α-helical coiled coil. The amino acids in the heptad sequence are marked A-B-C-D-E-F and G. Residues A and D are non-polar and form the hydrophobic core of the coiled coil structure. Residues E and G tend to be charged and can form ionic interaction stabilising the structure. The remaining residues tend to vary.

The mammalian Tm family comprises a large number of isoforms, so far 20 have been identified. Different isoforms are located in different cell types or are associated with different filaments within the same cell. These isoforms arise from the expression of four different genes TPM1, 2, 3 and 4 with alternative promoter and RNA processing (Lees-Miller and Helfman, 1991; Helfman 1994). TPM1 and TPM2 encode for the skeletal and smooth muscle α and β isoforms respectively (Figure 1.11). TPM1 gene has 15 exons, whereas TPM2 has only 13. In both genes exons 3, 4, 5, 7 and 8 are expressed in all α- and β-Tm isoforms. The different isoforms encoded by these two genes arise from the alternative splicing of the remaining exons (1a/b, 2a/b 6a/b, 9 a/b/c/d in TPM1 giving rise to at least nine isoforms and 1a, 2b, 6a/b, 9a/d in TPM2 giving rise to at least three isoforms). For instance, the main difference between skeletal and smooth α-Tm is in the alternative splicing of exons 2 and 9 whereas the main difference between skeletal and smooth β-Tm is in the alternative splicing of exons 6 and 9. The alternatively spliced exon 6a/b and 9a/b encode for the skeletal Tm domain responsible for binding the TnT head and tail domains respectively. Alternative exons in different isoforms provide sequence differences. For example, exons 9a and 9d of TPM1 both encode for 27 amino acids with only 4 identical residues. However, sequences of the same exons are highly conserved within different species.

Some parts of the Tm molecule are more conserved than others. The N-terminal end of Tm is highly conserved between isoforms with 18 out of 20 residues conserved in all vertebrate Tm. This N-terminal sequence along with the C-terminal sequence (encoded by exons 1 and 9 respectively) are responsible for the head-to-tail polymerisation of the Tm molecule giving rise to the filamentous structure of Tm (Perry, 2001).

Polymerisation of Tm dimers into a long filament involves the overlap of 8-9 amino acids at the C- and N-terminal ends of two molecules (McLachlan and Stewart, 1975). It is believed that the interaction between the side chains of these residues are of an ionic nature explaining the depolymerising effect high salt conditions have on Tm filaments. This head-tail arrangement also explains the reduction in the length of Tm in the filament (406 ± 1.4 Å) as compared to that of non-polymerised Tm (423 Å) (Philips *et al*, 1986).

The expression of the two major striated muscle Tm components α and β is dependent on both the tissue-type and the stage of development (Amphlett *et al*, 1976; Bronson and Schachat, 1982; Muthuchamy *et al*, 1993). Generally, in skeletal muscle the α-Tm isoform is more associated with fast-contracting fibres (Cummins and Perry, 1974; Heeley *et al*, 1983). In the heart muscle, the α-Tm, whose sequence is identical to that of skeletal α-Tm (Lewis and Smillie, 1980), is the predominant isoform with the β-Tm amount increasing in the slower beating hearts of bigger mammals (Perry, 2001). Amino acid sequence analyses of the α and β sequences revealed that differences between the two isoforms occur at the C-terminal end of the protein, the site for troponin complex binding. The cysteine content is also different as α-Tm contains one Cys residue at position 190 whereas β-Tm contains two Cys residues at position 36 and 190 (Mak *et al*, 1979; Mak *et al*, 1980). The two major forms present in muscle are αβ and αα. The ββ form has been reported to exist but in very small amounts in the cell. This is due to preferential heterodimer over homodimer formation (Lehrer and Qian, 1990; Lehrer *et al*, 1989). The significance of having two skeletal Tm isoforms and the biological properties of the different dimers is still not established. It has however been reported that in smooth muscle, heterodimers have stronger end-to-end interaction and stronger actin binding properties than homodimers (Lehrer *et al*, 1997).

All Tm isoforms have the same characteristic structure described above. In vertebrate cells, Tm molecules are either a 6 or 7-actin binding proteins with an amino acid sequence of 248 (fibroblast Tm) and 284 (muscle Tm) respectively. Both α and β Tm have 284 amino acids and span seven actin monomers or one actin structural unit. This can be demonstrated by co-sedimentation experiments where saturation of actin by Tm is achieved at a 7:1 ratio respectively under physiological conditions. Binding of Tm to actin has a cooperative nature and the binding affinity is strengthened by the presence of either Tn (Hill *et al*, 1992) or myosin (Cassel and Tobacman, 1996). In the same way, myosin affinity for actin is increased in the presence of Tm (Williams and Greene, 1983; Maytum *et al*, 1999; Tobacman and Butters, 2000). Tropomyosin is also found to stabilise the actin filament (increasing the filament stiffness) and to induce actin polymerisation (Fujime and Ishiwata, 1971; Wegner, 1982; Goldmann, 2000).

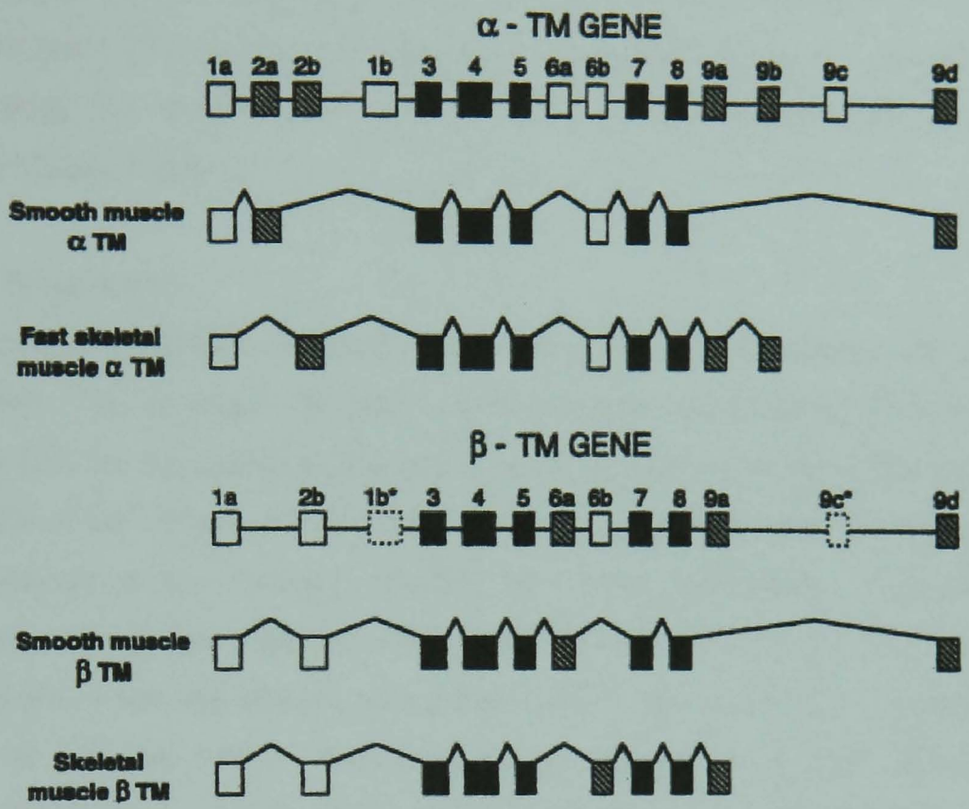

Figure 1.11: The coding sequence of the α- and β-Tm genes responsible for the expression of Tm in both skeletal and smooth muscles. Exons are represented by boxes and introns by lines. Exons expressed in both skeletal and smooth Tm isoforms are filled with black. Isoform diversity arises from the alternative expression of the remaining exons. The gene organisation represented above is that of chicken. Exons marked with dotted lines and stars have been detected in chicken but not in rat. This figure is taken from the review by Perry (2001) and is adapted from Lees-Miller and Helfman, 1991). Exon 6b represented as shaded in skeletal muscle β Tm should be clear.

1.2.2.3 Troponin proteins

The troponin (Tn) complex of proteins is composed of three subunits; the Ca^{2+}-binding subunit (TnC), the inhibitory subunit (TnI) and the tropomyosin binding subunit (TnT). Tn complex binds actin with a stoichiometry of 1:7 Tn:actin and with a periodicity of 38.5 nm along the thin filament. The structure and function of each subunit is discussed in details below.

1.2.2.3.1 Troponin C

TnC (18 kDa) is the protein responsible for binding Ca^{2+} in both skeletal and cardiac thin filaments. TnC protein is the only Tn subunit whose entire structure was resolved in solution both in the presence (Houdusse *et la*, 1997) and absence (Hezberg and James, 1985) of Ca^{2+} (Figure 1.12). TnC consists of two globular domains found at the N and C termini of the sequence separated by a long central helix. Each globular domain contains two cation-binding sites of the EF hand, helix-loop-helix type. The two sites at the N-terminal end are named site I and II, they bind Ca^{2+} with an affinity of about 10^5 M^{-1} and have a preferential binding for Ca^{2+} over Mg^{2+} (Potter and Gergely, 1974). The two sites at the C-terminal end are named sites III and IV. These have a higher Ca^{2+} affinity of about 10^7 M^{-1} and a high Mg^{2+} affinity (10^3 M^{-1}) resulting in their saturation with Mg^{2+} when the muscle is relaxed (under conditions where Ca^{2+} concentration is about 0.1 μM or less and the Mg^{2+} is at the millimolar level) (Zot and Potter, 1982). When muscle contraction is triggered, the Ca^{2+} levels rise in the cell to reach about 10 μM. Under these conditions, the Mg^{2+} in sites III and IV is exchanged by Ca^{2+} and sites I and II become also saturated. In this case muscle contraction is triggered as reflected by an increase in acto.myosin ATPase activity and force generation. The cardiac TnC isoform contains a single Ca^{2+}-binding site at the N-terminal domain of the protein. This is due to the substitution of three aspartic acids by a leucine, alanine and cysteine in site I (Van Eerd and Takahashi, 1976).

1.2.2.3.2 Troponin I

TnI is the inhibitory subunit of Tn. In the absence of Ca^{2+}, it binds tightly to the myosin-binding region on actin and inhibits muscle contraction. So far, three TnI isoforms are reported to be expressed in the mammalian muscle cell. These are the skeletal slow and fast isoforms and the cardiac isoform, with each one being the

product of a separate gene (Syska *et al*, 1974). There is about 60% homology between the three isoforms and about 80 % homology between the same isoform across different species. Skeletal TnI isoforms are a single 181 amino acid chain with a molecular weight of about 21 kDa. The cardiac TnI has a characteristic 30-amino acid extension at the N-terminal end of the molecule increasing its molecular weight to 24 kDa (Wilkinson and Grand, 1978). The cardiac extension is highly conserved and contains important phosphorylation sites. The protein is phosphorylated by protein kinase A (PKA) as a response to adrenaline stimulation (England, 1975; Solaro *et al*, 1976). PKA phosphorylates two adjacent serine residues (22 and 23 in human sequence) (Mittmann *et al*, 1992). Cardiac TnI phosphorylation has been reported to cause a decrease in the Ca^{2+} sensitivity of the system and will be further discussed in chapter 6 (for review on TnI properties and functions see Perry, 1999).

1.2.2.3.3 Troponin T

TnT is the Tn protein that holds the Tn complex and actin.Tm together. Therefore fulfilling an important structural role. In addition to that, it is required for the normal Ca^{2+}-sensitive acto.myosin ATPase activity in the presence of TnC-TnI (Potter *et al*, 1995) and it is believed to affect the Ca^{2+} sensitivity of the system. It has also been shown to alter the cooperative activation of the thin filament (Schaertl *et al*, 1995).

TnT is an extended molecule of about 185 ± 25 Å long and 20 Å wide as revealed under the electron microscope (Flicker *et al*, 1982). It has a molecular weight that varies between 31 and 36 kDa depending on the isoform. It is an asymmetric protein as it consists of an extended α-helical tail at the N-terminal end termed TnT1 and a globular domain at the C-terminal end termed TnT2. The two distinctive TnT domains can be obtained by chymotryptic digestion. TnT shows an antiparallel arrangement relative to Tm. The TnT1 region lies at the C-terminal domain of Tm including at the overlap region between two neighbouring Tm and extends towards the centre of the Tm molecule. This makes TnT influence Tm affinity for actin as well as Tm flexibility and cooperative effect (Section 3.3). Interestingly, the hypervariable region of the molecule is located at the part of TnT which interacts with Tm overlap region. The TnT2 domain lies one third of the way down from the Tm C-terminal end and interacts with both TnC an TnI as well as Tm. The binding of Tm to actin is enhanced by the

both TnT1 in a Ca^{2+}-insensitive manner and by TnT2 in a Ca^{2+}-sensitive manner (Pearlstone and Smillie, 1982; Heeley *et al*, 1987, Schaertl *et al*, 1995). The binding affinity of Tm to actin is reported to be more significantly affected by Ca^{2+} in the skeletal system i.e. six-fold decrease (Rosenfeld and Taylor, 1985) compared to the cardiac system where little change was observed (Dahiya *et al*, 1994). Hence, through its interactions with the other components of the thin filament, TnT controls the position of Tm on actin and determines the cooperativity of the filament, two aspects of a crucial importance in muscle regulation (for review on TnT see Perry, 1998).

1.2.3 Other muscle proteins

In addition to actin, myosin and the regulatory complex of proteins, muscle sarcomeres require other proteins that ensure normal assembly, structural integrity and normal function of the muscle cell. These include: α-actinin believed to be responsible for F-actin anchoring to the Z-disc, nebulin is implicated in the actin polymerisation process and is responsible for determining the length of F-actin during sarcomere assembly and titin the elastic element in muscle which acts as a spring (Squire, 1997 for review and refs therein). Additional thick filament proteins include protein-C, H and X all reported to be essential for thick filament assembly (Winegrad, 1999).

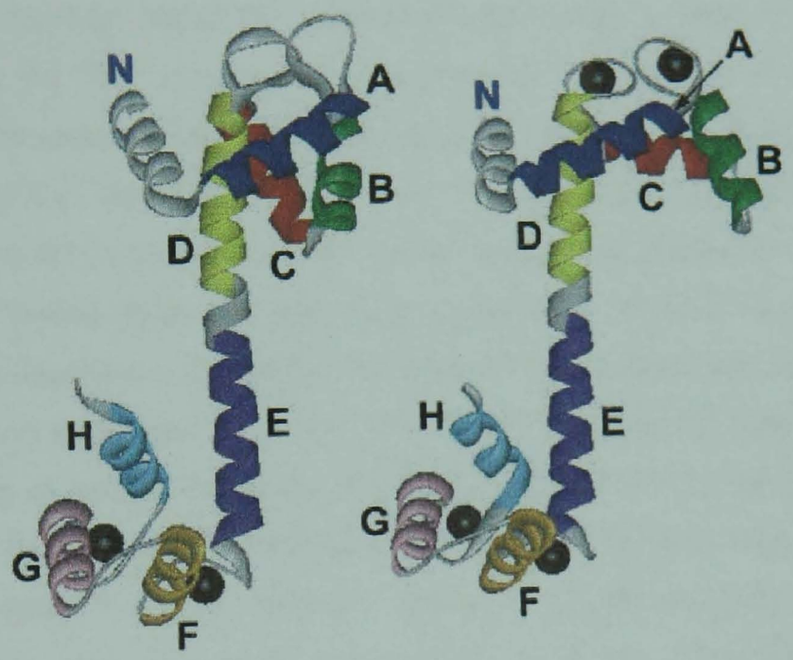

Figure 1.12: TnC crystal structure in the holo and apo states. On the left hand side is a ribbon representation of a Ca^{2+}-free skeletal turkey TnC molecule (Herzberg and James, 1985). The C-terminal Ca^{2+} -binding sites (III and IV) exhibit a high Ca^{2+} affinity and are always occupied under physiological conditions. On the right hand side is a ribbon representation of a rabbit fast skeletal TnC with Ca^{2+} bound at both C and N termini (Houdusse *et al*, 1997). ($Ca^{2+}$is represented by solid circles). Helices are colour coded and indicated by capital letters. (Figure taken from Gordon *et al*, 2000).

1.2.4 Calcium-dependent interactions of the thin filament proteins

The mechanism underlying regulation of muscle contraction is explained by a switching in the affinity of TnI for actin and for TnC as a function of Ca^{2+}. In the absence of Ca^{2+}, TnI is reported to have a high affinity for actin sterically inhibiting myosin heads binding. When Ca^{2+} binds TnC, the inhibitory effect of TnI is reversed as its affinity for TnC is increased weakening its interaction with actin. This is reflected by the co-migration of TnI and TnC as a single band on electrophoresis gel in the presence of Ca^{2+} (Head and Perry, 1974). The enhanced affinity of TnI for TnC can be explained at the molecular level by comparing the X-ray structures of TnC with and without Ca^{2+} bound (holo and apo states respectively) (Figure 1.12) (Hezberg and James, 1985; Houdusse *et al*, 1997). The structure revealed the presence of five helices in the N-domain designated N, A, B, C and D. The C-domain contains helices E, F, G, and H. Parts of helices D and E make up the interdomain helical linker. The Ca^{2+} binding sites (helix-loop-helix EF hands) are made up of helix A-loop-helix B (site I), helix C-loop-helix D (site II), helix E-loop-helix F (site III) and helix G-loop-helix H (site IV). Comparison between the two structures (with and without Ca^{2+}) revealed that the main differences arise in the interhelical angles at the N-domain of the molecule. In the Ca^{2+}-bound state, the helices A and B, C and D are perpendicular to each other. In the apo state however, the helices are almost parallel to each other with helices B and C folded down along the central helix. In the latter case, the N-domain of TnC is seen as a closed structure. Binding of Ca^{2+} therefore produces the conformational change required to move helices B and C away from the hydrophobic stretch of amino acid in the central helix. The change in helices orientation opens up the structure and allows TnI to interact with the TnC hydrophobic sequence, switching the site of interaction from actin to TnC. These structural changes indicated that the N-terminal lobe of TnC plays a regulatory role. Therefore, site I and II are referred to as the regulatory sites. The C-terminal lobe on the other hand plays a structural role as it binds to the N-terminal domain of TnI and anchors the TnC to the rest of troponin (Vassylyev *et al*, 1998). For this reason, sites III and IV are referred to as structural sites.

When the structure of the cardiac TnC in the presence of bound Ca^{2+} was resolved, it unexpectedly resembled the apo structure described above (Sia *et al*, 1997). This suggested that the Ca^{2+}-induced changes observed in the skeletal system were less

favourable in the cardiac system. To explain the mechanism by which TnC and TnI interactions take place, McKay *et al* (1999) suggested that TnI binding to TnC forced the N-terminal structure of TnC to open. This difference between the skeletal and cardiac systems could be at the heart of major differences in the Ca^{2+}-regulation of muscle contraction.

Understanding the nature of TnI interactions with the other thin filament proteins, in particular with TnC and actin required the identification of the TnI sequences which take part in such interactions. TnI sequence comprises two highly conserved regions important for its function. These have been identified as residues 17-23 and 97-121 in the rabbit skeletal isoform (Syska *et al*, 1976; Van Eyk *et al*, 1993). The latter comprises the inhibitory peptide, the TnI sequence that binds strongly to actin in the absence of Ca^{2+} (Figure 13). In fact, TnI interacts with every protein in the thin filament highlighting its key role in regulation. It therefore needs to adopt different conformations to fulfil its function.

Structural data on isolated TnI is not available, being a highly basic protein it tends to aggregate in solution. However, information about TnI interaction with TnC has been obtained using short TnI fragments in either NMR or X-ray crystallography studies (Campbell *et al*, 1991; Campbell *et al*, 1992; Farah *et al*, 1994; Krudy *et al*, 1994; Vassylyev *et al*, 1998). TnI fragments were produced by cyanogen bromide digestion and those selected for structural studies (peptides 1-21, 1-47 and 96-116) are not only highly conserved but they also bound to a TnC affinity column (Syska *et al*, 1976). The structural studies revealed the antiparallel orientation of the two proteins. The N-terminal end of TnI (residues 1-47) was found to interact with the C-terminal end of TnC (sites III and IV) in the presence of either Ca^{2+} or Mg^{2+} in what is referred to as the structural interaction, as it permits TnC to be anchored to the thin filament (Figure 1.13). Even though residues at the C-terminal end of TnI are strongly conserved between species, there was no evidence of that part of TnI binding to TnC from affinity chromatography experiments. NMR studies backed up by cross-linking experiments do however support an interaction of the C-domain of TnI (residues 115-131 in rabbit skeletal isoform corresponding to residues 148-164 in the human cardiac isoform) with the regulatory N-domain of TnC.

Actin is another key interaction partner of TnI. As with TnC, the TnI-actin interactions are complex and are at the heart of the regulatory process. The inhibitory region (residues 97-116) is not the only part of TnI that establishes contact with actin. This was clearly demonstrated by the fact that it is only 50 % efficient at inhibiting the actomyosin ATPase activity as compared to the full-length native TnI, suggesting the presence of additional actin-binding sites in TnI required for full inhibitory activity. Removal of residues 140-180 in rabbit skeletal TnI reduces its inhibitory action (Tripet *et al*, 1997) whereas removal of the inhibitory region results in complete loss of inhibition (Farah *et al*, 1994). This implies that the inhibitory function of residues 140-148 is complementary to that of inhibitory region and cannot take place in the absence of the latter.

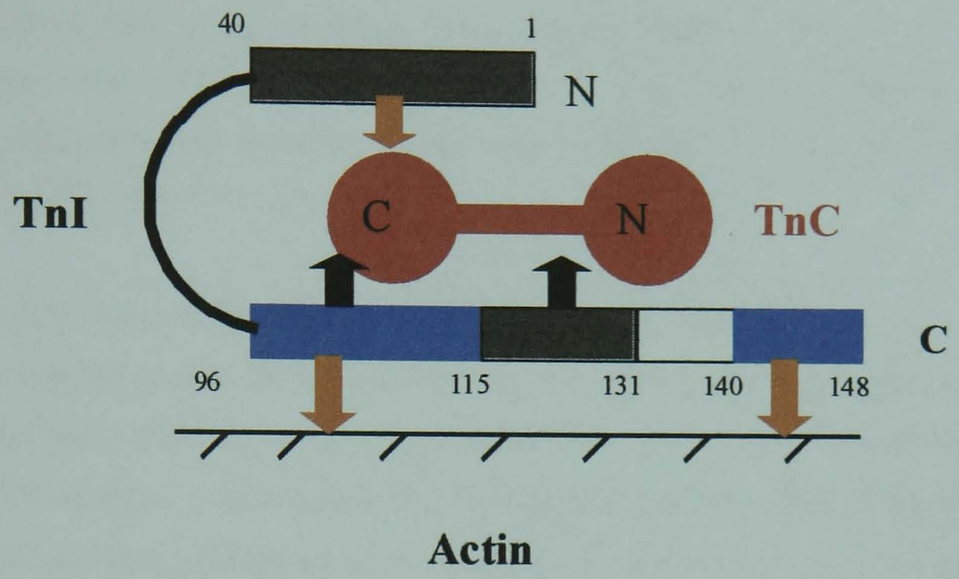

Figure 1.13: Model explaining the Ca^{2+}-dependent interactions of TnI with actin and TnC. The amino acid numbering corresponds to that of rabbit fast skeletal TnI. The corresponding sequence of rat cardiac TnI would be 32-73, 130-149, 149-165, 165-174 and 174-182. The regions implicated in establishing interactions are indicated by black arrows in the case where Ca^{2+} is bound to the N-domain of TnC and by orange arrows in the case where Ca^{2+} is absent. In absence of Ca^{2+}, residues 1-40 of TnI interact with TnC structural sites located at the C-domain. This interaction is believed to allow the anchoring on TnC to the thin filament. Residues 96-115 corresponding to the inhibitory region of TnI as well as residues 140-148 both interact with actin. These interactions sterically block the formation of an ATPase active acto.myosin complex. In the presence of Ca^{2+}, the inhibitory region switches sites of interaction to bind the TnC-C domain. Residues 115-131 on the other hand bind to TnC N-domain, more specifically the hydrophobic stretch of residues which becomes exposed upon Ca^{2+} binding to TnC (Adapted from Tripet *et al*, 1997)

1.2.5 The atomic structure of the human cardiac troponin complex

The core domain of human cardiac Tn, which consists of the TnC (residues 1-161), TnI (residues 31-210) and TnT2 (residues 183-288), in the Ca^{2+}-staurated form, was resolved at high resolution using X-ray crystallography by Maéda and co-workers (Takeda *et al*, 2003). This allowed for the first time the visualisation of how polypeptide chains of the three subunits are folded around each other in the troponin complex (Figure 1.14).

As already shown in the TnC-TnI binary complex published by Vassylyev *et al* (1998), the N-terminal portion of TnI (residues 43-79) corresponding to helix H1(I) interacts with the TnC C-lobe via its amphiphilic portion (residues 43-65) to form the first site of TnI-TnC binding. TnI residues 90-135 form a long α-helix (H2(I)) that interacts with TnT α-helix (H2(T2)) spanning residues 226-271 and giving rise to a parallel coiled-coil arm. This coiled-coil structure arises because of the presence of heptad repeats made up of residues highly conserved between species. At the C-terminal end of this coiled coil, TnT interacts with the C-lobe of TnC at the region where all three Tn subunits come together. The interaction of these three proteins is stabilised by the permanent presence of cations (Ca^{2+} or Mg^{2+}) at sites III and IV in the C-lobe of TnC. TnT residues 272-288, reported to interact with tropomysin, are not well defined in this structure. However, it is through that part of TnT that the TnC-TnI complex is integrated into the Tm.actin complex. TnT residues 204-220 of the C-domain form another α-helix (H1(T2)), positioned at 60° relative to the TnI-TnT coiled coil arm (Figure 1.14). This part of TnT extends into the TnT1 portion (N-terminal end) of the molecule (not present in the structure) which represents the second site for Tn anchoring to Tm and actin.

The TnI inhibitory region (cardiac sequence 137-148) is an extended α-helix followed up by another amphiphilic α-helix H3(I) (residues 150-159). The latter interacts with the conserved hydrophobic patch at the N-domain of TnC when it is Ca^{2+}-saturated (second TnI-TnC binding site). The C-terminal domain of TnI, previously identified as an actin-binding site (Tripet *et al*, 1997), was not defined in this structure apart from resides 164-188 which form the H4(I) helix that does not seem to interact with the rest

of the Tn molecule. The amphiphilic α-helix H3(I) is therefore positioned between two TnI actin-binding sites (the inhibitory peptide (residues 137-148) and the C-terminal helix (residues 164-210)) both required for full actomyosin ATPase inhibition by TnI in the absence of Ca^{2+} (Farah *et al*, 1994). Therefore, as previously speculated, the amphiphilic α-helix is the Ca^{+2}-dependent molecular switch whose binding to TnC in the presence of Ca^{2+} triggers the detachment of the two TnI inhibitory peptides from actin. The opposite happens when Ca^{2+} is removed from the system. The rigid TnI-TnT arm is also thought to play an important role in releasing inhibition and determining tropomyosin location on actin. It is positioned between the TnT1 portion of TnT and the mobile C-domain of TnI (two point of Tn attachment to Tm). The Ca^{2+}-dependent movement of TnI can thus cause the TnI-TnT arm to rotate (Figure 1.15).

The Tn core domain can therefore be divided into a number of subdomains namely the regulatory head domain, the TnI-TnT arm domain, the TnT1 domain, the TnT and TnI C-terminal domains. These subdomains are linked by flexible loops which would provide the whole molecule with the flexibility required for its function.

The Maéda structure despite describing the overall architecture of the Tn core complex does lack description of many of the potential actin and Tm sites on TnI and TnT. This was due to a poor definition of the electron map at those sites.

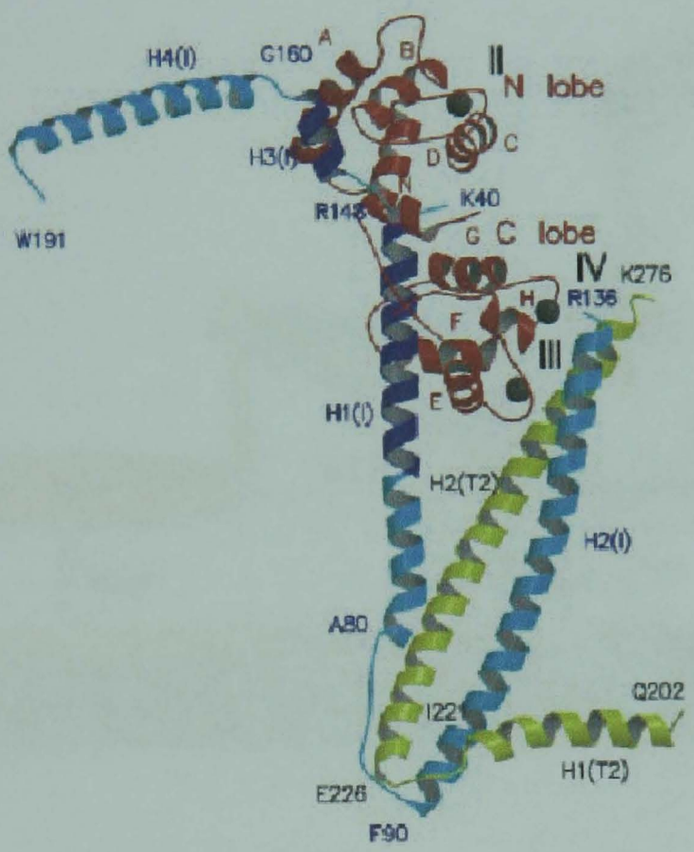

Figure 1.14: Crystal structure of human troponin core domain. TnC, TnT and TnI are coloured red, yellow and blue respectively. TnI helices that bind to TnC are coloured dark blue. The three Ca^{2+} ions bound to TnC are represented with filled black circles (Takeda *et al*, 2003)

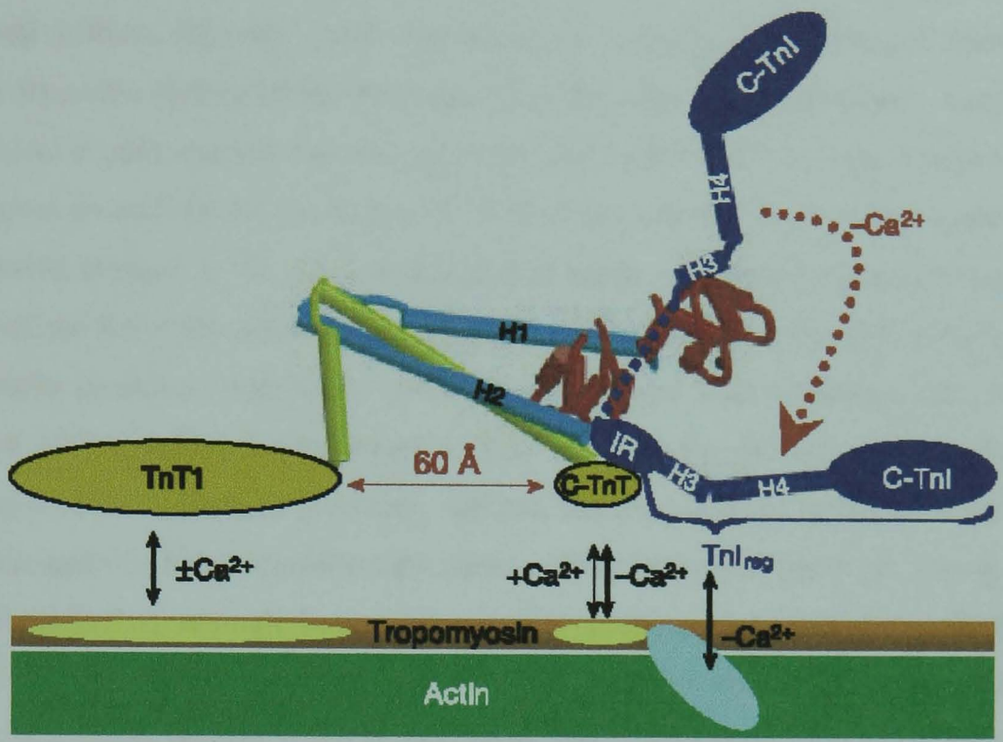

Figure 1.15: A proposed mechanism for the interaction of troponin with the other components of the thin filament. The parts of Tn not defined in the crystal structure are schematically represented by ellipsoids. These are the N- and C-terminal portions of TnT (yellow), the C-terminal end of TnI and the inhibitory region IR (dark blue). Sites of interaction with actin.Tm are indicated with black arrows (Takeda *et al*, 2003).

2 The molecular basis of muscle contraction

Though many details remain to be answered, the general mechanism underlying muscle contraction has been elucidated for many years. First, Huxley and Hanson as well as Huxley and Niedergerke (1954) explained the observation of sarcomere length shortening without filament length shortening by suggesting that muscle contraction resulted from the sliding of the thick and thin filaments past each other. Later on, a biochemical model was put forward by Lymn and Taylor (1971). This model was the first to give an account for the role of ATP hydrolysis by the myosin head in the cross-bridge cycle (Figure 1.16). It was found that when ATP was bound to myosin, the affinity of the latter for actin was significantly reduced, causing the dissociation of the acto.myosin complex. However, since the presence of actin accelerated the myosin-catalysed ATP reaction, it was suggested that rebinding to actin took place and helped the release of the hydrolysis products. Indeed, the myosin head bound to ADP.Pi can bind actin and this helps accelerate the release of the hydrolysis products, giving rise to the nucleotide-free, strongly-bound acto.myosin complex (rigor complex). Binding of an ATP molecule to myosin starts the cycle again. In this model, the power stroke or the conformational change in the myosin head which produces motility is coupled with the hydrolysis products release step. As successive cycles take place, myosin heads will appear to be rowing on the actin surface, producing the sliding effect.

The Lymn and Taylor model of the cross-bridge cycle, though giving an overall idea of the process, is an over simplified picture. The model is constantly refined as more information is obtained from both biochemical and structural work.

The movement of the myosin along the actin filament is the result of a change in the myosin affinity for actin combined with the tilting movement of the α-helical neck region of myosin (the lever arm) (Holmes, 1997). This is made possible through complex communications between the nucleotide-binding site, the actin-binding site and the converter region which is linked to the lever arm (it can be seen in the myosin head structure shown in Figure 1.5 that the nucleotide binding site is located where all the head domains come together). The affinity of the myosin head for actin depends on the type of nucleotide bound to myosin and vice versa. A cleft region extends from the nucleotide binding site into the actin-binding site of the 50K domain which it

divides into upper and lower 50K domains. The 50K domain also comprises two loops termed switch I (SWI) (upper domain) and switch II (SWII) (lower domain). SWI binds to the nucleotide and communicates with the actin-binding site. SWII interacts with the γ-Pi and communicates with the converter domain. It is these two switches which transmit conformational changes from one domain to the other during the cross-bridge cycle ultimately causing a 60° rotation of the converter region and resulting in the movement of the lever arm (about 10 nm) (see Geeves and Holmes, 1999 for review).

In 1980, Eisenberg and Greene proposed that myosin has two binding states to actin, a weak binding state when bound to ATP or ADP.Pi and a strong binding state when nucleotide-free or ADP bound. Goody and Holmes (1983) suggested that tighter binding of the nucleotide to myosin resulted in a weaker binding of myosin to actin and vice versa. When myosin is weakly attached to actin (A-state), it can reversibly isomerise to the strongly bound rigor complex (R-state) resulting in the reduction in the nucleotide affinity and its release. These changes in nucleotide affinities and actin binding affinities are coupled to the opening and closing of the switches as well as the cleft region. A tight binding to actin is linked to the closure of the cleft and happens when SWI is open. A weak binding to actin is linked to the opening of the cleft and happens when SWI is closed. SWI is open either when no nucleotide is bound or when a hydrolysis product is to be released and is closed once ATP is bound and is to be hydrolysed. The opening and closing of SWII will determine the conformation of the lever arm in either the pre- (closed SWII) or post-power stroke (open SWII) conformation and will result eventually in the movement of the lever arm (Smith and Rayment, 1996; Dominguez *et al*, 1998).

A description of the sequence of changes taking place is as follows. A nucleotide-free myosin binds actin tightly forming a rigor complex (A.M). In this case, both SWI and SWII are open and the 50K cleft is closed. Binding to ATP happens in two steps, first forming a weak complex with myosin which remains strongly bound to actin (A.M-ATP) and then weakening the acto.myosin interaction (A-M.ATP). The transition between these two states results from the closing of SWI and the opening of the 50K cleft. Up to this stage the lever arm is in the post-power stroke conformation. It is only

when a conformational change at the level of the nucleotide-binding site takes place to bring all residues required for the ATPase around the ATP molecule that the tail adopts the pre-power stroke conformation. Hydrolysis of ATP (which requires both SWI and SWII to be closed) into ADP and Pi will result in the rebinding of the myosin to actin. This will open SWI (weakening Pi binding to allow its release) and is followed by the closing of the 50K cleft subsequently resulting in an increase in the myosin affinity for actin. The release of Pi will result in the opening of SWII achieving the post-power stroke conformation. ADP, whose affinity is also weakened, is released and the cycle starts again (Geeves and Holmes, 1999; Holmes and Geeves, 2000).

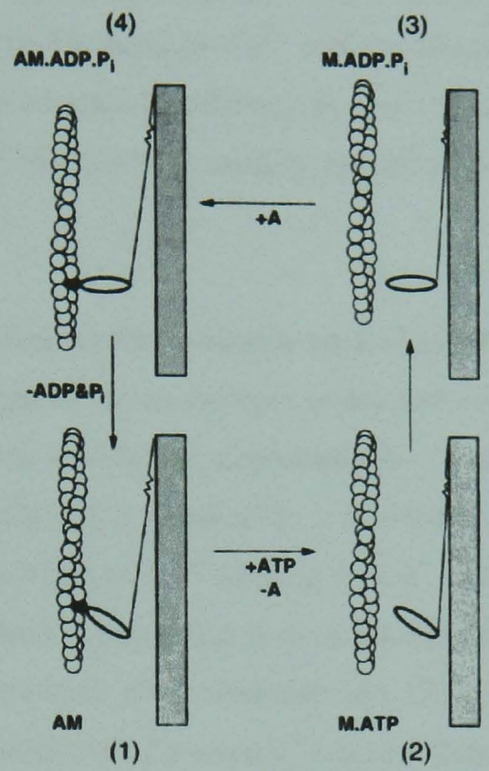

Figure 1.16: The Lymn and Taylor model of the crossbridge cycle. In the nucleotide-free state, the mysoin head (M) is strongly attached to actin (A) forming a rigor complex (1). Binding of ATP decreases the affinity of myosin to actin and subsequent dissociation takes place (2). ATP hydrolysis yields the M.ADP.Pi complex and results in a conformational change (3). Reassociation with actin takes place (4). Actin accelerates hydrolysis product release resulting in a second conformational change (the power stroke), the reverse of the first one (4-1 transition). This cyclic change of S1 conformation and affinity results in the sliding of the two filaments over each other producing muscle contraction (Lymn and Taylor, 1971).

3 Regulation of muscle contraction

The force-generating cyclic interaction of myosin heads with actin has to be tightly controlled. This is achieved by the action of the thin filament regulatory proteins, which respond according to the level of Ca^{2+} concentrations in the muscle cell. The mechanisms of regulation of muscle contraction have been extensively investigated. Below is a description of the working models put forward to try to understand the complexity of the system.

3.1 The McKillop and Geeves three-state model of regulation

Muscle contraction is triggered by an increase in the intracellular Ca^{2+} concentrations (Ebashi *et al*, 1969). This is reflected experimentally by the dependence of muscle tension production on pCa ($pCa=-\log[Ca^{2+}]$). However full activation of muscle contraction is not just dependent on Ca^{2+} binding to TnC. The rigor binding of myosin heads to actin is also required as suggested by both biochemical (McKillop and Geeves, 1993) and structural (Vibert *et al*, 1997; Wakabayashi, 2001; Craig and Lehman, 2001) evidence. Based on the biochemical evidence obtained from a combination of kinetic and equilibrium binding studies, McKillop and Geeves put forward the three-state model to account for the process of muscle regulation. Their model was a modification of the two-step steric-blocking model (Parry and Squire, 1973; Wakabayashi *et al*, 1975) as it takes into consideration the influence of myosin heads. The steric model described the binding of Ca^{2+} to TnC as being the only trigger for muscle contraction. Binding of Ca^{2+} ions to TnC causes a series of conformational changes within the thin filament leading ultimately the relocation of Tm, exposing the myosin-binding sites on actin. In the three-state model (Figure 1.17) the filament is believed to exist in a dynamic equilibrium between three myosin binding states namely Blocked (B-state), closed (C-state or the Ca^{2+}-induced state) and open (M-state or myosin-induced state). In the three-state model the ATPase activity is OFF when the filament is in the B- and C- states and it is turned ON when the filament is in the M-state. The three states are characterised by different Tm positions on actin. In the absence of Ca^{2+}, the filament is predominantly in the B-state as tropomyosin occupies the potential myosin-binding sites on actin preventing the formation of the acto-myosin complex. When Ca^{2+} binds to TnC, Tm moves away towards the inner region of actin allowing the formation of a weakly bound acto-myosin complex which does not exhibit an ATPase activity. The

binding of myosin heads shifts the position of Tm further switching the equilibrium into the M-state. Subsequently, the isomerisation from weakly to strongly-bound (rigor) myosin heads (A- to R-state transition) takes place. It is only in the R-state that the acto-myosin complex is ATPase active leading to force production. Thus, the full activation of muscle contraction is only achieved when both Ca^{2+} binds to TnC and when myosin binds actin in the rigor state.

3.1.1 The biochemical evidence for the three-state model of regulation

The existence of three states of the filament was deduced from S1 binding to actin as defined by both equilibrium and kinetic measurements. The binding of S1 to actin under equilibrium conditions (see chapter 3, section 3) follows a simple binding reflected by a hyperbolic curve. This suggested the non-cooperative nature of the binding, with actin monomers behaving as independent entities. In the presence of Tm or Tm.Tn complex, the binding curve is sigmoid which is indicative of the cooperative switching between two states of the filament induced by S1 binding. In the presence of the regulatory complex (Tm.Tn complex) and Ca^{2+}, 20% of the filament is found to be in the ON state. On Ca^{2+} removal, the figure goes down to 5%.

Evidence for a third state came from kinetic studies of the rate of S1 binding to actin using stopped-flow experiments under pseudo-first order conditions (either actin or S1 in a large excess over the other; see chapter 3, section 2). The results indicated that the rate of S1 binding to either actin, actin.Tm or actin.Tm.Tn complex in the presence of Ca^{2+} was similar. In the absence of Ca^{2+} and under the conditions where only few actin sites become occupied by S1 (i.e. actin in excess over S1) the rate of S1 binding to actin is a factor of 3 lower. The change in the rate of S1 binding to actin was explained in terms of a change in the fraction of actin sites available for binding. This meant that all the actin sites are available for S1 binding in the presence of Ca^{2+} (more than 95%) and only one third was available in the absence of Ca^{2+} (about 30%). The kinetic results therefore conflicted with the previously described equilibrium binding results. The most plausible explanation was that the two experiments described two different populations of the ON and OFF states. The three-state model could account for these differences. The distribution between the blocked, closed and open states is dependent on the proteins bound to actin and on the presence or absence of Ca^{2+}. When only Tm is bound to actin, the filament is mainly in the closed (80%) and open (20%) states, with

the blocked state not substantially populated (less than 5%). A similar distribution of the three states is reported when the Tm.Tn complex is bound to actin in the presence of Ca^{2+}. In the absence of Ca^{2+}, the filament is predominantly in the blocked (75%) and closed (25%) states with less than 5% in the open state. K_B and K_T, the equilibrium constants between blocked/closed and closed/open states respectively are Ca^{2+}-dependent, with a lesser effect of Ca^{2+} on K_T. The type of nucleotide bound to S1 will affect the K_2 value, the equilibrium constant for the isomerisation step (Figure 1.17).

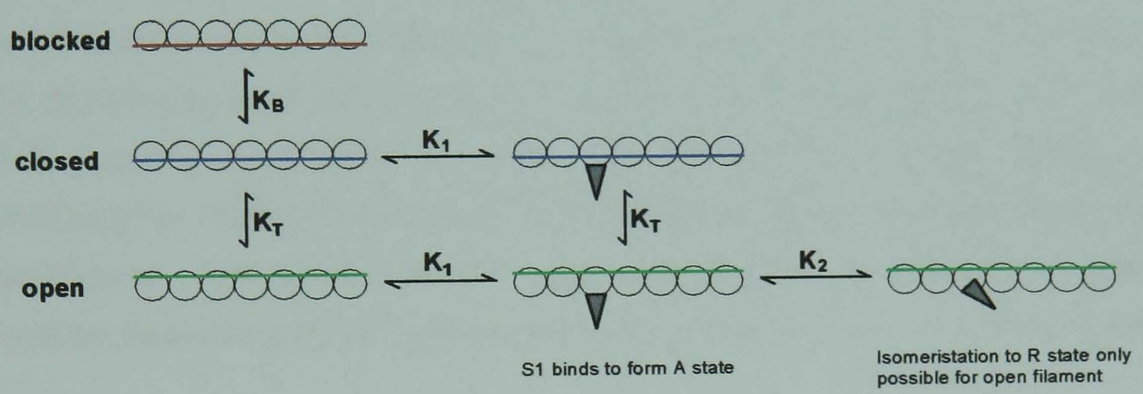

Figure 1.17: The three-state model for thin filament regulation. The thin filament is believed to exist in a dynamic equilibrium between three states namely: blocked, closed and open depending on Tm position on the filament. K_B defines the equilibrium constant between the blocked and the closed states, and K_T defines the equilibrium constant between the closed and open states. K_1 and K_2 represent the equilibrium constant of S1 binding to form an A state (weak binding) and R state (strong binding) respectively (McKillop and Geeves, 1993).

3.1.2 The structural evidence for the three-state model of regulation

The validity of the three-state model was confirmed later on by EM studies carried out on reconstituted thin filaments (Figure 1.18) (Vibert *et al*, 1997; Craig and Lehman, 2001). These images show clearly Tm occupying three different locations on the actin filament, both Ca^{2+} and S1-induced. These structural changes were in a good agreement with the biochemically defined blocked, closed and open states of the filament. The EM images show Tm interacting with the myosin-binding sites on actin in the absence of Ca^{2+}. The addition of Ca^{2+} shifts Tm to a position that allows the formation of acto-myosin complex but the isomerisation to the rigor complex is still sterically prevented. It is only in the presence of both Ca^{2+} and strongly-bound myosin heads that the Tm is moved further away allowing the formation of the ATPase active, rigor acto.myosin complex. The reconstruction of these high-resolution images required the use of helical averaging of a number of collected images. As a result of that, this technique, though allowing the localisation of the long helical molecule of Tm, did not give much information about the localisation and contribution of Tn which binds once every seven actins. To overcome this problem, the group of Wakabayashi (2001) applied single particle analysis to reconstruct the three-dimensional image of the thin filament. Their images where Tn could be visualised confirmed that full activation could not be achieved by Ca^{2+} only and the binding of myosin heads was also required.

Crossbridge and tropomyosin positions on actin

It is widely accepted that there are two states of myosin crossbridge binding to actin: weakly-bound state (attachment A-state) and strongly-bound (rigor R-state) (Eisenberg and Greene, 1980; McKillop and Geeves, 1993; Geeves and Conibear, 1995) with the transition between the two involving the force-generating conformational change or power stroke of the ATPase cycle. Structural data (Rayment *et al*, 1993b) supported by mutational analyses (see Sheterline *et al*, 1995 for review and refs therein) concluded that formation of an acto.myosin complex involved three types of interactions. The formation of a disordered (non-stereospecific) complex involving ionic interactions mainly between lysine residues located on the 50K to 20K junction loop of myosin and negatively charged acidic residues at the N-terminal end of actin subdomain 1. A stereospecific interaction arises as a result of hydrophobic interactions between the two helices at the lower 50K domain of the myosin head (Figure 1.5) and a number of

hydrophobic residues located at the interface between subdomains 1 and 3 of actin. The strengthening of this interaction involves the recruitment of additional loops from the upper 50K domain with interactions predominantly ionic in nature. These interactions are believed to extend to the adjacent actin monomer, making one myosin head bind two actin subunits and accounting for the myosin-induced polymerisation of actin.

The data obtained by Vibert *et al* (1997) is in good agreement with the proposed pattern of interactions described above. In the absence of Ca^{2+} (when the A-state formation is prohibited (blocked state)), the position of Tm as revealed by electron microscopy does not block the electrostatic binding site of myosin on the periphery of actin. The presence of Ca^{2+} shifts Tm position towards the inner region of the filament uncovering the strong binding sites of myosin (allowing the A-state formation) but still blocking the formation of the strong rigor complex as access to the all the residues required for the hydrophobic interaction is still sterically prevented. The conclusion was that in the absence of Ca^{2+}, there is the possibility for the formation of a non-stereospecific acto.myosin complex which precedes the formation of the A-state myosin crossbridge. This initial non-specific binding is thought to allow the myosin crossbridge to be in the vicinity of the stereospecific attachment site on actin (docking process).

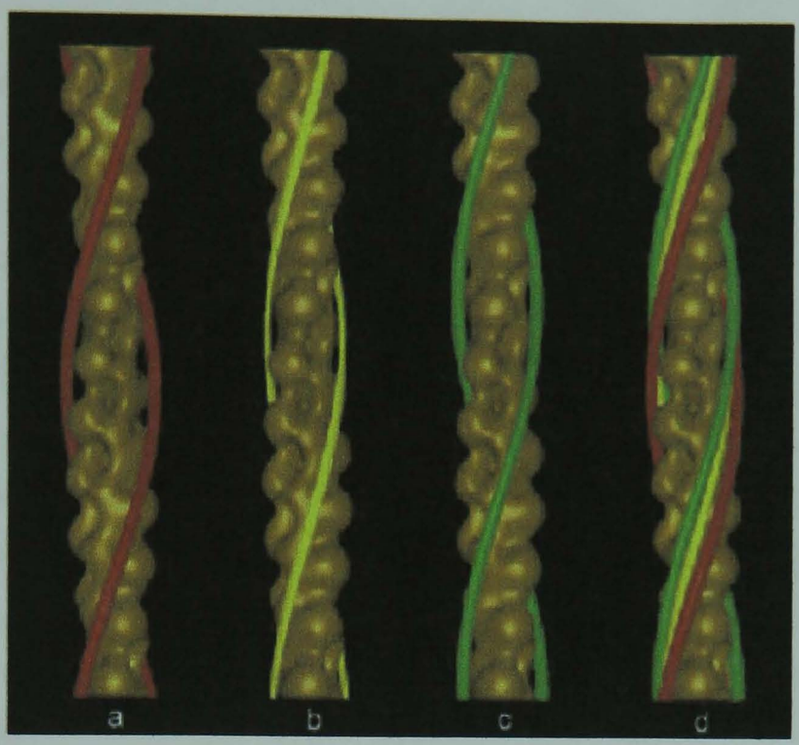

Figure 1.18: Structural evidence for the three-state model of thin filament regulation. The images are 3-D reconstructions of thin filaments under different experimental conditions **a)** relaxed filament in the absence of Ca^{2+} **b)** activated filament in the presence of Ca^{2+} **c)** in the presence of bound myosin heads (not shown on this figure). A shift of 25° in Tm position is observed as Ca^{2+} is added uncovering actin binding sites and allowing the formation of a weakly bound acto.myosin complex (image b). Binding myosin heads to the filament in the presence of Ca^{2+} causes a further shift of 10° in Tm position uncovering the sites required for the formation of a rigor acto.myosin complex (image c). The three Tm positions on actin are superimposed in image d. These three structural states of the thin filament are believed to correspond to the biochemically identified blocked, closed and open states (Craig and Lehman, 2001)

3.2 Cooperative binding reactions

Proteins with more than one ligand-binding site may display sigmoidal binding curves instead of hyperbolic ones, which is indicative of a cooperative binding of the ligand.

3.2.1 The Monod Wyman and Changeux (MWC) model

The Monod, Wyman and Changeux (MWC) cooperative model (1965) (Figure 1.19) was established by studying the binding of oxygen to haemoglobin. The multi-subunit protein is assumed to exist in equilibrium between two states or conformations; a low ligand- affinity and a high ligand-affinity state. When none of the sites are occupied, the low affinity conformation of the protein is predominant. As more sites become occupied the equilibrium is shifted toward the high affinity state each time by a given factor corresponding to the ratio between the two affinities. This mechanism of cooperative binding therefore allows a several fold increase in the equilibrium constant between the two states of the protein as a result of the binding of few ligand molecules. This way, the protein can switch between the two states over a small range of ligand concentration.

Most proteins that exhibit this sort of behaviour have been reported to be enzymes subject to feedback activation or inhibition. This explains the need for cooperativity, as it provides a more efficient and rapid means for the switching between the two states of the protein.

3.2.2 The Koshland-Némenthy Filmer (KNF) model

In the KNF model (1966), it is assumed that the switching between the two conformations of the enzyme happens in a sequential manner, as the conformation of each subunit changes upon ligand binding (Figure 1.20). In other words, in the absence of ligand only one conformation exists (low affinity state) and binding of the first ligand will induce a conformational change in the subunit (high affinity conformation) which is subsequently transmitted to the neighbouring site. It is only when all the sites become occupied that complete switching into the second conformation takes place (ON state).

Combining both the MWC and the KNF models would give rise to a scheme where all the possible substates are described. This sort of model is very complex as it contains too many binding parameters and protein conformations. Therefore, to simplify the analysis, experimental results are interpreted either in terms of MWC or KNF model.

3.3 Cooperativity in the muscle thin filament

The muscle thin filament is a complex structure made up of repeating units each comprising an assembled complex of at least 5 proteins (Figure 1.6). The nature of interactions between these proteins is very complex and is highly allosteric/cooperative (see chapter 3 section 3.2.3) both within and between the thin filament structural units (reviewed by Lehrer and Geeves, 1998).

Ca^{2+} binding to TnC is cooperative. The cooperativity is believed to occur between the two Ca^{2+} binding sites (I and II) of TnC (as revealed from Ca^{2+} binding to isolated TnC) (Potter and Gergely, 1975; Grabarek *et al*, 1983) and potentially over a long range as reflected by the large Hill coefficient value (> 2) obtained using fibre measurements (Brandt *et al*, 1980). This cooperativity is confirmed as the Hill value for Ca^{2+} binding to cardiac TnC, which has only one effective Ca^{2+}-binding site as compared to two sites in skeletal TnC, is lower. The affinity of Ca^{2+} for TnC is dependent on whether TnC is free or bound to TnI with Ca^{2+} affinity being higher when TnC is tightly bound to TnI. Similarly, the affinity of TnI for actin is dependent on whether TnC is Ca^{2+}-bound or free, as TnI binding to actin is tighter in the absence of Ca^{2+} (Potter and Gergely, 1974; Grabarek *et al*, 1983; Ingraham and Swenson, 1984). So as postulated by Geeves and Lehrer (2002) TnI can be regarded as an allosteric effector for Ca^{2+} binding to TnC, and in the same way Ca^{2+} can be regarded as allosteric effector of the thin filament conformation changes.

Myosin binding to the thin filament is also cooperative as indicated by the sigmoid equilibrium binding curves (Greene and Eisenberg, 1980; Hill *et al*, 1980; Geeves and Halsall, 1987; Maytum *et al*, 1999). The cooperative unit size switching between the B- and C-states (i.e. the number of actin monomers that switch between the two transition upon myosin binding and as a response to Ca^{2+} activation) was found to be no smaller than 7 (the size of a structural unit) (Head *et al*, 1995). The cooperative unit

size for the C- to M-state transition is found to be around 7 in the absence of Ca^{2+} and almost twice that in the presence of Ca^{2+} (Maytum *et al*, 1999). TnT1 influences the cooperative unit size of the filament (Schaertl *et al*, 1995). Owing to its location at the overlap region, it strengthens the head to tail interaction of two neighbouring Tm and therefore stiffens the Tm filament allowing an easier propagation of the signal (Maytum *et al*, 1999). This explanation is consistent with the results obtained with smooth Tm known to have stronger Tm-Tm contacts and a cooperative unit size of 12 (Lehrer *et al*, 1997). The cooperative unit size is independent of the length of Tm as fibroblast Tm (which binds 6 actins) has a similar cooperative size as the smooth Tm (which binds 7 actins) (Maytum *et al*, 2001). In the absence of Ca^{2+}, the cooperative unit size is no larger than the structural unit size as under these conditions the TnI is strongly bound to every seven actins producing a pinning effect and preventing a long range cooperativity. These findings led to the suggestion of the continuous flexible model for Tm by Maytum *et al* (1999). Tm is believed to form a continuous, dynamic cable along the actin filament with Tm stiffness being the determinant of the cooperative unit size (Figure 1.21).

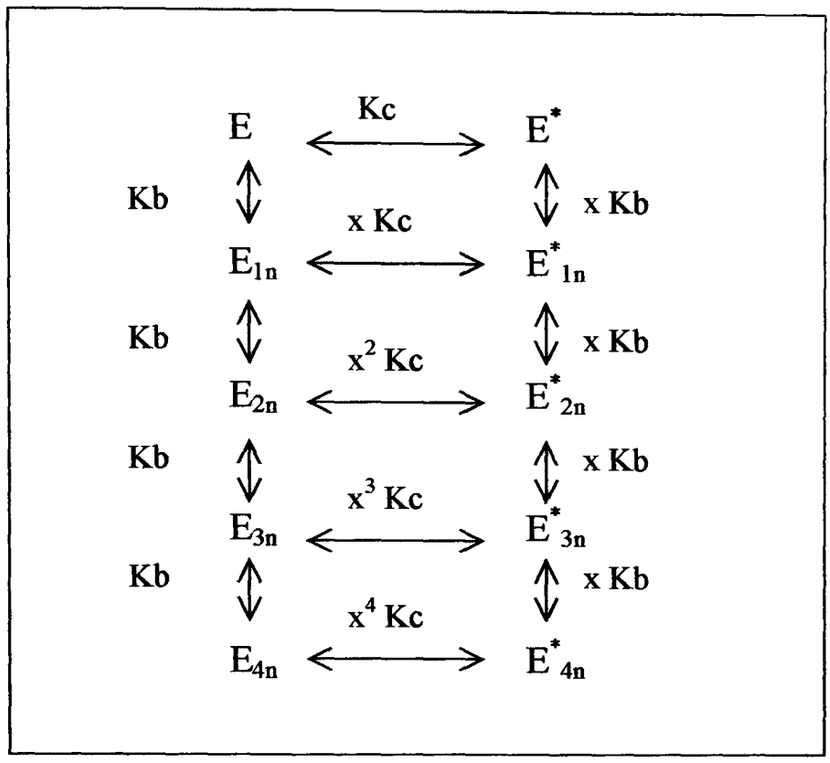

Figure 1.19: A scheme for the MWC cooperative model. The ligand (n) binds to the enzyme (E) which contains 4 ligand-binding sites. The enzyme is in equilibrium between two conformations E and E^* defined by the constant Kc. Binding of the ligand to the E conformation of the enzyme is defined by the equilibrium Kb which is increased by a factor x when the enzyme is in the E^* conformation. As more sites become occupied by the ligand the Kc equilibrium is increased by the factor x allowing a rapid switching between the two states of the enzyme. It is assumed that the different enzyme subunits are identical in each state. The ligand affinity for the enzyme should therefore remain unchanged as more sites become occupied.

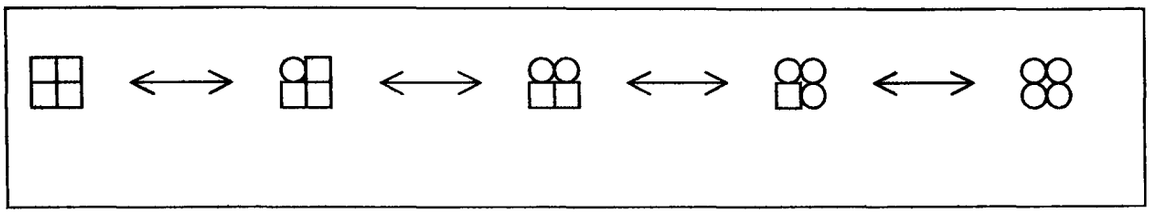

Figure 1.20: Schematic representation of the KNF model. The full switching between the low and high affinity conformations of the protein is only achieved once all the ligand-binding sites become occupied. Intermediate substates arise as the binding of a ligand to a vacant site changes its conformation and influences the conformation of the neighbouring site at the interface.

3.4 Other muscle regulation models

3.4.1 The Hill model

The McKillop and Geeves model is a refinement of the Hill *et al* (1980) model. In the Hill model, the filament is considered as a linear array of repeating structural units (seven actins, one Tm and one Tn complex) with each unit being in either the ON (ATPase active) or OFF (ATPase inactive) state. S1 binds each state with a different affinity. Hill *et al* included an extra cooperative parameter to take into consideration the influence of interaction between two adjacent units (Figure 1.21).

3.4.2 The Tobacman model

The Tobacman model tries to address the mechanism by which the C- to M-state transition occurs by assigning a role to actin in the process of regulation (Tobacman and Butters, 2000). It has been established by many groups that the affinity of myosin for actin is enhanced in the presence of tropomyosin (Williams and Greene, 1983; Maytum *et al*, 1999; Tobacman and Butters, 2000) and that the affinity of tropomyosin for actin is enhanced in the presence of myosin bound to actin (Cassel and Tobacman 1996; Maytum *et al*, 2001). Tobacman explains this mutual effect of myosin and Tm by an indirect interaction promoted by a conformational change in actin. In other words, there would be an allosteric effect from actin promoting the myosin-Tm interaction. The actin conformational change would happen upon myosin binding to actin and would subsequently strengthen the binding of Tm to the inner domain of actin. The same changes to actin would be promoted when Tm is bound to its inner region. To date, there is no structural evidence to back up the Tobacman hypothesis as no structural changes have so far been detected in actin.

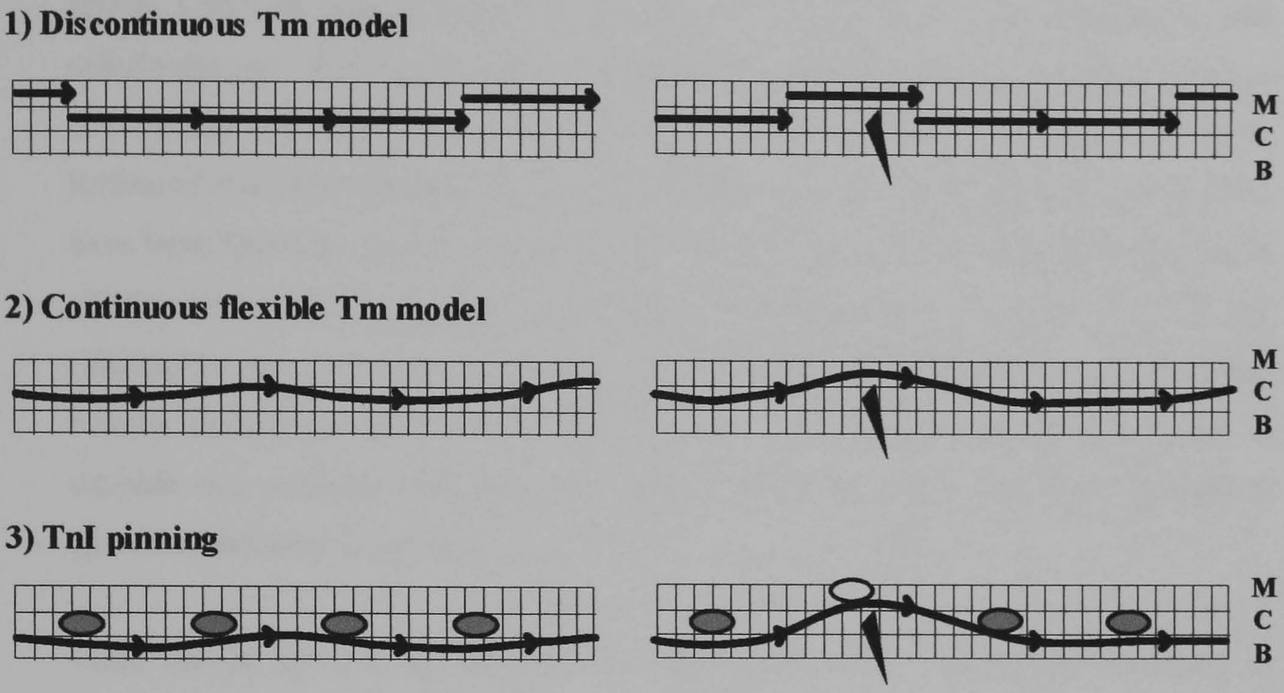

Figure 1.21: Discontinuous cooperative and continuous flexible models of Tm. Actin is shown with three potential Tm binding sites corresponding to the blocked (B), closed (C) and open (M) states of the filament. On the left is shown the filament in the absence of S1 and on the right is the filament bound to one S1 head. Panels 1 and 2 correspond to the state of the filament when it is either bound to Ca^{2+} or in the absence of Tn. In this case the Tm switches between the closed and open positions when S1 is bound. Model 1 was described by Hill *et al* (1980) and describes Tm as a rigid filament with only one unit switching between states but with an increased likelihood for the adjacent unit to also switch states. Panel 2 represents the Maytum *et al* model where Tm is shown as a dynamic flexible filament whose stiffness determines the extent of the cooperativity of the system. Panel C represents the effect of TnI (grey oval) on the extent of cooperativity when Ca^{2+} is absent. The strongly bound TnI to actin prevents the propagation of the signal between units as it pins the Tm down every seven actins. It also constrains Tm to the blocked and closed states (Maytum *et al*, 1999).

4 Hypertrophic cardiomyopathy mutations

Familial Hypertrophic Cardiomyopathy (FHC) is an autosomal dominant disease. It affects 1 in 500 individuals and is characterised by left ventricular hypertrophy and cellular disarray. FHC mutations are believed to be the cause of sudden death in young and healthy individuals (for reviews see Maron *et al*, 1995; Bonne *et al*, 1998; Redwood *et al*, 1999; Marian and Roberts, 2001). So far, the mutations that cause FHC have been found to arise in sarcomeric proteins namely myosin heavy and light chains (Watkins *et al*, 1993, Flavigny *et al*, 1998), actin (Mogensen *et al*, 1999) TnT and TnI (Thierfelder *et al*, 1994; Kimura *et al*, 1997), α-tropomyosin (Watkins *et al*, 1995) and myosin binding protein-C (Bonne *et al*, 1995). The severity of FHC mutations is variable and probably linked to the degree of structural and functional disruption caused by different mutations.

More details about FHC mutations in tropomyosin and troponin are discussed in chapters 5 and 6.

5 Project aims

So far most of the work on the three state model of regulation has been accomplished with skeletal muscle proteins. The aim of this study was to extend the initial studies to the cardiac system and to define all the parameters of the model in the presence of cardiac thin filament proteins. This would lead on to the investigation of the effects of cardiomyopathy mutations on the regulatory process and the definition of the subtle changes that can arise from these mild mutations. The kinetic methods used to define the three state model of regulation would be used to interpret the effect of phosphorylation of cardiac Tn on the Ca^{2+} sensitivity of the thin filament. The *in vitro* assay system in which reconstituted proteins are used offers a big advantage over the *in vivo* fibre measurements as factors which affect the Ca^{2+} sensitivity of the system, such as the level of Tn phosphorylation and the isoform type present in the Tn complex, can be defined and controlled.

Establishing a Tm expression system and the validation of the use of recombinant proteins would ultimately allow the expression of different Tm isoforms as well as Tm carrying FHC mutations in large quantities. A number of approaches would then be used to characterise these molecules. These would include both the kinetic and equilibrium techniques previously applied to define the three state model parameters, actin binding assays as well as a calorimetry technique to investigate protein thermal stability. This would be followed by the development of a procedure for the production and characterisation of the αβ Tm heterodimer.

The effect of cardiac TnI phosphorylation on the Ca^{2+}-dependent regulation of muscle contraction will be investigated for both the WT and FHC-carrying Tn complexes. The alterations brought about by phosphorylation and dephosphorylation can be accounted for by measuring specific rates and equilibrium constants within the model.

CHAPTER 2

MATERIALS AND METHODS

1 Protein biochemistry materials and methods

1.1 Materials

1.1.1 Chemicals

Unless otherwise stated, all the chemicals used in the preparations were purchased either from Sigma-Aldritch, Fisher, BDH or Melford. N-(1-pyrenyl)iodoacetamide was purchased from Molecular Probes.

1.2 Methods

1.2.1 Sodium Dodecyl Sulphate Polyacrylamide Gel Elecrophoresis (SDS-PAGE)

Protein purity was checked on SDS-PAGE gels made of 12.5 % resolving gel (6.25 ml of 30 % acrylamide, 5.55 ml of dH_2O, 3 ml resolving gel buffer (see section below), 150 µl of 10 % SDS, 10 µl TEMED (N,N,N',N'-Tetramethylethylenediamine) 100 µl of 10 % APS (Ammonium Persulphate) and 4.8 % stacking gel (0.8 ml of 30 % acrylamide, 3.6 ml dH_2O, 0.5 ml stacking gel buffer (see section below), 50 µl of 10 % SDS, 10 µl TEMED, 34 µl of 10 % APS). All protein samples had sample buffer added to them and were heated up to 100 °C for 3 minutes before loading. The gels were run in the running buffer (see section below) at 30 mA for 50 minutes. The gels were incubated with the staining solution until protein bands started to appear. The destaining was carried out until most of the background staining was removed.

SDS-PAGE standard buffers and solutions

Acrylamide solution	30 % Acrylamide 0.8 % N, N-methylenbisacrylamide
SDS solution	10 % SDS
Resolving gel buffer	23 g TRIS / HCl pH 8.8 in 100 ml total volume
Stacking gel buffer	7.56 g TRIS / HCl pH 6.8 in 50 ml total volume
Sample buffer	2.5 ml Stacking gel buffer

	1 g SDS
	2.5 ml 2-mercaptoethanol
	5.8 ml Glycerol
	5 mg Bromophenol blue
	dH_2O added up to a final volume of 50 ml
Running buffer	7.2 g l^{-1} Glycine
	1.52 g l^{-1} TRIS
	0.5 g l^{-1} SDS
Coomassie solution	5 g Coomassie G250
	0.5 g Coomassie R250
	solved in 50 ml methanol
	dH_2O added up to a final volume of 1 l
Staining solution	1 g Coomassie R
	40 % methanol
	10 % Acetic acid
	50 % water
Destaining solution	7 % Acetic acid
	25 % Methanol

1.2.2 Estimation of protein concentration

All protein concentrations were determined by photometric absorbance at 280 nm. The concentration of the protein-containing solution was calculated using the Beer-Lambert law where $A = \varepsilon . c . l$ (A: the solution absorbance, ε: the molar extinction coefficient (l mol^{-1} cm^{-1}), l: length of the light path (cm), c: protein concentration (mol l^{-1}))

1.2.3 Native muscle protein preparations

All steps of protein preparations were carried out at 4 °C unless otherwise stated. The purity of proteins produced in each preparation was verified by SDS gel electrophoresis.

Acetone powder, myosin and S1 preparations were all performed by our technician Ms Nancy Adamek.

The following muscle proteins were prepared from freshly killed white New Zealand rabbits. The back and leg muscles were minced and transferred into 3 l of Guba-Straub buffer (0.3 M KCl, 0.1 M KH_2PO_4, 0.05 M K_2HPO_4, pH 6.6). The mixture was stirred for 15 minutes and then centrifuged at 4, 500 g for 30 minutes. The resulting pellet was used for actin and regulatory control protein preparations, whereas the supernatant was used for myosin preparation.

1.2.4 Actin preparation

1.2.4.1 Acetone powder preparation

The pellet from rabbit muscle mixture (section 1.2.3) was transferred into 5 l of extraction buffer (4% $NaHCO_3$, 0.1 mM $CaCl_2$) and stirred for 30 minutes. This was followed by filtration through a double layer of muslin. The residue was transferred into 1 l of buffer containing 10 mM $NaHCO_3$, 10 mM Na_2CO_3 and 0.1 mM $CaCl_2$. 10 l of distilled water (20 °C) were added and the mixture was filtered again through a double layer of muslin. The residue was transferred into 2.5 l acetone, incubated for 20 minutes, and then filtered through a double layer of muslin. The latter was repeated four times. The residue from the final wash was dried on Whatman paper in a fume cupboard for 2 days. The powder was sifted through a mesh to remove unwanted tissue residues and was kept at -20 °C for several months.

1.2.4.2 F-actin preparation

The preparation of F-actin was based on a method previously described by Spudich and Watt (1971). 1-2 g of acetone powder was added to pre-chilled 10 mM TRIS, 0.5 mM ATP, 0.2 mM $CaCl_2$, 1 mM DTT pH 8.0 buffer and stirred for 30 minutes. The mix was then filtered under vacuum through a double layer of cheesecloth. The filtrate was used for the F-actin preparation and the solid residue was used for thin filament regulatory protein (Tm.Tn complex also referred to as control proteins CPs) preparation (see section 1.2.7).

The filtrate was centrifuged at 100, 000 g for 1 hour and the pellet was discarded. KCl and $MgCl_2$ were added to the supernatant to a final concentration of 100 mM and 2 mM respectively. The resulting solution was stirred for 1 hour at room temperature to

achieve actin polymerisation. The polymerised actin was collected by centrifugation at 100,000 g for 3 hours. The actin pellet was resuspended in depolymerising buffer (5 mM TRIS, 0.2 mM $CaCl_2$, 1 mM NaN_3 pH 7.5) using a homogeniser and dialysed overnight against the same buffer. The depolymerised actin was centrifuged at 100, 000 g for 1 hour and the concentration of actin present in the supernatant was measured by absorbance at 280 nm. The actin concentration was diluted to 1 mg ml^{-1} using depolymerising buffer and actin was then polymerised as previously described. Unlabelled actin was obtained by centrifugation at 100, 000 g for 3 hours. The pellet was redissolved in and dialysed against the appropriate experimental buffer (20 mM MOPS, 100 mM KCl, 5mM $MgCl_2$, 1 mM NaN_3 pH 7.0). The unlabelled actin was stored up to two weeks at 4 °C. The concentration of actin prepared following this protocol usually ranged between 100 and 200 μM (actin's extinction coefficient $\varepsilon = 1.104$ mg^{-1} ml cm^{-1} and its molecular weight is 42, 000 Da).

1.2.5 Pyrene labelled F-actin Preparation

The labelling of F-actin with the N-(1-pyrenyl)iodoacetamide (pyrene fluorophore) was based on a procedure by Criddle *et al* (1985). Pyrene (5mg ml^{-1} solved in DMF) was added to the stirred 1 mg ml^{-1} repolymerised actin solution (as described in section 1.2.4.2) very slowly to reach a final concentration of 0.8 % w/w (pyrene/actin). The pyrene labelling of actin was carried out by stirring the two components together over an 18 hour period in the dark at room temperature. The labelled actin was centrifuged at 7, 800 g for 1 hour to remove residual pyrene and denatured protein. The supernatant was then centrifuged at 100, 000 g for 3 hours. The pellet was resuspended in the appropriate experimental buffer (20 mM MOPS, 100 mM KCl, 5 mM $MgCl_2$, 1 mM NaN_3 pH 7.0) using a homogeniser, and dialysed overnight. In order to discard any precipitated pyrene-actin, the actin was spun in an Eppendorf centrifuge at maximum speed for 5-10 minutes. The concentration of the supernatant and the percentage of labelling were assessed by UV spectroscopy. These varied between 100-200 μM and 80-100% respectively. The pyrene label has an absorbance peak at both 280 nm ($\varepsilon = 1.059 \times 10^4$ M^{-1} cm^{-1}) and 344 nm ($\varepsilon = 2.33 \times 10^4$ M^{-1} cm^{-1}). By calculating the concentration of pyrene from the 344 nm absorbance peak, its absorbance at 280 nm can be subtracted and the actin concentration can be deduced at that wavelength. The pyrene-actin was stored at 4 °C for up to two weeks.

1.2.6 Phalloidin-stabilised F-actin preparation

Actin critical concentration (see chapter 1, section 1.2.2.1) is 0.1-1 μM depending on the buffer conditions. Therefore when low actin concentrations were used in an experiment, the fungal toxin phalloidin was added in a 1:1 molar ratio with actin. An overnight incubation allowed the stabilisation of the filamentous form of actin (Cooper, 1987; Kurzawa and Geeves, 1996).

1.2.7 Control proteins (CPs) preparation

Control proteins are made up of both the troponin complex (Tn) and tropomyosin (Tm) proteins. These are prepared as follows. The solid residue from the cheesecloth filtration in the F-actin preparation (section 1.2.4.2) was added to 10 mM TRIS, 2 mM DTT, 1 mM NaN_3 pH 8.0 buffer and stirred for 5 hours at room temperature. The resulting solution was filtered through a double layer of cheesecloth. The filtrate was subjected to a 40 % ammonium sulphate cut (0.24 g ml^{-1}) and stirred for 20 minutes in order to precipitate the actin. After a centrifugation step at 9, 800 g for 30 minutes, the supernatant was taken through a second ammonium sulphate cut (0.13 g ml^{-1}) reaching 60 % saturation and resulting in CPs precipitation. The proteins were recovered by centrifugation at 9, 800 g for 30 minutes. They were then resuspended in 5 mM TRIS, 0.5 mM DTT pH 8.0 buffer, against which they were dialysed 3-4 times. The concentration, which normally varied between 20-30 μM, was measured by absorbance at 280 nm (ε = 0.385 mg^{-1} ml cm^{-1}, Mwt = 136, 000 Da). CPs were stored for up to two weeks at 4 °C.

1.2.8 Skeletal tropomyosin and skeletal troponin preparation

In order to separate CP components, the following procedure was followed. CPs were dialysed overnight against 50 mM KCl, 10 mM TRIS, 0.5 mM DTT pH 8.0. The CP concentration was then diluted to 1 mg ml^{-1} using the same buffer. This was followed by 3-4 pH cuts where the pH was dropped slowly to 4.6, the isoelectric point for Tm. The Tm was collected in a pellet after each pH cut by centrifugation at 27, 000 g for 15 minutes, leaving the Tn in the supernatant. The supernatant of each pH cut had its pH readjusted to 8.0 and some DTT added to it. The Tm pellet from the final pH cut was redissolved in 250 mM KCl, 5 mM TRIS, 0.2 mM EDTA, 0.2 mM DTT pH 7.5 to

give a protein concentration of 1 mg ml^{-1}. The solution was spun at 17, 500 g for 30 minutes and this was followed by a 53 % ammonium sulphate cut (0.32 g ml^{-1}) and by 20 min stirring which allowed the precipitation of any remaining Tn in the pellet. The Tm-containing supernatant was heat precipitated at 30 °C for 30 minutes and the solution was centrifuged at 17, 500 g for 30 minutes. The pellet was then resuspended in storage buffer (10 mM KCl, 10 mM MOPS, 1 mM EDTA, 0.2 mM DTT, 1 % sucrose pH 7.5). The Tn-containing supernatants were pooled together and taken through a 70 % ammonium sulphate cut (0.47 mg ml^{-1}) in order to precipitate the Tn proteins. This was followed by a centrifugation step at 12, 000 g for 30 minutes. The pellet was then dissolved in storage buffer. Both protein concentrations were measured by UV spectroscopy (skTm's extinction coefficient ε = 0.276 mg^{-1} ml cm^{-1} and Mwt_{dimer} = 66, 000 Da. SkTn's extinction coefficient, ε = 0.45 mg^{-1} ml cm^{-1}, and Mwt =70, 000 Da). Both proteins were stored at -20 °C.

1.2.9 α -tropomyosin preparation

The preparation was based on a method described by Smillie (1982) with modifications. Control proteins from preparation 2.4.2 were dialysed against the following urea buffer (6 M urea, 50 mM TRIS, 1 mM EDTA, 5 mM DTT pH 6.5). The protein solution was then loaded on an anion-exchange chromatography column (Pharmacia Resource Q 6ml) and the proteins were eluted using a 0-300 mM NaCl gradient (Figure 2.1). The fractions from the α Tm-containing peak were pooled together and the protein was concentrated by a pH cut to 4.6. This was followed by a centrifugation step at 27, 000 g for 15 minutes. The pellet was then resuspended and dialysed against storage buffer (10 mM KCl, 10 mM MOPS, 0.2 mM EDTA, 0.2 mM DTT, 1 % sucrose pH 7.5). This preparation gave a protein yield of 15-20 mg (ε = 0.276 mg^{-1} ml cm^{-1}, and Mwt = 66, 000 Da). The protein was stored at –20 °C.

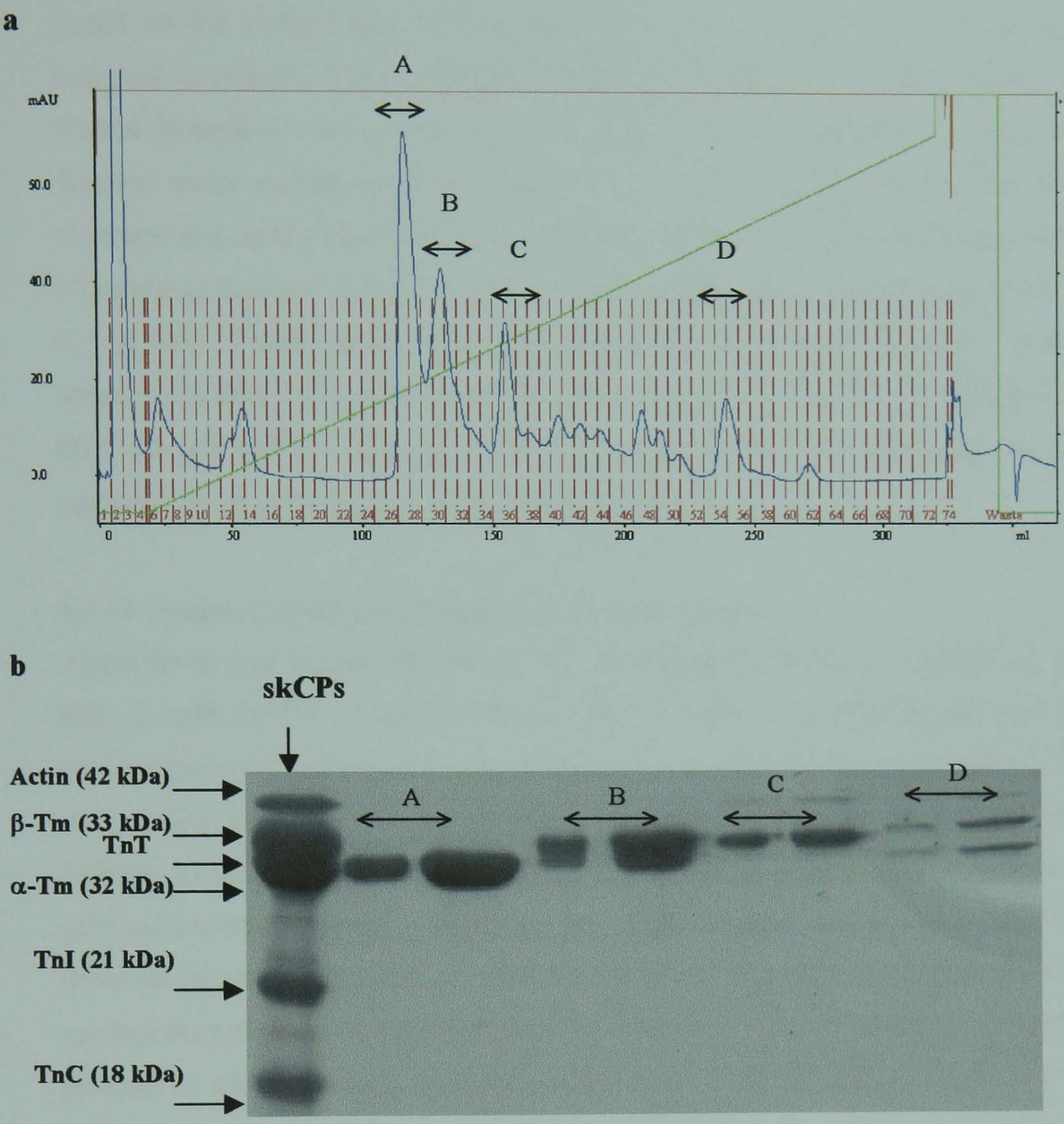

Figure 2.1: a) Protein elution profile from α-Tm preparation. The different peaks represent the 280 nm absorbance of different proteins as they elute from the column. The salt gradient is shown in green. **b) SDS-gel of the different protein peaks.** The different peaks were identified by running a 12 % SDS-Page gel. The different peaks are (A) α-Tm, (B) mixed α- and β-Tm, (C) TnT and finally (D) mixed α- and β-Tm

1.2.10 Myosin preparation

Based on the method described by Margossian and Lowey (1982) the myosin was prepared as follows. The supernatant from the rabbit muscle mixture (section 2.4) was filtered through a 1 cm layer of Whatman paper and then transferred into 30 l of cold distilled water causing myosin precipitation. The precipitate was allowed to settle overnight and most of the water was removed carefully. The excess water was removed by centrifugation at 4 500 g for 45 min. The myosin pellet was redissolved into 1 l of 0.5 M KCl. Further purification steps were undertaken by precipitation into distilled water. The final pellet was redissolved in 500 ml of 0.5 M KCl, 10 mM KPi, 1 mM DTT pH 6.5 buffer. Long term storage at –20 °C was possible when the myosin solution was mixed with an equal volume of glycerol.

1.2.11 Skeletal myosin subfragment (S1) preparation

About 10-20 g of myosin was dissolved in 1 l of digestion buffer (125 mM KCl, 10 mM KPi, 2 mM EDTA, 2 mM DTT pH 6.5). Addition of chymotrypsin to a final concentration of 0.1 mg ml^{-1} was followed by a 20 minute incubation at room temperature under a constant stirring. The digestion reaction was stopped by the addition of 0.5 mM PMSF (500 mM stock solution in ethanol) and the mixture was dialysed overnight against 10 l of 5 mM KPi pH 6.5 buffer. The undigested myosin was removed by centrifugation at 15, 000 g for 1 hour. The yield of the digestion was on average around 100-200 mg of S1 per 1 g of myosin. The S1 preparation was further purified by anion-exchange chromatography using a DEAE-Sephacel column (500 ml gel bed volume) equilibrated in 50 mM imidazol pH 7.0. The elution of the protein was achieved using a 0-250 mM KCl gradient and the presence of S1 was confirmed by the presence of absorbance peaks at 280 nm. The S1-containing fractions were pooled and dialysed against 10 l of 10 mM KPi pH 7.5. S1 was freeze-dried after the addition of an equal amount (w/w) of sucrose. For experimental uses, S1 was dissolved and dialysed against 20 mM MOPS, 30 mM KCl, 5 mM $MgCl_2$ pH 7.0. The concentration of S1 was determined using UV spectroscopy (ε = 0.79 mg^{-1} ml cm^{-1}, Mwt = 115, 000 Da). The S1 solution was stable at 4 °C for a couple of weeks.

2 Molecular biology materials and methods

2.1 Materials

2.1.1 Chemicals, enzymes, and kits

All chemicals were purchased from Sigma-Aldritch, Fisher, BDH or Melford. Molecular biology enzymes (restriction endonuclease, Taq polymerase and T4 DNA ligase enzymes) and their buffers were purchased from Roche. The purification kits (gel cleanup, plasmid purification, mini and midi prep kits) were purchased from Eppendorf.

2.1.2 Oligonucleotide primers

Primers were synthesised by MWG-Biotech. They were designed to create an *Nde*I site at the start codon and a *Bam*HI site directly downstream of the stop codon to enable the cloning into the pJC20 vector. The 5' end of the β-Tm gene (see appendix for sequence) had a dipeptide extension (Ala (GCG) and Ser (AGC)) inserted into its sequence upstream of the ATG start codon (see section 2.2.2.1 for more details).

Forward primer:

5'-GGAATTC**CATATG**GCGAGCATGGACGCCATCAAGAAGAAGATGC-3'

*Nde*I site → β Tm sequence

Reverse primer:

5'-CGC**GGATCC**TCAGAGGGAAGTGATGTCATTGAGCG-3'

*Bam*HI site → β Tm sequence

2.1.3 pJC20 vector

pJC20 vector (Figure 2.2) was purchased from ATCC. pJC20 vector is a pET derived expression vector. It has a T7 RNA polymerase-dependent promoter region and is suitable for transformation into BL21 cells which carry the gene for T7 RNA polymerase whose expression is controlled by the *lac*UV5 promoter (IPTG induced). The small size of the pJC20 plasmid and the presence of a powerful origin of replication makes it an ideal vector system for the cloning of large inserts and the production of high plasmid copy number. The plasmid shows a good stability in both XL1 Blue and BL21 *E-coli* cells. Moreover, protein expression is reported to be well regulated and

highly effective in BL21 cells (Rosenberg *et al*, 1987; Studier and Moffat, 1986; Studier *et al*, 1990; Clos and Brandau, 1994).

2.1.4 Bacterial strains

XL1 Blue and BL21 *E-coli* cells (Stratagene) were used for plasmid DNA amplification and for gene expression respectively.

2.1.5 Bacterial growth media

LB solution

10 g l^{-1} Bactopeptone
5 g l^{-1} Yeast extract
10 g l^{-1} NaCl
pH 7.5

LB-Agar plate

2 % agar in LB (w/v) autoclaved and allowed to cool down to about 50°. Ampicillin added to a final concentration of 100 mg l^{-1}. 25 ml poured into each plate and allowed to cool further until solidification.
Plates stored at 4 °C.

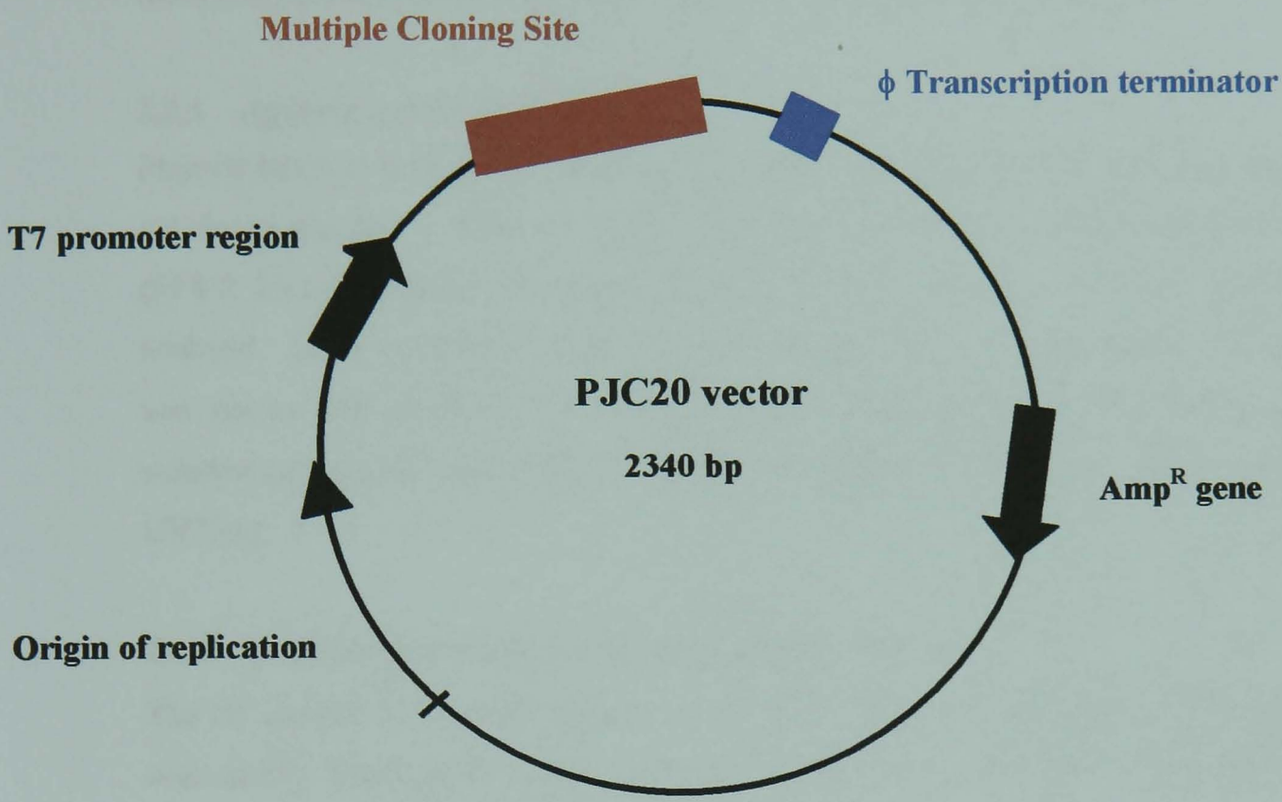

Figure 2.2: Schematic representation of the pJC20 vector. The pJC20 vector has a T7 RNA polymerase-dependent promoter region. It has a multiple cloning site which includes *Bam*HI and *Nde*I restriction sites. It also has a powerful origin of replication and an Ampicillin resistant gene.

2.2 Molecular biology methods

All molecular biology procedures were carried out under aseptic conditions. All the tubes and pipette tips were autoclaved prior to the start of the experiments.

2.2.1 Agarose gel electrophoresis

Plasmid DNA as well as PCR and restriction digest products were visualised by agarose gel electrophoresis. 1 % or 1.5 % agarose gels were made in TAE buffer (40 mM TRIS pH 8.0, 20 mM glacial acetic acid, 1 mM Na_2EDTA) depending on the DNA size to be analysed. DNA samples (1- 2 µl) were mixed with 2 µl of loading buffer and the gel was run in TAE buffer at 100 V. The gel was then incubated in ethidium bromide solution (0.5 µg ml^{-1}) for about 15 minutes and the DNA bands were visualised under UV light.

2.2.2 β-tropomyosin gene subcloning into pJC 20 vector

The rat skeletal β-Tm gene (sequence shown in appendix) cloned into a CGN plasmid was kindly donated by David Helfman (Cold-Spring Harbour). The gene was subcloned into a pJC20 expression vector as follows.

2.2.2.1 Polymerase chain reaction (PCR)

PCR was used in order to amplify the gene of interest and to introduce the desired restriction sites at both the 5' (*Nde*I) and 3' (*Bam*HI) ends of the gene. In this case it was also used to introduce a dipeptide extension (Ala-Ser) essential for the normal functioning of recombinant Tm (see chapter 4). Tm expressed with this N-terminal extension will be referred to from now on as Tm (n3) as it has a Met-Ala-Ser codons added to its sequence. The PCR reaction mixture was set up in 100 µl total volume and contained: 10 µl of 10x PCR buffer, 200 µM dNTPs, 25 mM $MgSO_4$, 20 ng of template DNA, 0.33 pM of each primer and 2 units of *Taq* polymerase. A thermal cycler was set for the following programme:

Denaturation at 95 °C for 2 minutes (1 cycle)

Denaturation at 95 °C for 30 seconds (25 cycle)

Annealing at 50 °C for 30 seconds (25 cycle)

Extension at 72 °C for 40 seconds (25 cycle)

The PCR reaction products were separated by size on a 1.5 % agarose gel by loading 5 µl of the reaction mixture and 1 µl of loading buffer. The size of DNA bands was compared to molecular weight markers λ DNA/ *Hind* III digested and ϕ X174 DNA/Hae III digested. The band corresponding to the β-Tm gene (864 base pairs) was cut from the gel and the DNA was extracted using gel cleanup kit following the manufacturer's instructions.

2.2.2.2 Restriction digest of the PCR product

The purified PCR product was digested with *Nde*I and *Bam*HI restriction enzymes (1 U μg^{-1} of DNA) in the manufacturer's supplied buffer at 37 °C for 1 hour. The β-Tm fragment was purified using a DNA purification kit. The protocol was carried out as instructed by the manufacturer.

2.2.2.3 Ligation of the β-Tm gene into pJC20 vector

The ligation of the cohesive β-Tm gene ends (0.2 µg) into the *Nde*I/ *Bam*HI restricted pJC20 vector (0.1 µg) was catalysed by 1 unit of the T4 DNA ligase enzyme in the manufacturer's supplied buffer at 4 °C overnight in a total volume of 20 µl.

2.2.2.4 Production of competent cells

Competent *E.coli* cells were prepared on the protocol described by Nishimura *et al* (1990). 50 ml of LB supplemented with 10 mM $MgSO_4$ and 0.2 % glucose was inoculated with 0.5 ml of a bacterial cell starter culture. The resulting culture was incubated at 37 °C until its optical density (OD_{600nm}) was between 0.6-1.0. The cells were then kept on ice for 10 minutes and pelleted down at 1, 500 g for 10 minutes at 4 °C. The pellet was gently resuspended with 0.5 ml of the pre-chilled supplemented LB buffer. 2.5 ml of storage buffer (36 % glycerin, 12 % polyethylene glycol, 12 mM $MgSO_4$ $7H_2O$ added to LB and sterilised by filtration) was added and mixed well. Aliquots of 100 µl were stored at –80 °C until use.

2.2.2.5 Transformation into XL1 Blue bacterial cells

Competent XL1 Blue cells (section 2.2.2.4) were transformed with the pJC20 vector containing the β-Tm gene in order to screen for positive clones and amplify the vector.

Transformation was performed as follows: 100 µl of competent XL1 Blue bacterial cells were thawed on ice. 5 µl of the ligation mix (section 2.2.2.3) was added to the competent cells and the mixture was stirred gently. The cells were incubated on ice for 30 minutes and then heat shocked at 42 °C for 2 minutes. This was followed by a 2 minute incubation on ice. LB was added to a final volume of 1 ml and the mixture was incubated for 1 hour at 37 °C. The cell culture was mixed and 100 µl was plated onto an ampicillin plate. The plates were incubated at 37 °C overnight.

2.2.2.6 Plasmid DNA amplification and purification

Single colonies from the transformed XL1 Blue plates (section 2.2.2.5) were used to inoculate 3 ml LB supplemented with 100 µg/ml of ampicillin. The cultures were incubated with shaking at 37 °C overnight. The plasmids from each cell culture were purified using DNA mini-prep kit as instructed by the manufacturer. 1 µl of each DNA plasmid preparation was run out on an agarose gel to determine concentration. The plasmid was then stored at -20 °C.

2.2.2.7 Restriction digest screening for positive clones

Restriction digests were set up as described in section 2.2.2.2. The presence of insert (864 base pairs) was verified by running agarose gel electrophoresis.

2.2.2.8 DNA sequencing

β-Tm DNA sequencing was performed by MWG-Biotech. The β-Tm fragment cloned in the pJC20 vector was sequenced both forward and backward. In that way, the full-length sequence was confirmed. For that purpose, primers corresponding to the vector T7 promoter sequence and the transcription terminator sequence were used. The sequences of which are shown below

T7 sequencing primer:

5'-GGTTTC CTC TAG AAT ATT TTG TTT ACT TTACG**AAGGAG**A**TATA**-3'

Shine -Delgarno TATA box

Transcription terminator sequencing primer:

5'-CTCAGCTTCCTTTCGGGC-3'

2.2.3 Recombinant tropomyosin expression and purification

The following recombinant Tm molecules: rat sk β-Tm (n3), and the rabbit/human sk α-Tm (n3) both WT and containing cardiomyopathy mutations D175N and E180G (cloning performed by Dr Robin Maytum) were expressed as described below.

2.2.3.1 Transformation into BL21 bacterial cells for protein expression

The *E.coli* bacterial strain BL21 was used for the β-Tm protein expression. These cells were made competent as described in section 2.2.2.4 and were transformed with 1 μl pJC20 vector as described in section 2.2.2.5.

2.2.3.2 Small-scale protein expression

Small-scale protein expressions were carried out in order to identify the BL21 clones that express the protein of interest.

Single colonies were inoculated into 3 ml of LB containing 100 μg/ml of ampicillin. The cultres were incubated for about 4 hours (until the optical density OD_{600} of the culture was between 0.6 and 1) at 37 °C with shaking. The cells were then induced by adding 0.4 mM isopropyl β-D-thiogalactopyranoside (IPTG). Prior to that, 0.5 ml of each cell culture was transferred into a fresh tube and was used as a control sample. Both the IPTG-induced and non-induced samples were incubated at 37 °C for 3-4 hours. Positive clones were identified by running SDS gel electrophoresis of 0.5 ml cultures. These were centrifuged and the resulting pellets were resuspended in 50 μl water and 10 μl sample buffer. 5 μl of each sample was run on a 12 % SDS gel. The appearance of a large protein band of correct size (33, 000 Da) indicated successful expression of the protein of interest.

2.2.3.3 Large-scale protein expression and purification

Clones containing the gene of interest were inoculated into 1 l flask containing LB-Amp media (100 mg of Amp) for large-scale protein expression. IPTG was added when the OD_{600nm} of the culture was between 0.6 and 1. This was followed by a 3 hour incubation at 37 °C with continuous shaking. The bacterial cells were then harvested by centrifugation at 6, 500 g for 15 minutes. The pellet was resuspended and homogenised in lysis buffer (20 mM TRIS, 150 mM NaCl, 1 mM $MgCl_2$ pH 7.5). Cell free lystates

were then produced by sonication (2 minute pulse, 2 minute rest and 2 minute pulse) Unlike many other proteins, tropomyosin is a heat-stable protein that is reversibly denatured if the temperature is increased up to 80 °C. The samples were therefore heated up to 80 °C for 10 minutes resulting in the irreversible denaturation of most of the bacterial proteins without affecting the structure and function of Tm. The solution was then placed on ice and allowed to cool down. Both RNAse and DNase enzymes were added (2 units ml-1) and incubated for about 1 hour. This was followed by a centrifugation step at 12, 000 g for 15 minutes to remove cell debris and precipitated proteins. The supernatant was then taken through a pH cut to 4.6 in order to precipitate the Tm. The protein was recovered in the pellet by centrifugation at 27, 000 g for 15 minutes and was resuspended in 5 mM PO_4 pH 7.0, 100 mM NaCl. The pH of the Tm solution was measured and readjusted to 7.0. The final purification of Tm was carried out using an ion exchange chromatography column (HiTrap 5 ml Q, Pharmacia product). The protein was eluted using a 0.1-1 M NaCl gradient (Figure 2.3). The protein-containing fractions were pooled together and pH cut to 4.6. This was followed by a centrifugation step at 27, 000 g for 15 minutes to recover the precipitated Tm. The Tm was then resuspended and dialysed against storage buffer (10 mM KCl, 10 mM MOPS, 1 mM EDTA, 0.2 mM DTT, 1 % sucrose pH 7.5). The resulting purified Tm was stored at –20 °C.

Protein concentrations were determined using an extinction coefficient (ε = 0.276 mg^{-1} ml cm^{-1}, and Mwt of 65, 679.6 Da for sk α-Tm (n3), 65, 677.6 Da for sk α-Tm D175N (n3), 65, 535.4 Da for sk α-Tm E180G (n3) and 65, 991.6 Da for sk β-Tm (n3).

a

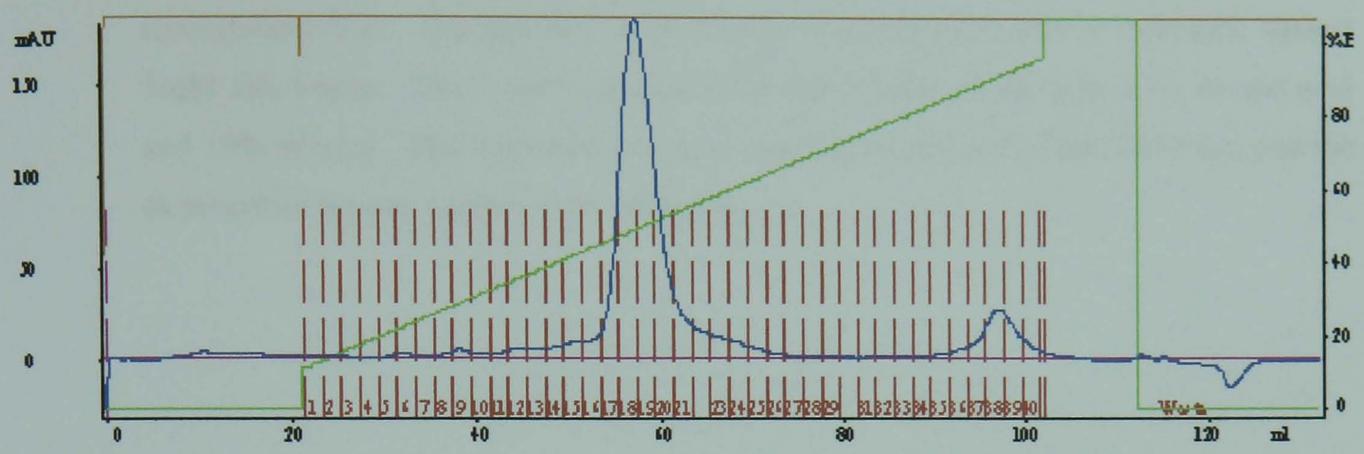

b

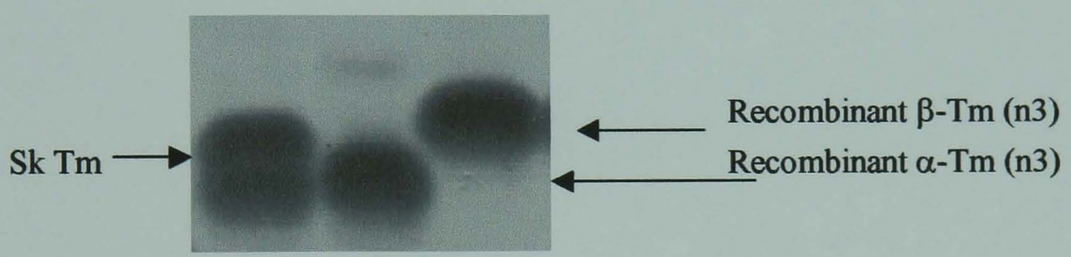

Figure 2.3: a) Elution profile of recombinant β-Tm (n3). The peaks represent the 280nm absorbance of the proteins eluting from the column. As most proteins are denatured during the 80 °C heating step, the Tm peak is the main one obtained during the ion-exchange chromatography step. The salt gradient is shown in green. **b) SDS-gel of α- and β-Tm (n3).** The samples were run on a 12 % SDS gel. The proteins molecular weights are 33, 000 and 32, 000 Da for β- and α-Tm respectively.

2.2.4 Mass spectrometry

Electrospray mass spectrometry was used to determine the molecular mass of expressed recombinant Tm. The protein samples were prepared by dialysing overnight against 5mM Tris buffer. The protein samples were then diluted 10 times in 0.1% formic acid and 10% ethanol. The mass spectrometry was performed by Dr Robin Maytum and the expected molecular weights were obtained.

CHAPTER 3

TECHNIQUES AND ANAYTICAL PROCEDURES

This chapter aims at introducing the techniques as well as the analytical methods applied in the study presented in this thesis.

1 Measurement of tropomyosin binding affinity for actin using co-sedimentation experiments and densitometry analyses

1.1 Co-sedimentation experiment

When actin is polymerised (F-actin form), it can be pelleted by centrifugation at 100, 000 g (Beckman TLA100A). Therefore, any protein that would normally remain in the supernatant will pellet when bound to actin. The concentration of bound and free protein can be deduced by adding increasing concentrations of the protein of interest to a fixed actin concentration, and then checking the content of both the pellets and the supernatants on as SDS-PAGE gel.

On this basis, the binding of different Tms to actin was investigated by co-sedimentation experiments. These were designed as follows: 0.2, 0.5, 1, 1.5, 2 and 3 μM of Tm were added to a fixed 10 μM actin concentration. The appropriate experimental buffer (20 mM MOPS pH 7.0, 5 mM $MgCl_2$ and 100-200 mM KCl) was added to reach a total volume of 100 μl. The samples were well mixed and were then incubated at room temperature for at least 1 hour. The samples were then spun at 100, 000 g for 20 minutes at 20 °C. The supernatants were transferred into fresh tubes and the pellets were resuspended with 100 μl dH_2O. 20 μl and 10 μl of sample buffer were added to the 100 μl pellet and 50 μl supernatant samples respectively. 12 μl of each sample was loaded on a 12.5 % SDS-gel (see chapter 2, section 1.2.1) (Figure 3.1).

1.2 Densitometry

The binding constants of Tm to actin were obtained from cooperative binding curves generated by combining co-sedimentation experiments with densitometry analyses. The stained gels (Coomassie Blue G250) from the co-sedimentation experiment were scanned with an Epson 1640 SU scanner and the obtained images were analysed using the Image-PC program (Scion Corp. based upon NIH-Image). The density of protein bands was measured by comparison to integrated optical densities (the scanner was

calibrated using a Kodak neutral density step tablet). A standard curve plotting the densities of Tm against known concentrations was used to work out the free Tm concentration in the supernatant (Figure 3.2). Both the dissociation binding constant ($K_{50\,\%}$) and the Hill coefficient (*m*) parameters were determined by plotting the ratio of Tm bound to actin (ratio of the two protein band densities) as a function of free Tm concentrations (Figure 3.3). The data was fitted to a Hill equation using Origin 6.0 software (see appendix, equation 1.1.3).

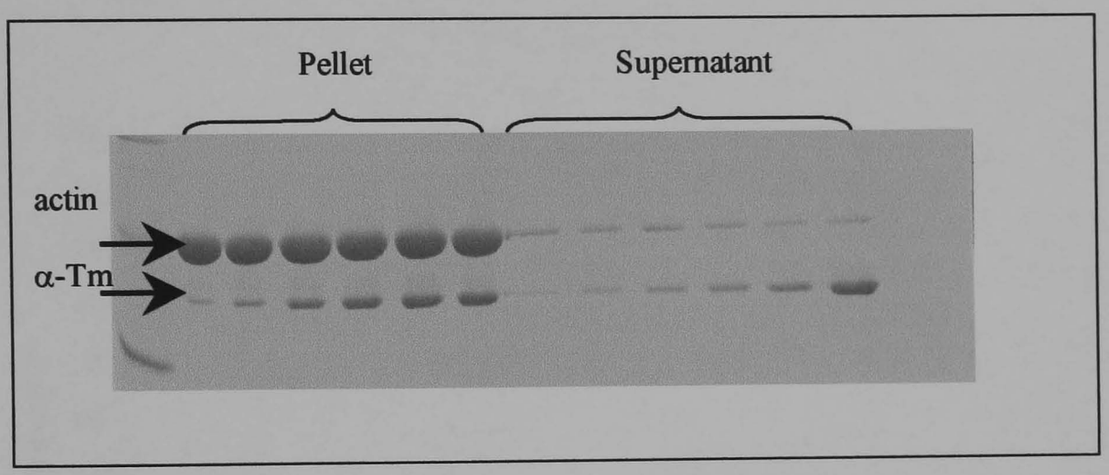

Figure 3.1: A co-sedimentation binding gel. 0.2, 0.5, 1, 1.5, 2 and 3 μM (left to right) of recombinant α-Tm (n3) were added to 10 μM actin. The experimental buffer was 20 mM MOPS, 100 mM KCl, 5 mM $MgCl_2$ pH 7.0.

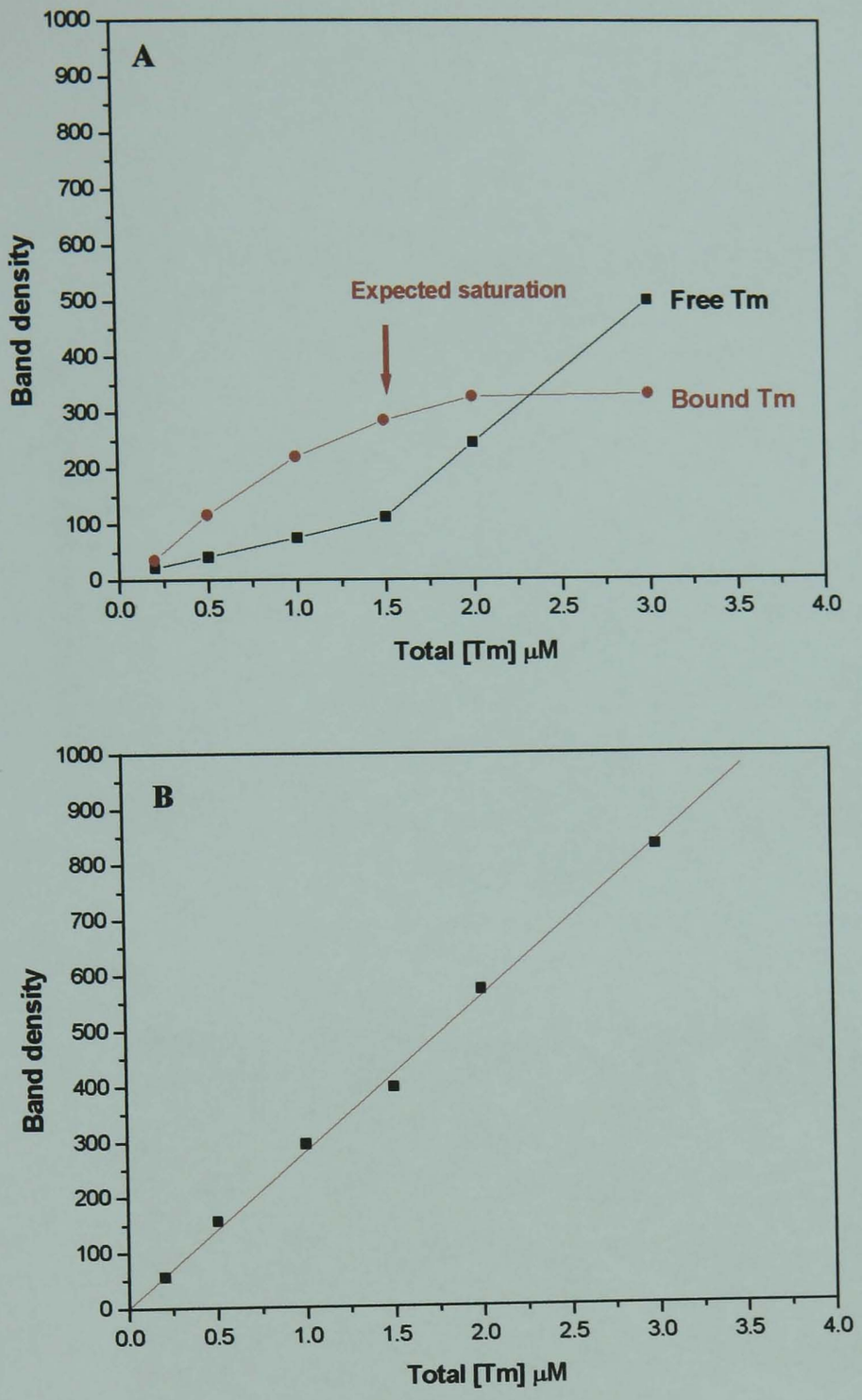

Figure 3.2: **(A)** graph representing the distribution of Tm in pellet (bound to actin) and supernatant (free) as a function of total Tm added to 10 μM actin. Saturation of actin occurs at stoichiometric concentration of about 1.5 μM as one Tm molecule binds every seven actins. **(B)** Tm calibration curve. The band density of known Tm concentrations was plotted against the corresponding concentrations. This allowed the deduction of the bound and free Tm concentrations.

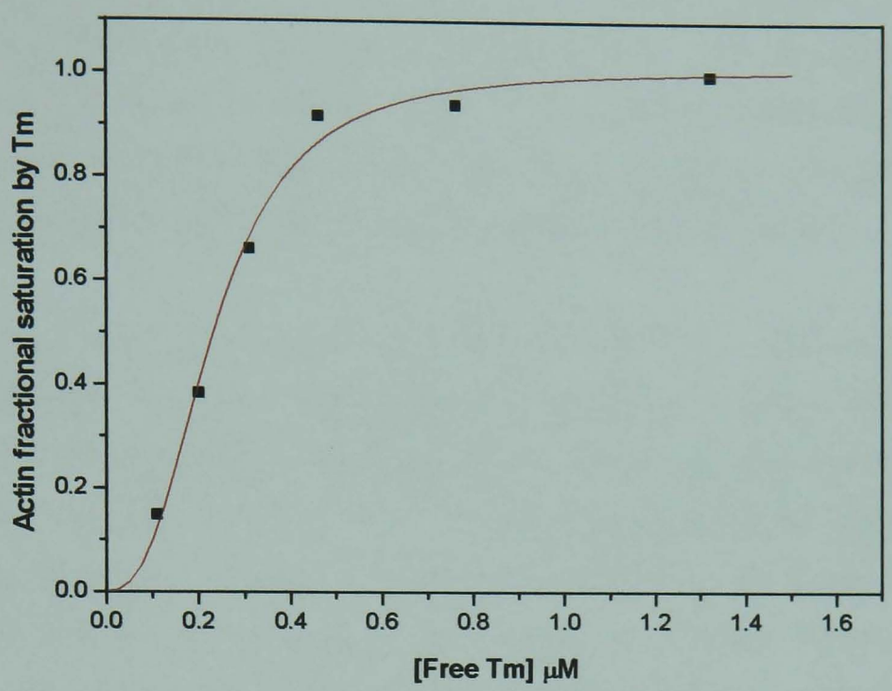

Figure 3.3: Binding curve of α-tropomyosin to actin. Actin fractional saturation by Tm (ratio of bound Tm band density and actin band density) is plotted as a function of free Tm (supernatant Tm) concentrations. The experimental conditions are detailed in the text. The sigmoid curve reflecting the cooperative binding of Tm to actin was fitted to a version of the Hill equation. Both the Hill coefficient *m* and the midpoint of the sigmoid curve $K_{50\%}$ were determined. The data was normalised to 1.0 by dividing Tm:actin ratio from densitometry by the Tm:actin ratio for saturating stoichiometric binding.

2 Kinetic measurements using the stopped-flow technique

2.1 The stopped-flow machine

The stopped-flow (SF) spectrophotometry technique enables the monitoring of fast reactions that occur at the millisecond time scale. The principle of this technique consists in the use of light scattering or fluorescence to measure the association or dissociation rates of a given reaction. It relies on a rapid mixing method and a suitable detection system that allows the reaction to be followed in real time.

The stopped flow instrument is represented in Figure 3.4. The instrument used for our experiments was a Hi-Tech Scientific Ltd (Salisbury, England) SF-51 apparatus. It consists of a rapid mixing system made up of two separated compartments in which the reactant solutions are placed. The solutions are pushed into the mixing chamber by air-compressed pressure driven pistons. The system is equipped with Teflon valves that control the direction of the flow into the right compartment. Once in the observation cell, the solution is excited with UV light produced by a Xenon/Mercury lamp (Hamamatsu 100-W). The desired wavelength is selected for by a monochromator (Photon Technology International LP S-20). The observation cell is designed in a way that allows the incident light to pass into one surface, and the emitted light, detected by a photomultiplier, to be monitored at 90°. A cut-off filter (KV 389 nm) is used in order to resolve the fluorescence emission from the scattered excitation light. The back syringe acts as a stopping device by hitting a metal block when a fresh solution flows into the observation chamber and pushes the old solution out. At this moment, the time resolved fluorescence recording is triggered and the obtained curves are visualised and analysed by computer using the software provided by Hi-Tech. The rate of the reaction is obtained by curve fitting the average of at least three consecutive data sets. The system is temperature-controlled by an external water bath and all the experiments described were carried out at 20 °C.

Equal volumes of the reactants are mixed each time and therefore half the initial concentrations are present in the reaction mixture. All the concentrations in the text refer to those in the mixing chamber of the instrument (for a review on SF spectroscopy, see Eccleston, 1991).

In all our experiments, we monitered the change of Pyrene fluorescence (actin is labelled with the pyrene fluorophore (365 nm excitation, 380 nm emission) at Cys 374 (see chapter 2, section 1.2.5). Binding of S1 to actin causes 70% quenching of pyrene fluorescence (Criddle *et al*, 1985).

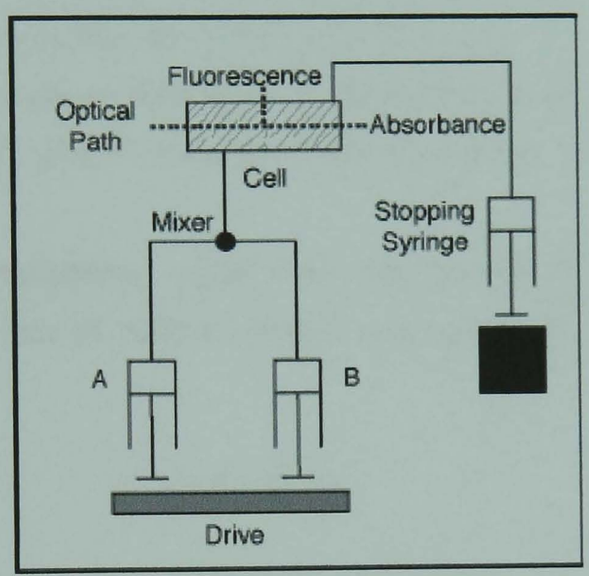

Figure 3.4: Schematic representation of the stopped-flow apparatus. (http://www.hi-techsci.co.uk/scientific/stoppedflow.html

2.2 Transient kinetic principles

In order to understand the data obtained from a SF experiment, one needs to consider the kinetics that describe the reaction under investigation. The following equations are of relevance for the study of binding reactions.

First order reactions: defines a reaction whose rate or velocity (rate of reactant disappearance or rate of product appearance measured in $M.s^{-1}$) is proportional to the first power of the reactant concentration.

$$A \xrightarrow{k} B$$

The rate of the reaction is proportional to the concentration of A at time t.

Rate of reaction = $d[B]_{(t)} / dt = -d[A]_{(t)} / dt = k\,[A]_{(t)}$

Integration of the above equation gives the following single exponential:

$[A]_{(t)} = [A]_0\, e^{-kt}$, where k is the first order rate constant of the reaction (s^{-1}).

Second order reactions: occur when two reactants come together to give rise to a product. The rate of such a reaction is proportional to the concentration of both reactants.

$$A + B \xrightarrow{k} C$$

Rate of reaction = $d[C]_{(t)} / dt = k\,[A]_{(t)}\,[B]_{(t)}$

However, considering the complexity of the analysis of the above equation, second order reactions are best studies under pseudo-first order conditions.

Pseudo-first order reactions: are described when the concentration of one of the reactants is in a great excess compared to the other so that it remains effectively constant over the course of the reaction.

$$A + B \xrightarrow{k} C$$

Rate of reaction = $d[C]_{(t)} / dt = k [A]_{(t)} [B]_{(t)}$, where k is the second order rate constant. Since [A] >>> [B] then, $[A]_{(t)} \cong [A]_0$. This gives rise to a new constant termed observed rate constant k_{obs} where $k_{obs} = k [A]_0$.

On integration, the following single exponential equation is obtained

$[B]_{(t)} = [B]_0 e^{-k_{obs} t}$, the k_{obs} (s^{-1}) is a linear function of [A].

2.3 Experimental conditions

In all the SF experiments we monitored the binding of S1 to pyrene-actin. For this purpose, the concentration of either actin or S1 was in 10-fold excess compared to the other (10 μM vs. 1μM or 5μM vs. 0.5 μM syringe concentrations). The experimental buffer used was 20mM MOPS, 140 mM KCl, 5mM $MgCl_2$ pH 7.0. 1 mM DTT was added to the buffer when Tn was present in the solution. The k_{obs} value of the binding reaction shows a linear dependence on the concentration of the reactant which is in excess. The buffer's ionic strength will also affect the k_{obs} value.

2.3.1 Excess actin case:

$$A + S1 \xrightarrow{k} A.S1$$

[A] >>> [S1]

The rate of the reaction: $-d[S1]_{(t)} / dt = k [A]_{(t)} [S1]_{(t)}$

Integration of the above equation predicts an exponential decrease in [S1]

$[S1]_{(t)} = [S1]_0 e^{(-k_{obs}t)}$ where $k_{obs} = k [A]_0$

Under these conditions, few actin sites will be occupied by S1 (one or less S1 every one actin structural unit). Therefore, the observed rate constant is that of the first S1 molecule that binds to actin and is dependent on the actin concentration available for S1 binding (actin sites in the ON state).

2.3.2 Excess S1 case:

As described above, when [S1] >>> [A], $[A]_{(t)} = [A]_0 e^{(-k_{obs}t)}$ where $k_{obs} = k [S1]_0$

Under these conditions, S1 will occupy all the sites on actin. The initial binding of S1 is restricted by the number of actin sites available for binding. So, if a fraction of actin

sites is in the OFF state, a lag phase is obtained. As more S1 heads bind to actin, the filament is turned into the ON state allowing faster S1 binding. The rate of the fast binding follows a single exponential described by the above equation.

2.4 Measurement of the calcium sensitivity of the thin filament complex

2.4.1 Calcium-dependence of S1 binding to actin:

The binding of S1 to the thin filament is a Ca^{2+}-dependent reaction. In the case of excess actin over S1, a 3-fold decrease in k_{obs} value is observed on Ca^{2+}- removal (see Figure 3.5).

This decrease in the S1 binding observed rate constant is explained by a 3-fold decrease in the fraction of actin sites available for binding.

Assuming that actin exists between two states ON (that can bind S1) and OFF that cannot bind S1 with the equilibrium between the two defined by K_B.

$$A_{OFF} \xleftrightarrow{K_B} A_{ON}$$

$K_B = [A_{ON}] / [A_{OFF}]$

The fraction of actin sites in the ON state is $[A_{ON}] / [A_0]$, where $[A_0] = [A_{ON}] + [A_{OFF}]$

Therefore: $[A_{ON}] / [A_0] = K_B [A_{OFF}] / ([A_{ON}] + [A_{OFF}])$

$[A_{ON}] / [A_0] = K_B / (K_B + 1)$

$[A_{ON}] = [A_0] K_B / (K_B + 1)$

Since S1 only binds to actin in the ON state.

$$A_{ON} + S1 \xrightarrow{k} A.S1$$

The rate of the reaction $-d[S1] / dt = [S1] [A_{ON}] k$, where $k_{obs} = [A_{ON}] k$

Therefore: $k_{obs} = [A]_0 K_B / (K_B + 1)k$

The fact that $k_{obs}(Ca^{2+})/k_{obs}(-Ca^{2+}) = 3$ is explained by a 3-fold decrease in the fraction of actin sites available for S1 binding. In other words $K_B / (K_B + 1) = 0.3$, giving K_B a value of about 0.42 in the absence of Ca^{2+}. In the presence of Ca^{2+}, the k_{obs} value is similar to

that obtained for S1 binding to actin alone suggesting that all the actin sites are available for S1 binding. The K_B value in the presence of Ca^{2+} is therefore at least 10.

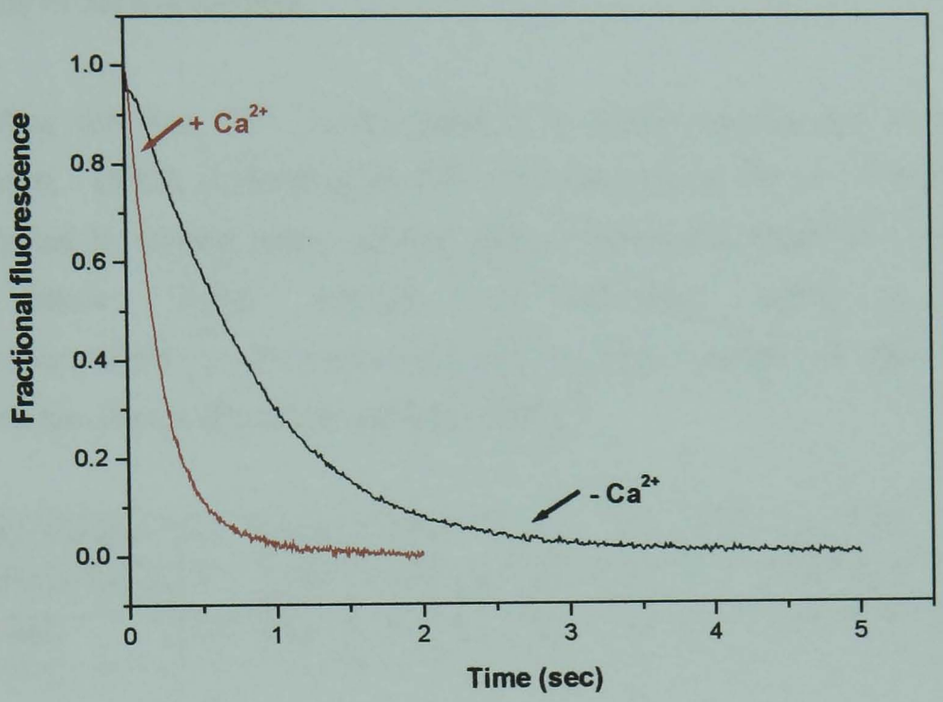

Figure 3.5: Effect of Ca^{2+} on the observed rate constant of S1 binding to actin. Stopped-flow transients for S1 (0.25 μM) binding to Pyrene-actin (2.5 μM) in the presence of control protein complex (1 μM) both in the presence and absence of Ca^{2+}. Fractional fluorescence values (F_{frac}) were calculated using the formula $(F-F_{final})/(F_{initial}-F_{final})$.

2.4.2 The generation of calcium sensitivity curves:

Measuring the rate of S1 binding to actin as a function of Ca^{2+} concentrations or pCa (pCa = -log [Ca^{2+}]) gives an indication on the Ca^{2+} sensitivity of the system. It is therefore a good assay for looking at the effect of different control protein isoforms as well as the effect of mutations that arise in the regulatory proteins on the Ca^{2+} sensitivity of the thin filament.

Controlling the free Ca^{2+} concentration is a crucial requirement in this type of experiment. This is achieved using Ca^{2+} chelators such as EGTA. The pCa solutions are obtained by mixing given volumes (ml) of EGTA and CaEGTA as shown in the table below. These volumes are calculated using a programme (http://www.stanford.edu/~cpatton/webmaxclitel15.htm) where all the Ca^{2+}-binding constants are entered (Harrison and Bers, 1987).

[EGTA] (100 mM)	0	0.05	0.075	0.12	0.2	0.3	0.4	0.6	1.0	1.5	2
[CaEGTA] (100 mM)	2	1.95	1.925	0.88	1.8	1.7	1.6	1.4	1.0	0.9	0
pCa (2 mM)	4.6	5.0	5.2	5.4	5.6	5.8	6.0	6.2	6.6	7.0	8.9

Ca^{2+}-sensitivity curves are obtained by measuring the k_{obs} values for S1 binding to a regulated thin filament at different pCa values (Figure 3.6). The k_{obs} values are then plotted as a function of pCa as shown in figure 7. The sigmoid curve obtained is fitted with a Hill equation (see appendix, equation 1.1.4) and both the midpoint of the curve ($K_{50\%}$) and the Hill coefficient (h) are derived. A shift in the $K_{50\%}$ value is an indication of a change in the Ca^{2+}-sensitivity (Figure 3.7). The h value is a measure of the cooperativity of the system and is about 1.8 in the case of skeletal Tn and 1.2 in the case of cardiac Tn (see chapter 1, section 3).

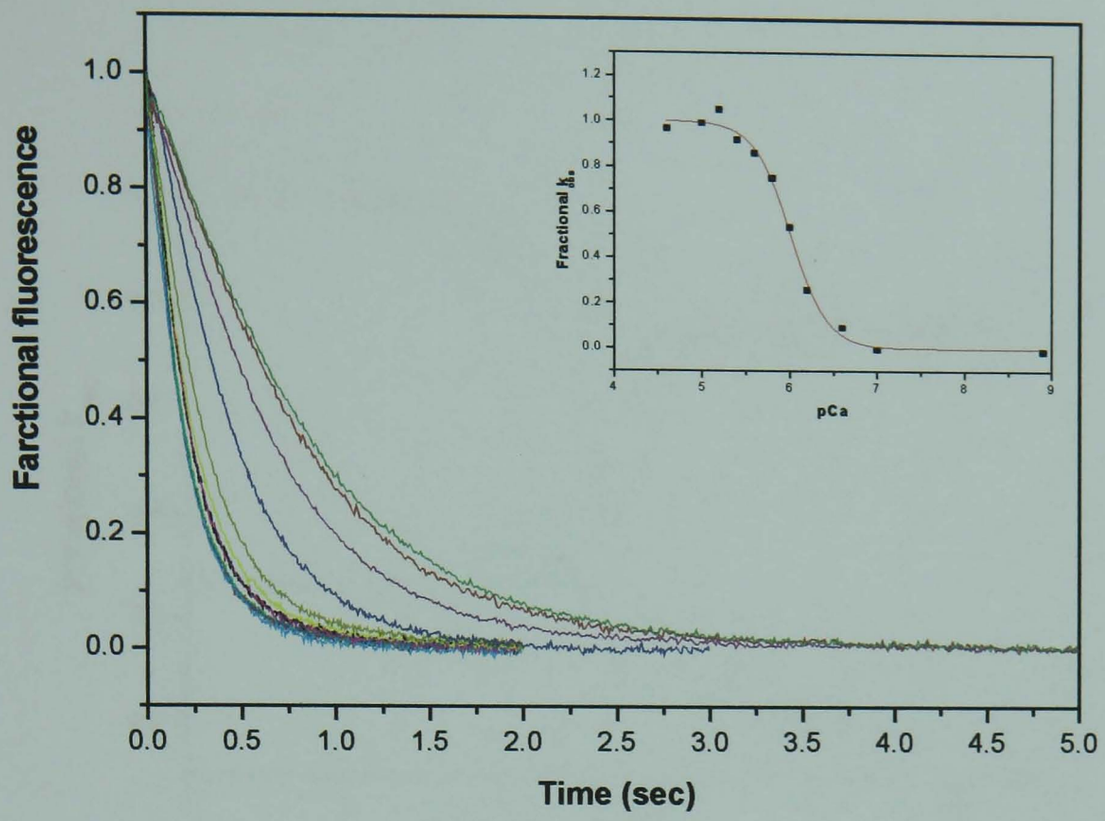

pCa	4.6	5	5.2	5.4	5.6	5.8	6.0	6.2	6.6	7.0	8.9
k_{obs} (sec^{-1})	5.30	5.40	5.65	5.10	4.85	4.40	3.50	2.35	1.65	1.25	1.22

Figure 3.6: Stopped-flow transients for S1 binding to pyrene-actin in the presence of regulatory proteins. S1 binding, monitored by fluorescence quenching, was recorded at different Ca^{2+} concentrations or pCa (pCa = -log[Ca^{2+}]). The observed rate of binding (k_{obs}) is Ca^{2+}-dependent and decreases as Ca^{2+} concentration is lowered. The raw k_{obs} values, obtained from fitting the transients to a single exponential, are shown in the above table. Experiment conditions were as follows: protein concentrations were 2.5 μM Pyrene-actin, 1 μM regulatory proteins pushed against 0.25 μM S1. The buffer used was 20 mM MOPS, 140 mM KCl, 5 mM $MgCl_2$, 1 mM DTT, pH 7.0. Fractional fluorescence values (F_{frac}) were calculated using the formula $(F-F_{final})/(F_{initial}-F_{final})$.

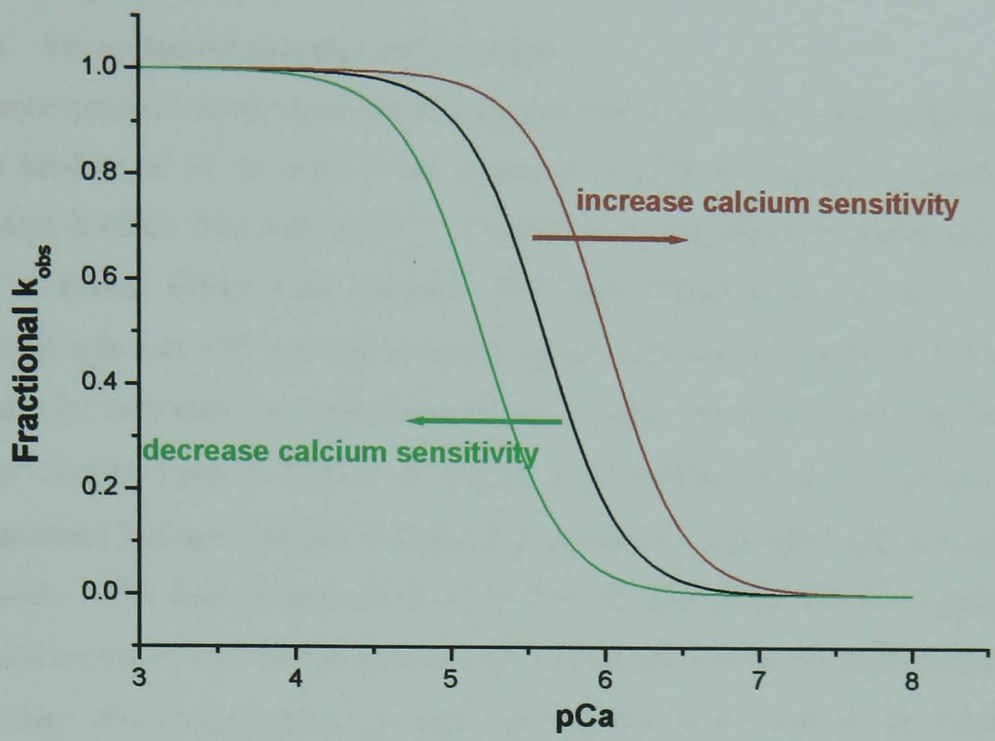

Figure 3.7: Simulation of a Ca^{2+} sensitivity curve for S1 binding to pyrene-actin in the presence of regulatory proteins. Ca^{2+}-sensitivity curves are obtained by plotting the k_{obs} values (see figure 3.6 legend) as a function of pCa. The sigmoid curve is fitted to a version of the Hill equation and both the $K_{50\%}$ (midpoint of the curve) and the *h* (Hill coefficient) values are obtained. A shift in the $K_{50\%}$ is indicative of a change in the Ca^{2+}-sensitivity of the system. The *h* value is a measure of the degree of cooperativity and is defined by the slope at the midpoint. The *h* value used for this simulation was 1.8 and the $K_{50\%}$ values were 5.2 (green), 5.6 (black) and 6.0 (red).

3 Steady-state measurements using fluorescence titration experiments

3.1 Fluorescence titration experiments

Fluorescence titration experiments were performed in order to define the parameters for the binding of S1 to actin in the presence of different regulatory proteins when the system is either fully ON or OFF. Fluorescence titration experiments were carried out on a Perkin Elmer Life Sciences 50B spectrofluorimeter at 20 °C. Excitation wavelength was 365 nm and emission wavelength was measured at 405 nm. The slit width for both excitation and emission was 15 nm. The S1 (10 μM stock concentration) was titrated from a 100 μl Hamilton glass syringe by a syringe pump (Harvard Apparatus Syringe Infusion Pump 22) at a rate of 12 μl min^{-1} into a constantly stirred cuvette. The latter contained 2 ml of 50 nM phalloidin- stabilised pyrene-actin and 2 μM excess of Tm. When titrations were performed in the presence of both Tn and Tm proteins, the concentration of each was reduced to 0.2 μM as the whole regulatory protein complex has a much higher affinity for actin as compared to Tm alone (Wenger and Walsh, 1981; Heald and Hitchcock-DeGregori, 1988). The experimental buffer used was 20 mM MOPS pH 7.0, 5 mM $MgCl_2$, 200 mM KCl (1 mM DTT was added to the buffer when Tn was present in the mixture). Binding of S1 to actin causes 70% quenching of the pyrene fluorescence. Therefore, the change in fluorescence gives a measure of the proportion of actin bound to S1. The fluorescence recording was triggered using a contact switch attached to the syringe drive-plate and connected to the TTL trigger input of the fluorimeter. The titrations were carried out for a period of 250 s^{-1} and data points were collected every 0.5 s^{-1}. The software Scientist was used for the plotting and fitting of the obtained fluorescence curves. These were fitted to the three-state model equation or to a two-state version of that equation when only Tm is bound to actin (see appendix, equations 1.2.2 and 1.2.3).

Fitting data is achieved by a systematic fitting procedure where the parameters are defined and only few of them are allowed to vary (K_T, K_1). The best fit is that with the lowest standard deviation value from the fit as the *n* value is varied from 5 to 12.

3.2 Steady-state kinetics

3.2.1 Equilibrium binding reactions

S1 binding to actin can be represented by the following reaction

$$A + S1 \xleftrightarrow{K_d} A.S1$$

The dissociation constant of the reaction K_d = [S1][A]/[A.S1], where [S1], [A] and [A.S1] are concentrations of reactants and product at equilibrium.

$K_d = 1/K_{ass}$ (K_{as} is the equilibrium association constant) and has units of concentration (M).

Since $K_d/[S1] = [A]/[A.S1]$, then K_d represents the equilibrium S1 concentration at which the concentration of free actin equals that of actin.S1 complex i.e. when 50 % of actin is bound to S1.

Since $[A]_0 = [A] + [A.S1]$ and $[S1]_0 = [S1] + [A.S1]$

Then $K_d = ([A]_0 - [A.S1])([S1]_0 - [A.S1]) / [A.S1]$, and the following quadratic equation can be derived

$[A.S1]^2 - [AS1]([A]_0 + [S1]_0 + K_d) + [A]_0[S1]_0 = 0$

For the equation:

$ax^2 + bx + c = 0$

$$x = \left(-b \pm \sqrt{b^2 - 4ac}\right)/2a$$

In this case, x or [A.S1], is the concentration of actin.S1 complex at equilibrium.

$$x = \frac{([A]_0 + [S1]_0 + K_d) \pm \sqrt{([A]_0 + [S1]_0 + K_d)^2 - 4[A]_0[S1]_0}}{2}$$

α the fractional saturation is the fraction of actin that binds to S1. $\alpha = [A.S1]/[A]_0$

Therefore,

$$\alpha = \frac{([A]_0 + [S1]_0 + K_d) \pm \sqrt{([A]_0 + [S1]_0 + K_d)^2 - 4[A]_0[S1]_0}}{2[A]_0}$$

α is proportional to the quenching of pyrene fluorescence as S1 binding to actin causes fluorescence change (see Figure 3.8).

Therefore α = Bound actin/total actin = $(F_0\text{-}F)/(F_0\text{-}F_\infty)$

$F = F_0\text{-}\alpha\ (F_0\text{-}F_\infty)$

$$F = F_0\left[\frac{([A]_0 + [S1]_0 + K_d) \pm \sqrt{([A]_0 + [S1]_0 + K_d)^2 - 4[A]_0[S1]_0}}{2[A]_0}(F_0 - F_\infty)\right]$$

3.2.2 Experimental conditions

The concentration of actin (50 nM) was in the range of the K_d for S1 binding to actin. This allowed the observation of hyperbolic binding curves from which the different binding isotherms were derived (see appendix, equation 1.2.1). The titration of a total of 250 nM S1 (5 times the actin concentration) should saturate the actin filament.

The system was shown to be in equilibrium as stopping the S1 titration was followed by no further fluorescence quenching (Maytum *et al*, 1999).

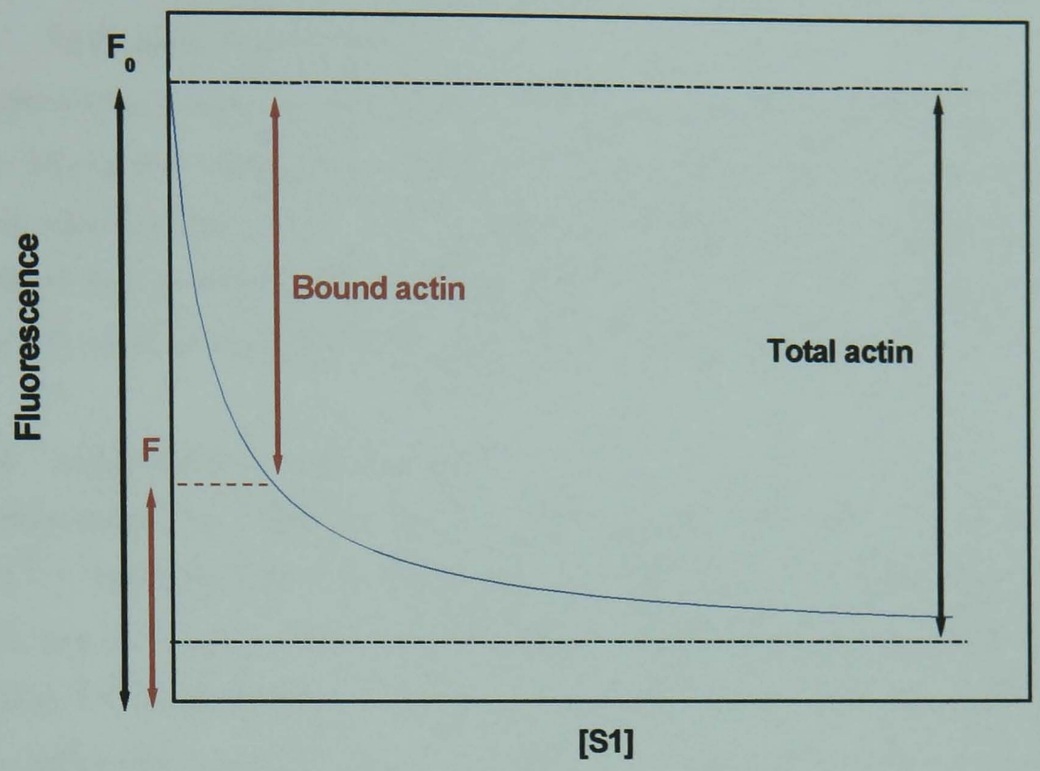

Figure 3.8: A simulation of the change in pyrene fluorescence (F) as a function of S1 concentrations. The quenching of pyrene fluorescence is proportional to the formation of the actin.S1 complex. The fractional saturation ($[A.S1]/[A]_0$) is therefore proportional to the fluorescence quenching and can be represented as $(F_0-F)/(F_0-F_\infty)$.

4 Measurement of protein thermal stability using Differential Scanning Calorimetry

Differerential Scanning Calorimetry (DSC) is a very useful technique for investigating the thermal unfolding of protein domains or subdomains either isolated or in complex with other proteins (Freire, 1995; Privalov and Privalov, 2000). In this work, we used DSC to look at the effect of cardiomyopathy mutations expressed in tropomyosin on the stability of the protein both in the presence and absence of actin.

4.1 Experimental conditions

Tropomyosin was dialysed into the following experimental buffer 20 mM Hepes, pH 7.3, 100 mM KCl, 2.5 mM $MgCl_2$. Measurements were performed both in the presence and absence of 1 mM β-mercaptoethanol as the state of oxidation/reduction affects Tm thermal stability. Phalloidin-stabilised actin was used each time as it shifted the actin melting transition by 20 °C above the Tm melting transition. In all cases, actin concentration was 46.7 μM but Tm concentrations varied depending on the experiment. The DSC apparatus used was a differential adiabatic scanning microcalorimeter DASM-4M (Institute of Biological Instrumentation, Pushchino, Russia) with scanning performed at a constant pressure of 152 kPa and a heating rate of 1°C $minute^{-1}$. The traces obtained are analysed and plotted using Origin software package.

The reversibility of Tm unfolding was assessed by heating up to 65 °C to achieve full denaturation, then cooling the sample down and scanning again. The protein unfolding is said to be reversible if similar transitions are reproduced (similar melting temperatures and amplitudes). Performing two heating scans also allows the reduction of Tm disulfide bonds. The first heating scan will result in the denaturation of the two Tm chains, facilitating the accessibility of the reducing agent (β-mercaptoethanol in this case) to the cysteine residues which allows the protein to be fully reduced.

4.2 The DSC technique

Protein unfolding is a heat driven reaction, the heat energy input of the system increases when the specific protein melting temperature is reached. DSC is therefore a useful

method, not only for providing an insight into protein melting temperatures, but also information concerning thermodynamic changes associated with such a process.

DSC is a calorimetric method that allows the measurement of the heat capacity (Cp) of the system of interest. In other words, it allows the investigation of the change in the amount of heat energy (μW) as a function of temperature (°C). Hence the name scanning microcalorimeter as, it continuously heats the calorimetric cell at a constant rate and measures the heat capacity over a range of temperatures. Scanning calorimeters are differential instruments as they measure the difference in heat capacity between two identical cells which only differ in their protein content. One of the cells is loaded with the protein-containing solution whereas the other one contains the buffer in which the protein is found. The difference between the two heat capacities should correspond to the protein's heat capacity. This is achieved by sustaining the same temperature in both cells and monitoring the difference in power produced by the electrical heater. The difference between the power output of the two cells is recorded over a range of temperatures.

The cells are filled with liquid through two capillary inlets and they are thermally isolated from the surroundings to avoid heat loss by thermal shells providing adiabatic conditions. Once the cells are filled with the liquid, a small constant pressure is applied in order to exclude the presence of any bubbles in the cell which might interfere with the recording of the traces. The constant pressure also decreases the boiling temperature of the solution.

CHAPTER 4

BACTERIALLY EXPRESSED STRIATED TROPOMYOSIN ISOFORMS

1 Introduction

1.1 N-terminal acetylation of tropomyosin

Most proteins expressed in eukaryotic cells undergo a number of co- and post-translational modifications, one of which is acetylation of the amino terminal residue (Kendall *et al*, 1990). The full biological significance of such a process is still an open question but it is known that acetylation affects different proteins in different ways. In some cases, the loss of an acetyl group decreases the thermal stability of the protein, whereas in other cases it decreases the half-life of proteins by increasing their susceptibility to proteolytic degradation (Polevoda and Sherman, 2000).

Acetylation of the N-terminal methionine of tropomyosin is fundamental for the normal function of the protein. Tropomyosin expressed in bacteria and which does not undergo acetylation is characterised by impaired head to tail polymerisation, weaker actin binding and deficient inhibition of acto-myosin ATPase activity (Heald and Hitchcock-DeGregori, 1988). However, the expression of Tm with a fusion peptide upstream of the N-terminal methionine residue was reported to restore the native-like properties of the protein. Monteiro *et al* (1994) showed that Tm expressed with the dipeptide Ala-Ser fused to its N-terminal end had similar actin binding affinities, head to tail polymerisation, inhibition of acto-myosin ATPase and Ca^{2+} regulation properties as those of native, tissue purified Tm. Therefore, it was concluded that the Ala-Ser extension was a good substitute for the acetyl group as it restored all the functional properties of the protein.

A likely explanation for this finding can be drawn from the fact that the initiation methionine carries no net charge when blocked by acetylation and has a positive charge on its amino group when unacetylated. Since methionine occupies position *a* of the heptad, it is involved in making hydrophobic interactions which contribute to the formation of the hydrophobic core of the coiled-coil tropomyosin. The presence of two protonated amino groups at positions a and a' of the coiled-coil is likely to result in repulsive forces which could disrupt the local structure and result in molecule dysfunction. The presence of the fusion peptide neutralises that charge by forming the amide bond that would normally arise from acetylation. A crystal structure of a recombinant 81 residue N-domain fragment of Tm revealed a slight opening at the

unacetylated N-terminal end which has been shown to be fully helical in the native acetylated protein (Brown *et al*, 2000). This finding is consistent with the crucial role of acetylation for the normal functioning of Tm.

The ability to produce a modified recombinant Tm with native-like properties is a valuable tool as it would permit the expression of different Tm isoforms and introduce desired changes potentially useful for the investigation of structure/function relationship in Tm. In addition, it would allow the expression of Tm cardiomyopathy-causing mutations and examine the effect these have on the function of the molecule. Considering the subtle changes in regulation that would arise from small changes in the system, it is important to exclude the likelihood that the behaviour noticed is a consequence of differences between recombinant and native protein.

In order to validate the use of recombinant proteins, we expressed rabbit skeletal α-Tm with the Ala-Ser extension at the N-terminal end of the protein in *E-coli* (referred to in the text as recombinant αα Tm (n3), (see chapter 2, section 2.2.2.1). We also purified native α-Tm from rabbit skeletal muscle and we carried out a number of measurements to compare the behaviour of the two molecules. In this chapter, we determined the parameters described in the 3-state model of regulation (chapter 1, section 3.1) in each case using both transient kinetic and equilibrium measurements (described in chapter 3, sections 2 and 3). We also investigated the thermal stability of the two proteins using the DSC technique (chapter 3, section 4).

The results presented here will show that the recombinant protein is very similar to the native one and no significant differences in behaviour could be detected using our assays.

1.2 Striated tropomyosin isoforms

Skeletal Tm can be fractioned into two major isoforms, α and β, which were identified when running a preparation of rabbit skeletal Tm on acrylamide gel electrophoresis (Cummins and Perry, 1973). Sequence analysis revealed that the two isoforms had the same number of amino acids (284). Most of the amino acid differences (25 out of 39) are located at the C-terminal part of the protein where the troponin complex binds (see amino acid sequence comparison in Figure 4.1) (Mak *et al*, 1980). Most of the residue substitutions between the two isoforms are chemically similar and should not introduce major changes in the protein coiled coil structure. Investigating the frequency of residue substitution suggested that residues at position *a*, *d*, *e* and *g* which are crucial for the formation and the stabilisation of the coiled coil structure are more conserved than those responsible for making interactions with the solvent and other proteins of the thin filament (residues *b*, *c*, and *f*). In fact, only one charge substitution out of the total two that occur in the β-Tm happens at position *e* of the heptad (serine residue in α-Tm replaced by glutamic acid in β-Tm at position 229). Introducing a negative charge at that position is therefore likely to change the local structure of the β-Tm. Another important difference between the two Tm components is the number of Cys groups present in each isoform. In α-Tm one Cys residue is found at position 190, whereas two such residues are found in β-Tm at position 36 and 190.

The significance of having two major Tm isoforms has not been established but the differential tissue expression of the two components suggests a relationship between muscle function and the type of Tm associated with it. It has been reported that the ratio of α and β Tm varies from one muscle type to another and within the same muscle type during development (Amphlett *et al*, 1976; Bronson and Schachat, 1982; Muthuchamy *et al*, 1993). In general, the ratio of α to β chains is greater than 1 in fast-contracting muscles and is close to 1 in slow-contracting muscles (Cummins and Perry, 1974; Heeley *et al*, 1983). Since there is evidence for preferential heterodimer over homodimer formation (Lehrer and Qian, 1990), this suggests that fast-contracting muscles are likely to contain both αα homodimers and αβ heterodimers whereas the slow-contracting muscles are more likely to have mostly αβ heterodimers. The ββ homodimer is believed to be less stable than the αβ heterodimer and is therefore not expected to exist in very large amounts in the muscle cell.

In the cardiac muscle, α-Tm, which is identical in its sequence to the skeletal α-Tm (Lewis and Smillie, 1980), is the predominantly expressed isoform. However, while completely absent in the heart of small mammals, β-Tm is present in small amounts (up to 20 %) in the slower-beating hearts of bigger mammals.

Transgenic mice lines have been produced where β-Tm was over-expressed. These mice showed severe cardiac abnormalities that were lethal (Muthuchamy *et al*, 1995; Muthuchamy *et al*, 1998) and were reported to have a significant increase in the Ca^{2+} sensitivity of the cardiac muscle (Palmiter *et al*, 1996).

In this work, the functional differences between the two Tm isoforms were investigated in order to gain an insight into the biological significance of having two different Tm components. For this purpose, we expressed the β-Tm protein with an Ala-Ser extension at its N-terminal end (referred to in the text as recombinant ββ Tm (n3), (see chapter 2, section 2.2.2.1)) and we used a number of *in vitro* assays to compare the behaviour of recombinant αα and ββ Tm. We looked at the binding affinities of the two proteins to actin, the Ca^{2+} sensitivities in the presence of either cardiac or skeletal Tn complex, the thermal stability of the two isoforms in the presence and absence of actin and the effect of β-mercaptoethanol on each.

The results obtained demonstrated that the ββ Tm dimer causes an increase in the Ca^{2+} sensitivity of the thin filament when associated with cardiac Tn complex. Also, the ββ Tm was found to be considerably less stable than the αα Tm dimer. This explains why the β-Tm chain is predominantly found as a heterodimer and mainly in the skeletal muscle.

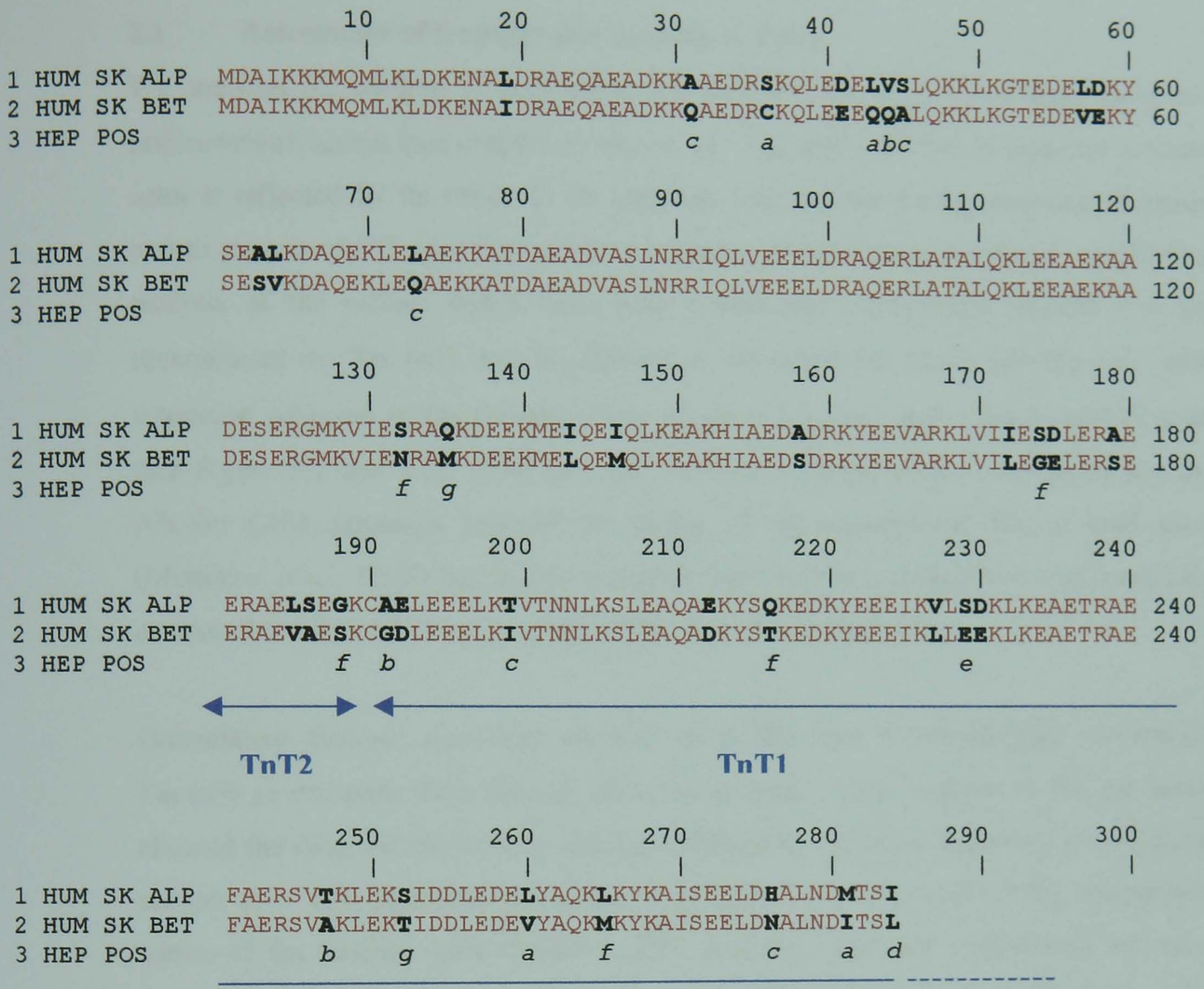

Figure 4.1: Sequence comparison between human α and β Tm chains. Line 1 and 2 correspond to the amino acid sequence of α and β Tm chains repectively. The differences in amino acids are highlighted in black and are mostly found at the C-terminal part of the protein where the Tn complex binds. In line 3 the heptad position of the non-conserved amino acids are indicated. The binding location for both TnT fragments are shown. TnT2 is the globular domain of TnT which binds to TnI and TnC. TnT1 is the TnT tail which binds mainly to Tm and extends to the overlap region between two neighbouring Tm.

2 Results

2.1 Assessment of tropomyosin binding to actin

We analysed the binding of both native and recombinant αα Tm to F-actin using co-sedimentation assays (see chapter 3, section 1). The ability of Tm to bind and saturate actin is reflected by its ability to co-sediment with F-actin during ultra-centrifugation and to saturate the F-actin filament at a 1:7 ratio of Tm:actin respectively. Qualitative analysis of the protein bands from both pellets and supernatants showed that the recombinant αα Tm (n3) was as efficient as the native αα Tm in binding actin with saturation achieved at Tm concentrations of about 1.5 μM when using 10 μM of actin (see Figure 3.2 and 3.3). This not only confirmed the previous observations that the Ala-Ser (AS) extension restored the ability of the unacetylated Tm to bind actin (Monteiro *et al*, 1994) but it also indicated that the Tm concentration was accurately estimated and that all Tm is properly folded and able to bind actin.

Quantitative analyses were also carried out in the case of recombinant αα and ββ Tm (n3) to compare their binding affinities to actin. Densitometry of the gel bands allowed the determination of Tm binding affinities to F-actin as described in chapter 3, section 1. The sigmoid binding curves (Figure 3.3), which reflect the cooperative nature of the binding, were fitted to a Hill equation. Both the midpoint of the curve ($K_{50\%}$) and the Hill coefficient (*m*) were determined and are shown in table 4.1. Our results indicated that no affinity difference exists between the two homodimers regardless of their oxidised/reduced state. The measurements were carried out both in the presence and absence of β-mercaptoethanol (ME) (Tm was heated to 65 °C in the presence of 1 mM ME and the resulting Tm was then assayed for actin binding). The effect of reduction was investigated as the thermal stability of Tm is found to be sensitive to the oxidation state of the protein (section 2.6 of this chapter). This is because α Tm has one Cys residue at position 190 while the β Tm has two residues at position 36 and 190.

The affinity values for the two Tm homodimers binding to actin at 100 mM and 200 mM KCl concentrations are shown in table 4.2. The binding affinities of recombinant αα Tm (n3) to actin were of the order of 0.2 μM and 0.6 μM at 100 mM and 200 mM salt concentrations respectively. This is comparable to the published

0.5 μM obtained at 150 mM salt concentration. The reported data for native αα Tm binding is also within the same range (Monteiro *et al*, 1994). Like with the αα Tm, the affinity of the ββ Tm at 200 mM KCl also decreased by a factor of 3. Therefore, the relative affinities remained the same.

	$K_{50\%}$ ± SD (μM)		*m* ± SD	
	+ME	-ME	+ME	-ME
αα Tm (n3)	0.16 ± 0.02	0.21 ± 0.02	1.3 ± 0.20	2.05 ± 0.66
ββ Tm (n3)	0.27 ± 0.05	0.24 ± 0.04	1.3 ± 0.13	1.6 ± 0.4

Table 4.1: Parameters for αα and ββ Tm (n3) binding to actin. The Tm binding curves to actin were generated as explained in chapter 3, section 1 both in the presence and absence of 1mM β-mercaptoethanol (ME). The buffer conditions were 20 mM MOPS, 100 mM KCl, 5 mM $MgCl_2$ at pH 7.0. The parameters obtained from fitting the binding curves to a Hill equation are $K_{50\%}$ (the midpoint of the curve) which gives a measure of the binding affinity and *m* (the Hill coefficient). The SD values were obtained using data from three independent measurements (N=3).

	100 mM KCl		**200 mM KCl**	
	$K_{50\%}$ ± SD (μM)	*m* ± SD	$K_{50\%}$ ± SD (μM)	*m* ± SD
αα Tm (n3)	0.21 ± 0.02	2.05 ± 0.66	0.58 ± ND	3.35 ± ND
ββ Tm (n3)	0.24 ± 0.04	1.6 ± 0.4	0.60 ± ND	2.80 ± ND

Table 4.2: Salt concentration effect on Tm binding affinity for actin. A three-fold decrease in the affinity of Tm for actin is reported on increasing the salt concentration of the buffer from 100 to 200 mM KCl in the case of both αα and ββ Tm (n3). The measurements were carried out in the absence of ME. ND stands for not determined.

2.2 Assessment of normal tropomyosin function

The ability of Tm to regulate the binding of S1 to actin was assessed by stopped-flow measurements of the rate of S1 binding to a reconstituted thin filament both in the presence and absence of Ca^{2+} (in the presence of either 2 mM $CaCl_2$ or 2 mM EGTA respectively; see chapter 3, section 2.4). The thin filament was reconstituted by mixing 5 μM pyrene-actin, 2 μM Tm and 2 μM Tn (either phosphorylated human cardiac Tn or tissue purified skeletal Tn) to ensure saturation of the filament. Figure 4.2 shows the fluorescence transients obtained in the case where pyrene-actin is in a large excess over S1 (10:1 ratio of actin: S1; see chapter 3, section 2.3.1). S1 binding to actin causes quenching of the fluorescence of the pyrene label attached to actin. The curves obtained were fitted to a single exponential (chapter 3, section 2.2). The superimposed raw and fitted traces indicated that pseudo-first order conditions were met. The observed rate constant (k_{obs}) of the reaction (S1 binding to actin) was derived from curve fitting and the k_{obs} values obtained with different Tm are presented in table 4.3. As previously reported, Ca^{2+} removal from the system causes a decrease in the rate of S1 binding to pyrene-actin. A 3-fold decrease was measured in the presence of skeletal control protein complex and a 2 to 2.5-fold decrease was recorded in the presence of cardiac control protein complex (control proteins are the tissue purified Tm.Tn complex) (McKillop and Geeves, 1993; Head *et al*, 1995; Reiffert *et al*, 1999). The values presented in table 4.3 are comparable to the results obtained with the control protein complex and are similar for both native αα Tm and recombinant αα/ββ Tm (n3). This suggests the following: 1) the reconstitution of the different regulatory protein components is successful in giving rise to a fully functional regulatory complex, 2) similarly to the native protein, recombinant Tm binds both skeletal and cardiac Tn proteins to form a Tm.Tn complex able to function as a mediator of the Ca^{2+}-dependent regulation of the acto-myosin interaction.

2.3 Characterisation of the blocked state:

The observed rate constant for S1 binding to an excess of actin was determined in the presence of native αα Tm, recombinant αα Tm (n3) or recombinant ββ Tm (n3). S1 binds to actin filament both in the presence and absence of Tm with the same rate, suggesting that there is no detectable blocked state in the presence of Tm (McKillop and Geeves, 1991) (chapter 3, section 2.4.1). It was therefore important to determine if any blocked state would be induced by the presence of the Ala-Ser extension in the recombinant protein or by switching isoforms. Our results (Figure 4.3) showed that S1 binds to the actin in the presence and absence of Tm with the same rate (about 5 sec^{-1}) regardless of what Tm was associated with actin, suggesting the absence of a blocked state.

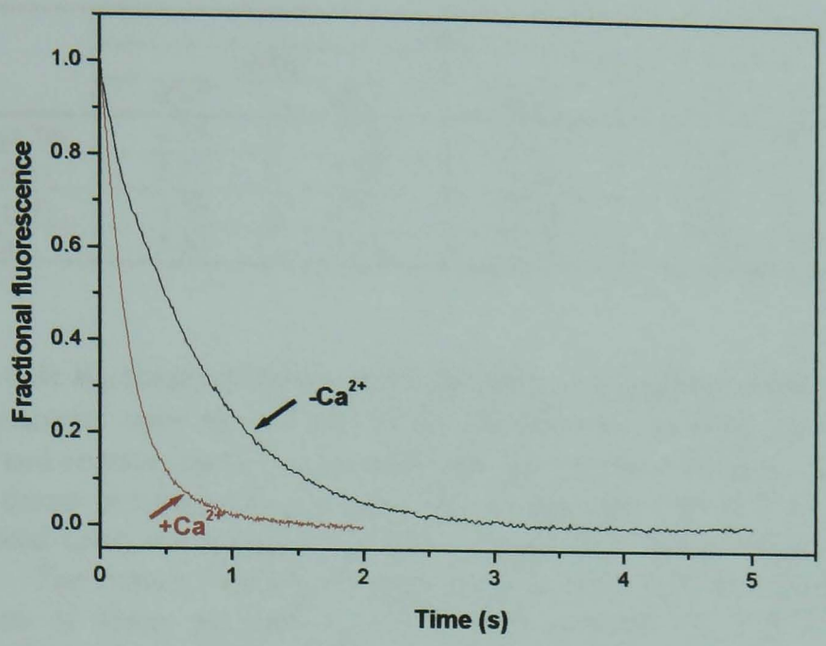

Figure 4.2: Stopped-flow transients for S1 binding to a reconstituted thin filament in the presence and absence of Ca^{2+}. The thin filament was reconstituted with 2.5 μM pyrene-actin, 1 μM Tm and 1 μM Tn. The thin filament complex was pushed against 0.25 μM S1. Buffer conditions were 20 mM MOPS, 140 mM KCl, 5 mM $MgCl_2$, pH 7.0, 1 mM DTT. The curves represented in this graph are those of recombinant αα Tm (n3) in the presence of sk Tn. Fitting these curves to a single exponential gave the following k_{obs} rates of 4.35 and 1.15 s^{-1} for (+) and (–) Ca^{2+} respectively representing a 2.9 fold decrease. When cardiac Tn was used k_{obs} values were 3.20 and 1.25 s^{-1} representing a 2.5 fold decrease in the rate. The results for the native αα Tm protein were very similar. The results with reconstituted thin filament were also very similar to those obtained with tissue purified control protein complex.

	k_{obs}				K_B	
	skTn		cTn			
	$+Ca^{2+}$	$-Ca^{2+}$	$+Ca^{2+}$	$-Ca^{2+}$	skTn	cTn
Native αα Tm	4.50	1.20	3.40	1.25	0.35	0.55
ααTm (n3)	4.35	1.15	3.20	1.25	0.35	0.66
ββ Tm (n3)	4.55	1.10	3.35	1.15	0.33	0.55
Sk Tm	4.50	1.35	2.85	1.10	0.42	0.60

Table 4.3: K_B measurements of S1 binding to regulated actin filaments. The K_B measurements were carried out in the presence of different Tm isoforms (αα (both native and recombinant), recombinant ββ Tm (n3) or mixed αα and αβ (skTm)) and either tissue purified rabbit skeletal or recombinant human Tn. The K_B value was calculated using the equation k_{obs} $(-Ca^{2+})/k_{obs}$ $(+Ca^{2+})=K_B/(1+K_B)$ (Chapter 3, section 2.4.1). The experimental conditions were as described in Figure 2 legend. In the presence of tissue purified control protein complex (sk Tm.Tn complex) the k_{obs} values obtained were 4.8 and 1.5 s^{-1} (+) and (-) Ca^{2+} respectively.

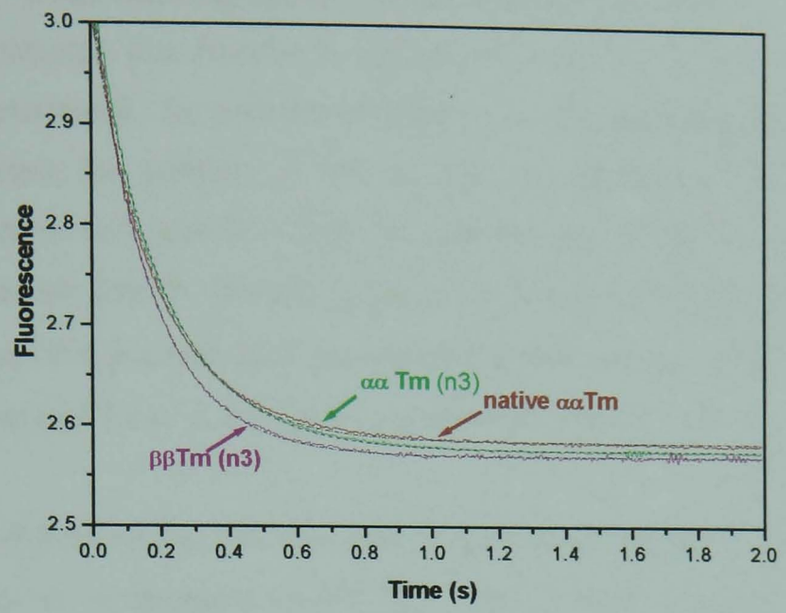

	k_{obs} ± SD (s^{-1})
native αα Tm	5.35 ± 0.09
αα Tm (n3)	5.30 ± 0.38
ββ Tm (n3)	5.30 ± 0.44

Figure 4.3: Stopped-flow transients for S1 binding to actin either in the presence of native αα, recombinant αα Tm (n3) or recombinant ββ Tm (n3). 2.5 μM pyrene-actin and 1 μM Tm were pushed against 0.25 μM S1. The buffer conditions were 20 mM MOPS, 140 mM KCl, 5 mM $MgCl_2$, pH 7.0. The curves were fitted to a single exponential. Both the raw (continuous) and fitted (dashed) curves are shown. In the table are shown the observed rate constants (k_{obs}) obtained from curve fitting. These are averages of 3 independent measurements. The rate of S1 binding to actin in the absence of Tm was also about 5 s^{-1}.

2.4 Determination the three-state model parameters:

The parameters that describe the three-state model of regulation (chapter1, section 3.1) were determined for each Tm in order to determine whether the affinity of S1 for actin (K_1 value), the position of Tm on actin at equilibrium (K_T value) as well as the cooperative unit size (*n* value) are affected by 1) the N-terminal extension of the recombinant Tm (by comparing native αα Tm with recombinant αα Tm (n3)), 2) the presence of a β component (by comparing pure αα with mixed αα αβ (sk Tm which had a ratio of 3:1 of α to β chains corresponding to a 1:1 ratio of αα and αβ Tm)).

Figure 4.4 shows the raw data of a titration curve for the binding of S1 to actin in the presence of recombinant αα Tm (n3). The titration of very low actin concentrations (50 nM) with S1 required the use of phalloidin to stabilise the actin in the filamentous form (F-actin). The use of phalloidin does not affect the affinity of S1 for actin (Criddle *et al*, 1985). As shown in the figure 4.4, working at 50 nM actin provided a high enough concentration to obtain a reasonable fluorescence signal with relatively low levels of noise. The initial fluorescence value (F_0) was about 350 fluorescence units with normally about 5 % variations. The F_∞ value obtained from the fit is 112 and corresponds to 68 % fluorescence quenching. Since binding of S1 to pyrene-actin results in 70% fluorescence quenching, this is consistent with there being no substantial background fluorescence in the buffer.

The affinity of Tm for actin under our experimental conditions (200 mM KCl concentration) was determined by co-sedimentation experiments to be at about 0.6 μM (Table 4.2). Consequently, the presence of a large excess of 2 μM Tm in the cuvette ensures actin filament saturation. The S1 binding curves in the presence of Tm are of a sigmoid nature reflecting the cooperative binding of S1 to the filament. The S1-actin binding curves were fitted to a 2-state version of the 3-state model equation (see appendix, equation 1.2.3). This is because no blocked state was detectable in the stopped-flow measurements when only Tm is bound to actin (see previous section). The filament is in equilibrium between closed and open states (less than 10 % blocked state) and therefore the K_B value is excluded from the equation. Considering the complexity of the equation and the number of parameters that describe it, the fitting can

only be carried out by fixing few parameters with either known or independently determined values (total actin concentration, K_2, F_0 and n) and systematically varying the other parameters (K_1, K_T and F_∞). For instance, the K_2 value (the equilibrium constant for the isomerisation from weakly to strongly bound acto-S1 complex) was previously determined to have a value of 200 in the absence of nucleotide (Coates *et al*, 1985). Fits were repeated for a range of n values (n varied from 6-12 and was fixed each time). The best fit was the one that offered the lowest deviation from the raw data (Table 4.4) (Maytum *et al*, 1999).

Figure 4.5 represents the binding curve of S1 to actin when bound to either recombinant pure αα Tm (n3), native pure αα Tm or to native sk Tm (mixed αα and αβ dimers). 8 curves were analysed in each case. The best fit parameters for each curve were averaged and are shown in Figure 4.5 table. In all cases, the best fit was obtained for an n value of 7-8. The K_1, K_T values for both native and recombinant αα Tm were very similar ranging between 145-150×10^3 M^{-1} and 0.075-0.08 respectively. In the presence of sk Tm, S1 was found to bind with a significantly higher affinity (K_1 is 185×10^3 M^{-1} for sk Tm and 150 × 10^3 M^{-1} for αα Tm) as revealed with a statistical analysis using the student T-test at p=0.05. The K_T value was however not affected by the presence of the β component of Tm on actin.

These results suggest that the type of isoform that makes up the Tm dimer does not affect the equilibrium position of Tm on actin but does increase the binding affinity of S1 for actin.

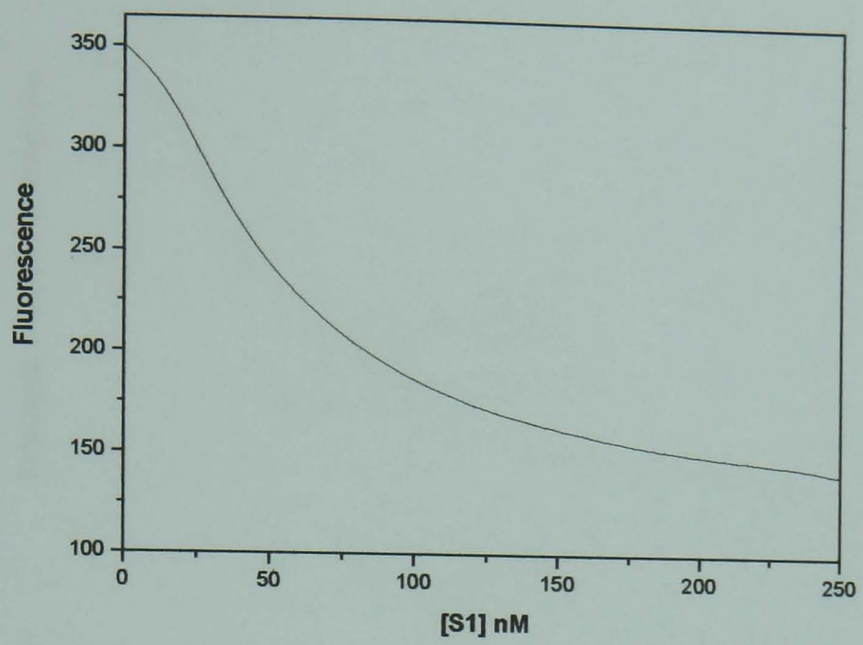

Figure 4.4: Raw titration data for S1 binding to pyrene-actin in the presence of recombinant αα Tm (n3). S1 was continuously titrated into a stirred cuvette that contained 50 nM pyrene-actin and an excess of 2 μM Tm. S1 binding was monitored by fluorescence quenching. The measurements were carried out at 20 °C and the buffer was 20 mM MOPS, pH 7.0, 200 mM KCl, 5 mM $MgCl_2$.

n	6	7	**8**	9	10	11	12
SD	0.92	0.66	**0.51**	0.52	0.60	0.85	1.2
K_T	0.17	0.125	**0.09**	0.68	0.05	0.04	0.028
K_1 ($x10^3$)	165	158	**153**	150	148	140	135

Table 4.4: Fitting of S1 titration curves over a range of *n* values. The fitting of S1 titration curves is achieved by varying the *n* value from 6 to 12. The best fit parameters are those obtained with the lowest standard deviation (SD) value (highlighted in bold). The data shown in the table is that of a curve obtained in the presence of recombinant αα Tm (n3).

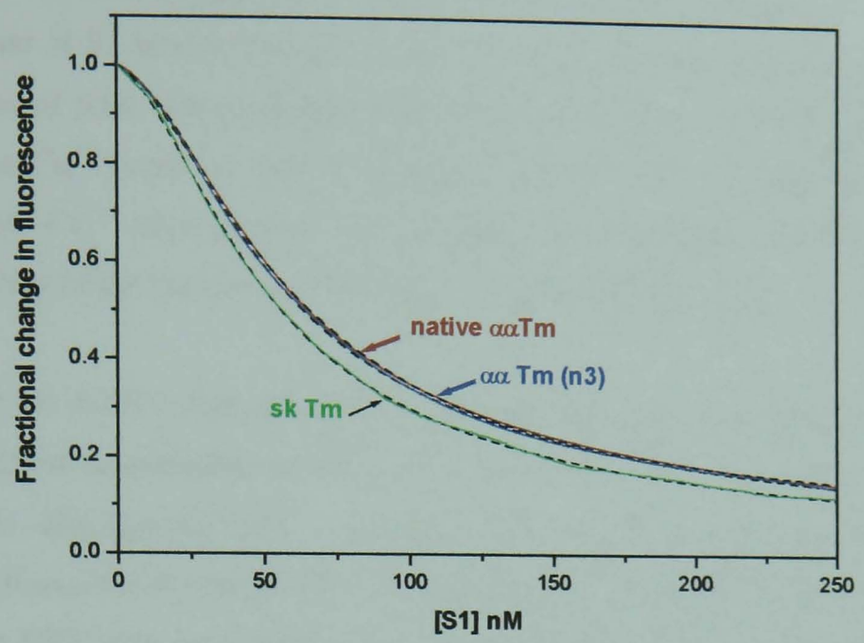

	$K_1 \pm SD$ (M^{-1})	K_2	$K_T \pm SD$	*n*
native αα Tm	145 ± 25	200	0.075 ± 0.02	7-8
αα Tm (n3)	150 ± 20	200	0.08 ± 0.03	7-8
sk Tm	185 ± 20	200	0.08 ± 0.03	7-8

Figure 4.5: S1 binding curve to actin in the presence of either native αα Tm, recombinant αα Tm (n3) or sk Tm (mixed αα and αβ Tm). The curves were fitted to a 2-state version of the McKillop and Geeves 3-state model equation. The raw (continuous) and fitted (dashed) data are superimposed. For ease of comparison, the data was normalised to 1.0 $(F-F_\infty)/(F_0-F_\infty)$. The parameters obtained from curve fitting are represented in the table. K_1 and K_2 are the equilibrium constants for weak and strong S1 binding to actin respectively (S1 affinity for actin is K_1K_2). K_T is the equilibrium constant for the transition between closed and open states of the filament. *n* is the cooperative unit size (the number of actins that switch between the two states of the filament). The K_1, K_T and *n* values represented are averages calculated from analysing 8 curves (N=8).

2.5 Measurement of the calcium sensitivity of the system

The rate of S1 binding to actin is a Ca^{2+}-dependent reaction as it is proportional to the number of actin sites available for S1 binding which in its turn is dependent on whether TnC is Ca^{2+}-bound or free (chapter 3, section 2.4). S1 binding to pyrene-actin at different Ca^{2+} concentrations (pCa) is therefore a good assay for investigating the Ca^{2+} sensitivity of the system under different conditions (Figure 3.7).

Figure 4.6 and 4.7 represent Ca^{2+}-sensitivity curves for S1 binding to pyrene-actin in the presence of recombinant αα Tm (n3) or recombinant ββ Tm (n3) bound to either sk Tn or cTn. The sigmoid curves were fitted to a Hill equation and both the midpoint of the curve $K_{50\%}$ (which reveals the Ca^{2+} concentration at which filament switching from the ON to OFF state takes place) and the Hill coefficient *h* are represented in the figure tables. The data obtained is of good quality as the data points have low scatter from the fitted curve. Also, the standard error (SE) obtained from the fit is within the same range for each parameter in each set of experiment. The differences between the two Tm homodimers were observed in terms of a shift in the Ca^{2+}-sensitivity curve midpoints. Interestingly, a 0.23 pCa shift (curve midpoint shift from pCa 5.57 to pCa 5.80) corresponding to 1.10 μM shift in Ca^{2+} concentration from 2.69 μM to 1.58 μM, was observed in the case of ββ Tm but only when bound to cTn complex. No difference in Ca^{2+}-sensitivity was observed between the two isoforms in the presence of skTn.

Unlike skTnC which has two functional Ca^{2+}-binding sites, cTnC has only one. This is reflected by the *h* value of 1.0 in the presence of cardiac Tn complex and the much higher value of 1.7 in the presence of skTn. Therefore, this result is compatible with each Tn complex operating independently.

This experiment was repeated with proteins from different preparations and with the same pCa solutions to minimise the error that could potentially arise from variations in Ca^{2+} concentrations. The results were reproducible as the same pCa shift is reported each time.

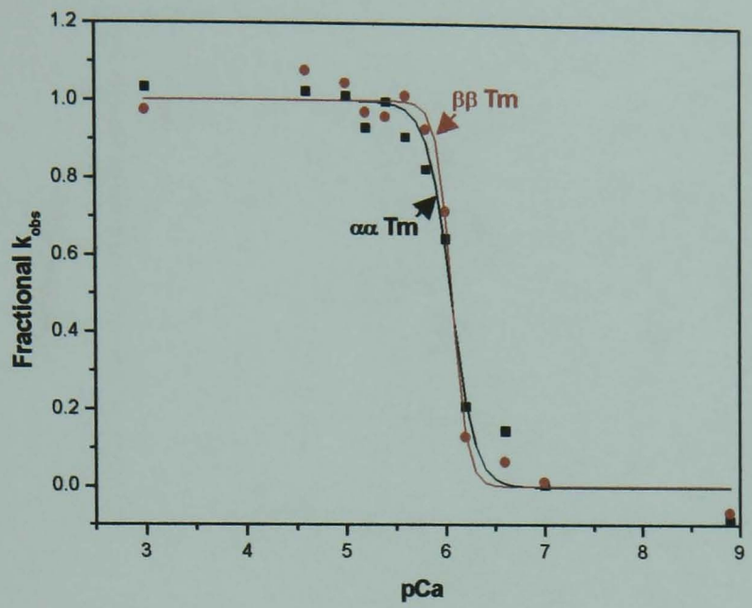

	h ± SE	$K_{50\%}$ ± SE	Midpoint $[Ca^{2+}]$ (μM)
αα Tm (n3)	1.50 ± 0.07	6.05 ± 0.03	0.89
ββ Tm (n3)	1.68 ± 0.08	6.06 ± 0.01	0.87

Figure 4.6: Ca^{2+}-sensitivity measurements for S1 binding to pyrene-actin in the presence of either αα Tm (n3) or ββ Tm (n3) and sk Tn. The Ca^{2+}-sensitivity curves were obtained by plotting the k_{obs} values for S1 binding to pyrene-actin as a function of pCa (see chapter 3, figures 6 and 7). The curves were fitted to a Hill equation to determine both the midpoint of the curve ($K_{50\%}$) and the Hill coefficient (*h*). Parameters obtained from curve fitting are shown in the table above. The standard error (SE) was obtained from fitting the data shown in this graph.

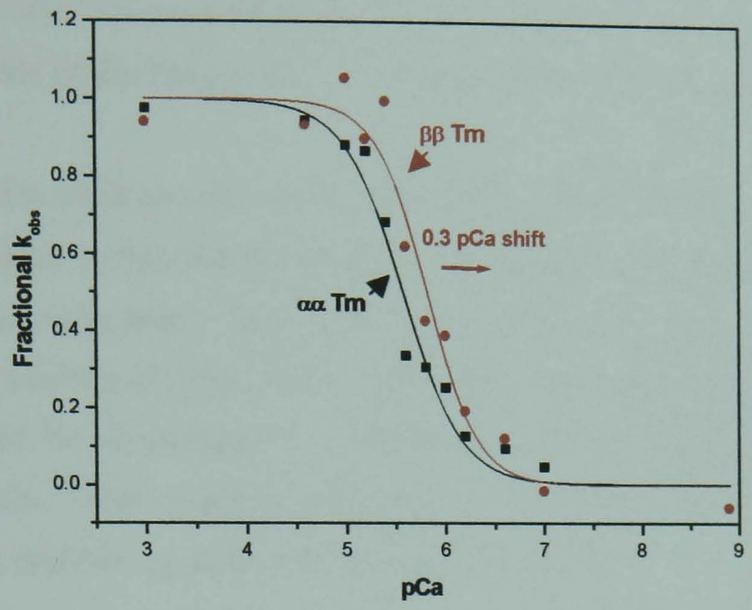

	h ± SE	$K_{50\%}$ ± SE	Midpoint [Ca^{2+}] (μM)
αα Tm (n3)	1.15 ± 0.09	5.57 ± 0.08	2.69
ββ Tm (n3)	1.20 ± 0.10	5.80 ± 0.07	1.58

Figure 4.7: Ca^{2+}-sensitivity measurements for S1 binding to pyrene-actin in the presence of either αα Tm (n3) or ββ Tm (n3) and cTn. The data was obtained and analysed as explained in Figure 6. The presence of ββ Tm (n3) caused a 0.3 pCa shift in the midppoint of the curve. The midpoint values of the curves are also shown in Ca^{2+} concentration.

2.6 Protein thermal unfolding using DSC:

The thermal stability of native αα, recombinant αα Tm (n3) and recombinant ββ Tm (n3) was assessed both in the presence and absence of actin. The effect of disulphide bridge reduction by β-mercaptoethanol (ME) was also investigated.

The α-Tm chain contains one Cys residue at position 190 (C-domain of the protein), the β-Tm chain on the other hand has two Cys residues, at positions 190 and 36 (C- and N-domains respectively) (see Figure 4.1 for sequence). In all cases, these Cys residues occupy position *a* of the heptad, and since the two Tm chains are parallel and in register, they can be cross-linked by the formation of a disulphide bond under oxidising conditions. That would potentially give rise to a single cross-linked αα Tm dimer or either a single or a double cross-linked ββ Tm dimer.

As previously demonstrated by Williams and Swenson (1981) the unfolding of the C-domain part of αα Tm is sensitive to the oxidation state of Cys 190. This was verified by using strong oxidising agents, chemically blocking the SH-groups of Cys190 (equivalent to the reduced state of the protein) and producing N- and C-domain fragments of Tm. All these modifications showed that when the SH-groups are blocked, two melting transitions are obtained. However, when Tm is oxidised only the high temperature transition is seen. The use of the N- and C-domain fragments confirmed that the presence of a disulphide bond at the C-domain of Tm stabilises the protein and causes a shift of the low temperature transition into the high temperature transition. Therefore, under oxidising conditions, the N- and C-domain transitions overlap. The low-temperature transition was assigned to the melting of the C-domain with reduced Cys 190, whereas the high-temperature transition was assigned to the melting of both the C-domain with oxidised thiol groups and the N-domain of Tm.

Figure 4.8 shows the melting profile of recombinant αα Tm (n3) in the absence of ME. Two separate melting transitions were observed during the first heating with maxima at 42 °C and 54 °C. During the second heating, the low temperature peak completely disappeared and only the 54°C peak was observed. In the presence of 1 mM ME (Figure 4.9) two melting transitions were also observed during the first and second

heating. However, the size of the two peaks was altered. A reduction in the size of the higher temperature peak (maximum at 52 °C) and an increase in the size of the lower temperature peak (maximum at 42 °C) were recorded. This finding is in good agreement with the explanation proposed by Williams and Swenson (1981). The low-temperature peak corresponds to the melting of the C-domain of the protein with Cys 190 reduced. The second high-temperature peak is composed of two overlapping transitions: the melting transition of the protein N-domain and that of the C-domain with cross-linked thiols of Cys 190. Therefore, when Tm becomes reduced after the first heating in the presence of ME, there is a shift of the higher temperature peak to the lower-temperature peak. This explains the increase in the size of the first peak and the reduction in the size of the second peak. This was further confirmed by measuring the thermal unfolding of C190S Tm mutant, which mimics the reduced state of the protein (data not shown).

In the presence of phalloidin-stabilised actin, three heating steps were performed. First, the sample was heated up to 65 °C to reversibly denature Tm and allow the reduction of Cys 190 residues. In this case, actin remains intact as its melting transition is at 80 °C. After cooling to 5 °C, the sample was heated again to 90 °C resulting in the irreversible denaturation of actin. The third heating was to 65 °C and should give results similar to that of reduced free Tm.

Figure 4.10 describes the DSC profile of recombinant αα Tm (n3) in complex with F-actin. A new sharp transition with maximum at about 47 °C was observed. During the third heating and after irreversible denaturation of actin, only the peaks corresponding to the thermal unfolding of free Tm (42 °C and 52 °C) were observed. This indicated that the new transition at 47 °C obtained in the presence of actin reflects the thermal denaturation of actin-bound Tm. As explained above, the reduction in the size of the most thermostable peak in the second heating is due to the reduction of Cys 190 groups. Comparing the size of peaks of the fully reduced free Tm (third heating) with those from the second heating (i.e. in the presence of actin) suggests that only the first thermal transition (the one corresponding to the melting of reduced C-domain of Tm) is sensitive to the presence of actin.

The thermal unfolding of native αα Tm obtained from rabbit skeletal muscle was very similar to that of recombinant αα Tm (n3) both in the presence and absence of actin. The comparison was made in terms of maximum temperatures of the melting transitions and the response to reduction by ME.

Figure 4.11 shows the thermal unfolding of recombinant ββ Tm (n3) both in the presence and absence of 1 mM ME. Tm samples will have a mixture of oxidised and reduced molecules, as the state of the Tm molecule will vary depending on the sample history. Because β-Tm has two Cys groups located both at the C- and N-domains, a mixture of single/double cross-linked or fully reduced molecules can arise. The first heating, which will either reduce or oxidise Tm depending on conditions (presence or absence of ME), will give different melting profiles for different samples. Therefore, for ease of interpretation only the second heating is shown. In the case of ββ Tm, two melting transitions were obtained at 37 °C and 52 °C. The size of the lower temperature peak was bigger in the presence of ME, and the size of the higher temperature peak bigger in the absence of ME.

Figure 4.12 represents the thermal unfolding of ββ Tm (n3) in complex with F-actin in the presence of 1 mM ME. As with αα Tm, a new sharp transition, corresponding to the melting of actin-bound Tm, was observed but in this case at about 41 °C. Interestingly, the third heating, which corresponds to the melting of reduced free Tm, had only one transition at 37 °C. The high temperature transition at 52 °C completely disappeared.

By analogy with the αα Tm, the high temperature peak at 52 °C should correspond to the melting of the more stable oxidised domains, whereas the low temperature transition should correspond to the melting of reduced domains. Since the higher temperature peak completely disappeared after the third heating with actin (Figure 4.12), it suggested that 1) ββ Tm unfolds as a single transition at 37 °C when fully reduced, 2) Unlike αα Tm, ββ Tm was not fully reduced after the first heating in the absence of actin.

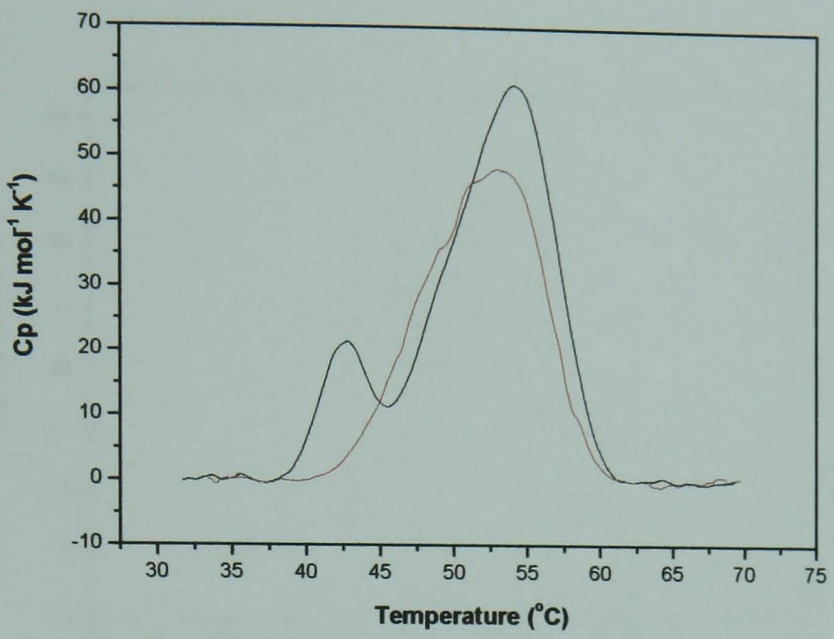

Figure 4.8: DSC profile of αα Tm (n3) in the absence of ME. 20 μM Tm present in 20 mM Hepes, 100 mM KCl, 2.5 mM $MgCl_2$, pH 7.3 was scanned twice at a constant heating rate of 1 °C min^{-1}. The first heating (black line) shows the presence of two melting transitions with maxima at 42 °C and 54 °C. The second heating (red line), shows the complete disappearance of the low-temperature peak.

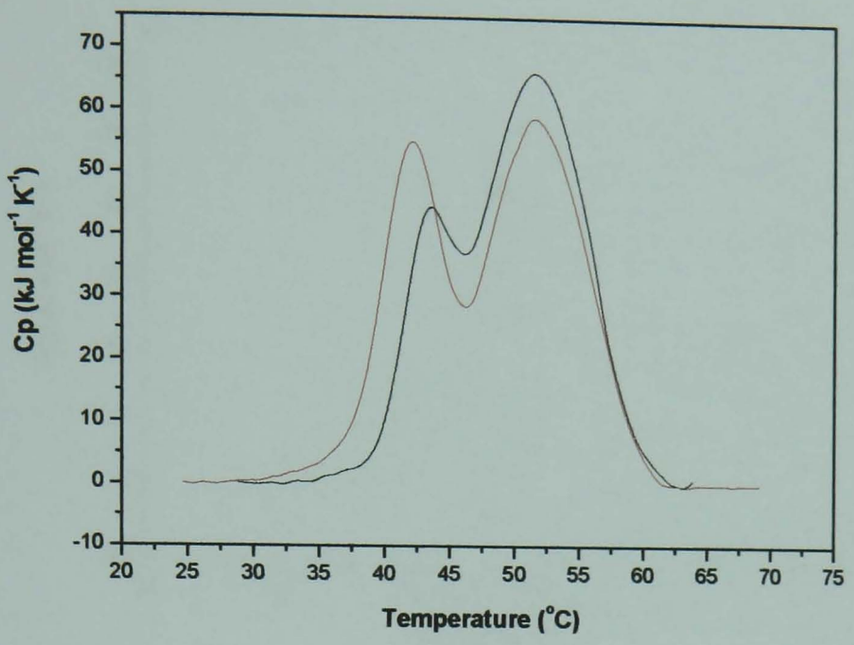

Figure 4.9: DSC melting profile of recombinant αα Tm (n3) in the presence of ME. Experimental conditions used were the same as desribed in Figure 4.8 legend except for the presence of 1 mM ME. Tm concentrarion used was 30 μM. The first scan (black) shows the presence of two melting transitions with peaks at 42 °C and 52 °C. The second scan (red), shows an increase in the size of the first peak (42 °C) and a decrease in the size of the second peak (52 °C).

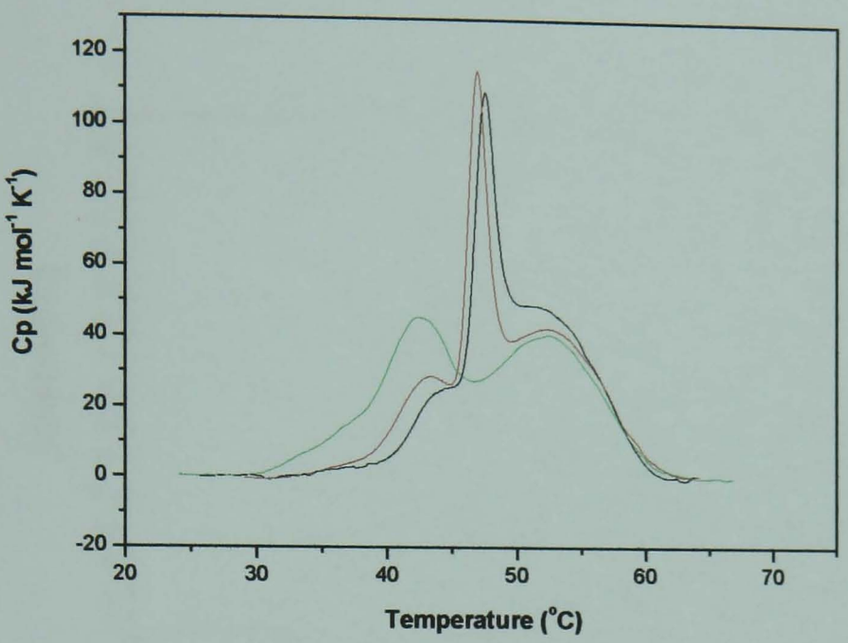

Figure 4.10: DSC melting profile of recombinant αα Tm (n3) in complex with F-actin. The complex was obtained by mixing 30 μM Tm with 46.7 μM phalloidin-stabilised actin. Experimental conditions used were the same as desribed in Figure 4.8 legend except for the presence of 1 mM ME. The mixture was first heated to 65 °C (black), then to 90 °C (red) and finally to 65 °C (green). The actin melting transition with maximum at 80 °C is not shown. In the presence of actin, a new sharp peak at 47°C appeared. The peaks were at 42°C, 47°C and 52°C.

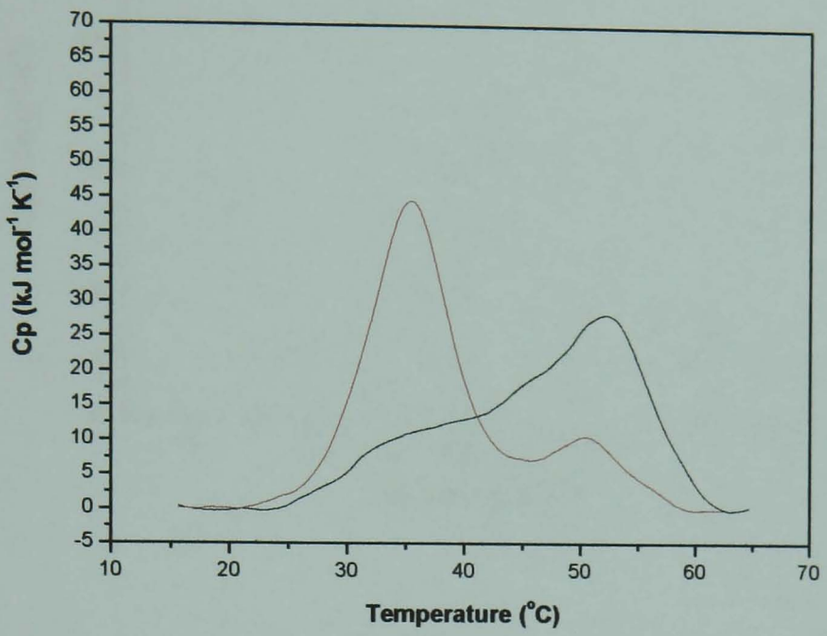

Figure 4.11: DSC melting profile of ββ Tm (n3) both in the presence and absence of ME. 30 μM of ββ Tm (n3) was scanned twice up to 65 °C both in the absence (black) and presence (red) of 1 mM ME. The buffer conditions were as described in Figure 4.8 legend. In both cases only the second heating is considered for ease of analysis (see text) Two main melting transitions were observed with values for maximum melting temperatures at 37 °C and 52 °C.

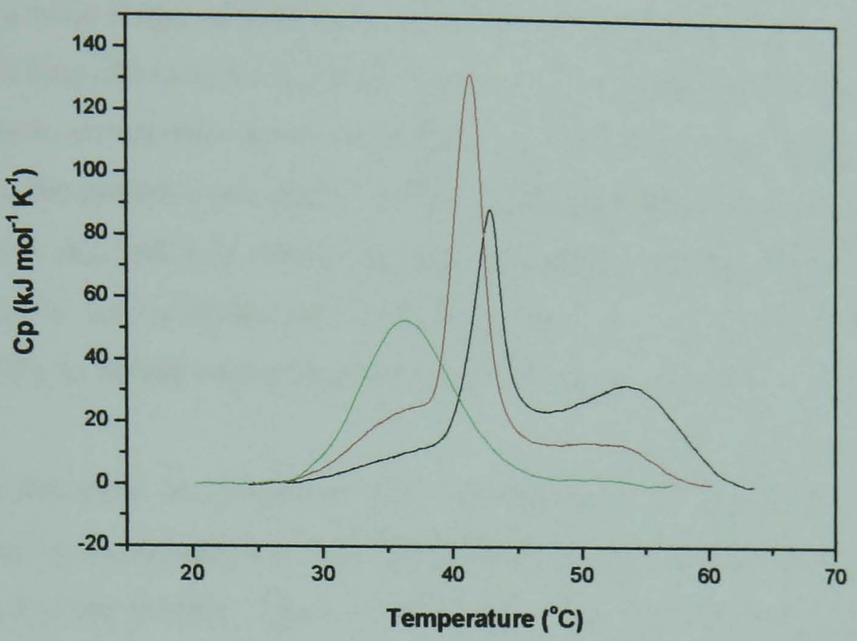

Figure 4.12: DSC melting profile for recombinant ββ Tm (n3) in the presence of actin. The complex was obtained by mixing 15 μM ββ Tm (n3) with 46.7 μM phalloidin-stabilised actin. Experimental conditions used were the same as desribed in Figure 4.8 legend except for the presence of 1 mM ME. Three heating scans were performed, the first to 65 °C (black), the second to 90 °C (red) and the third to 65 °C (green). Maximum melting temperatures are 36 °C, 41 °C and 53 °C.

3 Discussion

Comparing the regulatory and thermal properties of native and recombinant αα Tm using a wide range of techniques revealed the similar behaviour of these two proteins. The binding affinities for actin and the ability to mediate the Ca^{2+}-dependent regulation of muscle contraction were comparable in both cases. The affinity of S1 binding to actin in the presence of either protein was indistinguishable and so were the equilibrium constants (K_B and K_T), which describe the position of Tm on actin. The DSC melting profiles for both proteins were identical in terms of maximum melting temperatures and the ability to unfold reversibly and so was the response to ME.

It can therefore be concluded that the expression of an Ala-Ser (AS) extension is efficient in substituting for the lacking acetyl group without interfering with the normal function of the protein. This is in good agreement with the conclusions published in the Monteiro *et al* paper (1994).

The data obtained from comparing the regulatory properties of α and β Tm isoforms clearly suggests that significant differences in the properties of the thin filament would arise by switching between αα and ββ Tm. The ββ Tm, if existent in the cell, is found in very small amounts. The β Tm chain is found mainly associated with the α Tm chain as a heterodimer, mostly in slow contracting muscles and in slower beating hearts of big mammals (Cummins and Perry, 1974; Heely *et al*, 1983). This is not surprising as the thermal unfolding profiles obtained with DSC noticeably suggest that ββ Tm is thermally less stable than the αα Tm. ββ Tm protein is unstable at 37 °C, the normal temperature of the body. Though, binding to actin stabilises the protein by shifting the maximum melting temperatures by 5°C to 41-42 °C, it is still a temperature that the muscle can reach during exercise. Tn complex is reported to provide additional stability to Tm (Kremneva *et al*, 2003). However, prior to control protein assembly and binding to actin, the ββ Tm will be unstable in the cytoplasm especially if the cellular environment is reducing (Hwang *et al*, 1992). In the future, it will be important to study the thermal unfolding of the physiologically more relevant αβ Tm heterodimer as it is abundant in the skeletal muscle. The αβ heterodimer production and characterisation was not possible due to time limitations.

In the presence of actin, the thermal stability of Tm is increased, notably that of the low temperature melting transition (5 °C shift is observed for both αα and ββ Tm). The high temperature melting transition is unaffected by the presence of actin. The temperature at which Tm dissociates from actin under condition similar to those of the DSC second heating was investigated by Kremneva and Levitsky (Bach Institute of Biochemistry, Moscow). The results obtained showed that αα Tm dissociates from actin at 46.4 °C whereas ββ Tm dissociates at 40.5 °C (data not published). This finding explains why only the low temperature transition is sensitive to the presence of actin, as the N-domain and the cross-linked C-domain unfold at a temperature higher than that of Tm dissociation from actin. The sharp character of the actin-induced transition can be explained by the cooperative dissociation of Tm from actin being simultaneously followed by unfolding of the reduced C-domain. The low temperature transition was still observed in the presence of actin because Tm was in large excess. It therefore represents the melting of reduced C-domain of non-actin bound Tm.

The DSC experiments performed on the two Tm homodimers were very useful in giving an insight into the thermal stability properties of the two proteins. However, an appropriate comparison of the melting profiles was made difficult by the fact that the measurements are sensitive to the oxidised/reduced states of the starting protein samples. To facilitate the analysis, future experiments should be conducted with homogeneous samples. This can be achieved by either fully reducing (heating up to 65 °C in the presence of strong reducing agents like DTT) or fully oxidising Tm samples prior to the start of the experiments.

The distribution between the three states of the thin filament is not affected by the type of Tm isoform bound to actin. Both K_B (measured in the presence of either skTn or cTn) and K_T values were very similar for both αα and ββ Tm dimers. The K_B value was however larger when Tm was bound to cTn (Table 4.3). This would suggest that the proportion of actin sites not available for S1 binding is smaller in the cardiac system when the muscle is relaxed as compared to the skeletal system. Therefore the cardiac system is less off than the skeletal system, which is consistent with its function as it constantly beats and hence does not relax for a long period of time.

The equilibrium measurements revealed that the presence of the β component in Tm, as opposed to pure αα Tm, resulted in a significant increase in the binding affinity of S1 for actin. It has already been established that the affinity of S1 for actin was enhanced in the presence of Tm (Maytum *et al*, 1999; Tobacman and Butters, 2000). Two different explanations were put forward by these two groups. Tobacman and Butters speculated that a conformational change in actin induced by Tm movement, promotes the S1-actin interaction. Maytum *et al* on the other hand, speculated that electrostatic interactions between S1 and Tm would favour S1 interaction with actin. Both these hypotheses can be accounted for by the difference in amino acid sequence between the α and β Tm chains.

The constants for the S1 binding reaction to actin in the presence of Tm were defined by both kinetic and equilibrium measurements. The binding rate constant, measured with stopped-flow, is unchanged (k_{obs} is about 5 sec^{-1}) in the case of both αα and ββ Tm. However, the overall affinity of S1 binding to actin (K_1 value) is higher in the presence of the β component of Tm. This indicates that the two different Tm isoforms affect the dissociation rate constant of S1 for actin. This could be confirmed by measuring the ATP-induced dissociation of S1 from an actin filament both in the presence and absence of Tm in the stopped-flow machine.

Earlier studies (Palmiter *et al*, 1996) demonstrated that α to β Tm isoform switching in the mice heart altered the Ca^{2+}-induced activation of the thin filament. An increase in Ca^{2+} sensitivity of the thin filament results in activation of muscle contraction occurring at lower free Ca^{2+} concentrations. The Ca^{2+} sensitivity measurements carried out with isolated proteins in solution reinforce the idea of a change in Ca^{2+} sensitivity as a result of a change in Tm isoforms. We report an increase in Ca^{2+} sensitivity in the presence of the ββ Tm. Interestingly, this finding is only valid when Tm is in association with cardiac Tn complex. This shows that the presence of ββ Tm in the cardiac muscle would render the thin filament more sensitive to Ca^{2+} i.e. contraction would still happen at Ca^{2+} concentrations at which the filament should normally be turned off.

A change in the Ca^{2+} sensitivity of muscle can be linked to either a change in the affinity of Ca^{2+} for TnC, or to an alteration in the inhibitory action of TnI (due to changes in the nature of interaction between Tn.Tm and actin). Binding of Ca^{2+} to TnC has been reported to decrease the affinity of the Tm.Tn complex to actin. This effect has been reported to be more significant in the skeletal system as compared to its cardiac counterpart (Rosenfeld and Taylor, 1985; Dahiya *et al*, 1994). This is consistent with the results presented in this chapter. The midpoint of the Ca^{2+} sensitivity curve obtained with the reconstituted skeletal complex (αα Tm in complex with skTn) is at pCa 6.0 (corresponding to a midpoint Ca^{2+} concentration of 1 μM) whereas that obtained with the cardiac complex (αα Tm in complex with cTn) is at pCa 5.6 (corresponding to a midpoint Ca^{2+} concentration of 2.5 μM). This suggests that more Ca^{2+} has to be removed from the system for the skeletal muscle to be turned into the OFF state. This could be linked to the greater effect Ca^{2+} has on Tn.Tm and actin interactions in the skeletal muscle. Therefore, the nature of interactions between the thin filament regulatory proteins could influence the Ca^{2+}-dependent filament switching from ON to OFF states.

The Ca^{2+} sensitivity curve for ββTm is identical to that of αα Tm when both bound to skTn but shifted when bound to cTn. This could be attributed to cTn interacting differently with different Tm isoforms. TnT subunit of Tn is an important player in the Ca^{2+}-mediated regulation of muscle contraction (Potter *et al*, 1995). TnT is responsible for holding the whole Tn-Tm complex together. Tm binding to TnT happens mainly through the TnT1 region of the protein but it is the TnT2 region that interacts with the TnI-TnC components of Tn. Most of the sequence differences between the 20 different TnT isoforms occur at the N-terminal part of the protein (TnT1 region) (Perry, 1998 for review). This hypervariable region of TnT is therefore likely to provide functional modulations, which could account for the differences that arise between the different muscle systems. It would therefore be interesting to compare the binding properties of cTnT to both αα and ββ Tm, in the presence and absence of Ca^{2+}.

CHAPTER 5

STUDY OF FHC MUTATIONS EXPRESSED IN TROPOMYOSIN

1 Introduction

Familial Hypertrophic Cardiomyopathy (FHC) is a genetic disorder caused by mutations in sarcomeric proteins. So far, four of these mutations (A63V, K70T, D175N and E180G) have been found to arise in the α-Tm gene making up 5 % of all reported mutations (Thierfelder *et al*, 1994; Nakajima-Tanigushi *et al*, 1995; Watkins *et al*, 1995). The two mutations D175N and E180G have been of a particular interest over the last few years probably due to their location in the TnT binding region of Tm, more precisely the Ca^{2+}-sensitive TnT region. Residues 175 and 180 of the α-Tm chain are found at positions *g* and *e* of the heptad respectively. They could therefore be involved in either intra- or inter-chain salt bridge formation. In both cases, the mutation leads to the substitution of a charged residue with a non-charged one, and in the case of E180G, it results in the introduction of a small residue (glycine) also known as a helix breaker. Consequently, considering the nature of the changes and the position at which they occur, both within the helix heptad and relative to the location of the Tn binding site, it is not surprising that these two mutations have been reported to alter the normal function of the thin filament (Golistina *et al*, 1997; Coviello *et al*, 1997; Bottinelli, 1998; Bing *et al*, 1997; Bing *et al*, 2000). Studies on transgenic mouse lines that encode these FHC mutations showed that while D175N mutation causes mild hypertrophy (Muthuchamy *et al*, 1999), E180G mutation leads to severe cardiac dysfunction and death in mice (Prabhakar *et al*, 2001). This suggests that the E180G mutation is more disruptive than the D175N mutation. These two FHC mutations are also in the vicinity of Cys 190 whose state of oxidation has been demonstrated to be crucial for determining the stability of Tm (see chapter 4, section 2.6).

In this study, the effects of the two FHC mutations D175N and E180G on 1) the ability of Tm to bind actin, 2) the thermal stability of Tm both in the presence and absence of actin, and 3) the Ca^{2+}-sensitivity of the system were investigated. Both WT and FHC mutant αα Tm were overexpressed in *E.coli* (chapter 2, section 2.2.3) with the N-terminal extension (Ala-Ser referred to as the n3 extension) that mimics the N-terminal acetylation (Monteiro *et al*, 1994) (also see chapter 4). The results obtained showed that both D175N and E180G decrease the affinity of Tm for actin and cause an increase in the Ca^{2+}-sensitivity of the thin filament but with a more significant effect from E180G mutation. Also, the actin-induced stabilisation of E180G Tm, as measured with DSC,

was found to be significantly less than for WT and D175N Tm. This could therefore explain why the E180G mutation has more dramatic consequences on the heart's function.

2 Results

2.1 Effect of FHC mutations on tropomyosin binding to actin

The binding of recombinant αα Tm (n3) carrying the FHC mutations D175N and E180G was investigated using co-sedimentation assays (chapter 3, section 1) both in the presence and absence of ME. This is because reduction of Cys 190 residues is found to have an effect on Tm thermal stability and could potentially affect Tm ability to bind actin.

Figure 5.1 shows plots of the cooperative binding curves of different Tms to actin. The binding parameters i.e. the Tm concentration at which half of actin filaments are saturated ($K_{50\%}$) and the Hill coefficient *m*, were obtained by fitting the curves to a Hill equation. The parameter values are shown in Figure 5.1 table. The $K_{50\%}$ values obtained were 0.18 μM for WT αα Tm (n3), 0.51 μM for αα D175N Tm (n3) and 0.68 μM for αα E180G Tm (n3). The relative affinities remained the same when measured at 200 mM KCl concentration as the three affinities decreased by a factor of 3 (data not shown). This indicates that both mutations cause a decrease in the affinity of Tm binding to actin with a greater effect in the case of E180G mutation. The *m* value, which reflects the cooperative nature of the binding, is also affected by the two FHC mutations. The *m* value appears to be inversely proportional to the affinity of Tm for actin and is increased from 1.5-2 in the case of WT αα Tm (n3) to 2.5-3 and 3.5-4 in the case of αα D175N Tm (n3) and αα E180G Tm (n3) respectively. A change in the *m* value indicates a change in the cooperativity of the Tm binding to actin.

In order to investigate the effect of Tm reduction on the binding to actin, a sample of each of the three Tm was heated to 65 °C in the presence of 1 mM ME. The resulting Tm was then assayed for actin binding as detailed in chapter 3, section 1. No detectable change on the affinity for actin was apparent in the case of each Tm (see Figure 5.1 table).

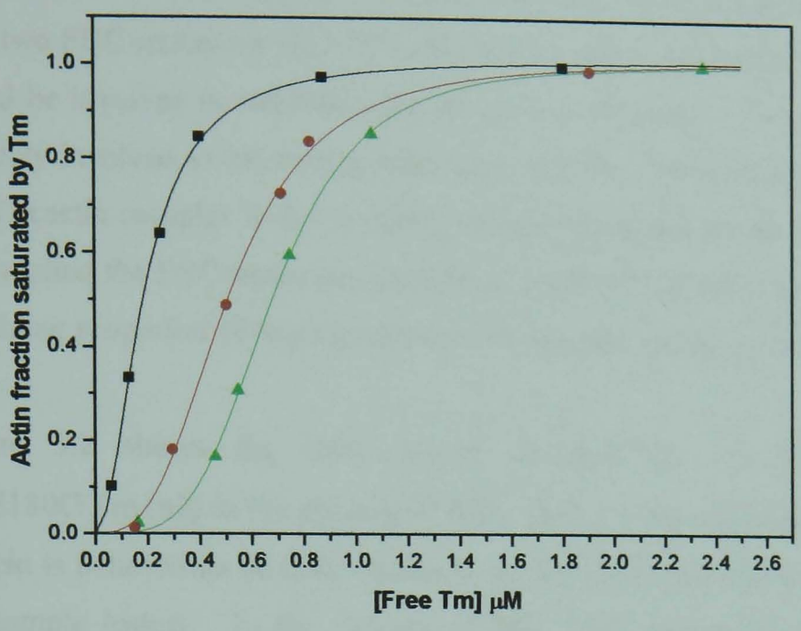

		$K_{50\%}$ (μM)	*m*
αα Tm (n3)	- ME	0.18	1.98
	+ ME	0.14	1.40
αα D175N Tm (n3)	- ME	0.51	2.98
	+ ME	0.44	2.53
αα E180G Tm (n3)	- ME	0.68	3.95
	+ ME	0.59	3.31

Figure 5.1: Binding curves of tropomyosin to actin. The binding of WT recombinant αα Tm (n3) (black) and its FHC mutants αα D175N Tm (n3) (red) and αα E180G Tm (n3) (green) to actin was investigated using co-sedimentation assays. The experiment details are outlined in chapter3, section 1. The curves are fitted to a Hill equation and the values obtained for both the $K_{50\%}$ (the concentration of free Tm at which half actin is saturated) and *m* (the Hill coefficient) are shown in the table.

2.2 Effect of FHC mutations on tropomyosin thermal stability

The two FHC mutations D175N and E180G result in the substitution of residues which could be involved in stabilising the coiled coil structure. These two residues are also possibly involved in interacting with actin and Tn. Therefore, the stability of Tm and the Tm.actin complex in the presence of such mutations could be significantly affected. We applied the DSC technique (chapter 3, section 4) in order to investigate the thermal unfolding properties of these proteins when free and bound to actin.

Figure 5.2 shows the DSC curves obtained for αα D175N Tm (n3) and αα E180G Tm (n3) in the absence of ME. Only the second heating is shown (when the protein is believed to be fully oxidised), as the first heating was variable depending on the sample history. In the absence of ME, both proteins showed a melting profile similar to that obtained with WT αα Tm (n3) (Figure 4.8), except for the presence of a small thermal transition at 35 °C for αα D175N Tm (n3) and 26 °C for αα E180G Tm (n3). Since these low-temperature transitions were not observed in the WT protein, they could therefore be assigned to the melting of the mutation-containing region of Tm. The E180G mutation therefore appears to have more destabilising effect compared to D175N mutation.

Figure 5.3 shows the thermal melting obtained from the second heating of αα D175N Tm (n3) in the presence of ME. As with the WT αα Tm (n3) (Figure 4.9), two melting transitions were obtained. The first peak at 42 °C corresponds to the melting of the C-domain of Tm with reduced Cys 190, the second peak at 52 °C is attributed to the melting of the N-domain part of Tm as well as the C-domain part with oxidised thiol groups (see chapter 4, section 2.6). The small transition at 35 °C can still be seen as a shoulder to the 42 °C peak. Interestingly, the αα E180G Tm (n3) under the same conditions showed a very small transition at 38 °C combined with the loss of the low temperature transition at 26 °C (Figure 5.4).

These results suggest that the E180G mutation, unlike the D175N, significantly affects the stability of the reduced C-domain of Tm and its ability to undergo reduction.

In the presence of actin three heating scans were performed on the same sample. During the first heating (shown in black) the sample was heated to 65 °C in order to reversibly unfold Tm and reduce its Cys groups. Actin remains intact in this case (actin melting transition happens at 80 °C and is not affected by the presence of Tm). After cooling the sample to 5 °C, it was heated again to 90 °C achieving the irreversible denaturation of actin. This allows the observation of the actin-induced transition under the conditions where Tm is reduced (see chapter 4, section 2.6). The third heating (shown in green) was to 65 °C and aimed at confirming the reversibility of Tm melting. DSC experiments with Tm.actin complexes were performed in the presence of ME.

The melting profile of WT αα Tm (n3) in complex with actin (Figure 4.10) showed the appearance of a new peak at 47 °C. This new peak was attributed to the melting of reduced C-domain of actin-bound Tm as it was not present in the third heating.

Figure 5.5 represents the DSC melting of αα D175N Tm (n3) when bound to actin. As with WT αα Tm (n3) (Figure 4.10) a new sharp peak appeared at 47 °C. As previously explained (chapter 4 discussion), Tm thermal denaturation only occurs upon dissociation from actin. Like with the WT αα Tm (n3), αα D175N Tm (n3) dissociates from actin at 46.5 °C (Kremneva and Levitsky, data not published). The 42 °C transition (in this case only seen in third heating), which in the presence of actin represents the melting of reduced C-domain of unbound Tm, was completely absent in both first and second heating. This is because actin was almost saturated with Tm (actin:Tm ratio of 1:6). As Tm becomes reduced in the second heating, a reduction in the size of the 52 °C peak is accompanied by an increase in the size of the 42 °C peak (chapter 4, section 2.6) under the conditions where Tm is in large excess. However, under the conditions where actin is not fully saturated by Tm, an increase in the size of the actin-induced peak at 47 °C was expectedly observed during the second heating. This is consistent with the assumption that the actin-induced transition at 47 °C originates from the melting transition of reduced C-domain. Overall, αα D175N Tm (n3) is indistinguishable from the WT protein.

The αα E180G Tm (n3) melting profile (Figure 5.6) showed significant differences to the WT αα Tm (n3) when bound to actin. The profile obtained from the first heating

was similar to that obtained in the absence of actin and ME (Figure 5.2) except for the complete disappearance of the small 26 °C transition and the appearance of a peak at 38 °C. This peak could therefore be assigned to the stabilisation by actin of the region of Tm where the mutation is located. During the second heating, a sharp new transition was observed at 42 °C. This transition was lost after the irreversible unfolding of actin (third heating). Also during the second heating a decrease in the size of the most thermostable transition was observed due to the reduction of Cys 190 residues. The profile from the third heating was similar to that obtained with free reduced αα E180G Tm (n3) (Figure 5.4).

Thus, DSC results show that significant differences exist between αα E180G Tm (n3) and WT αα Tm (n3), αα D175N Tm (n3) in the ability to undergo the actin-induced changes of the thermal unfolding of Tm.

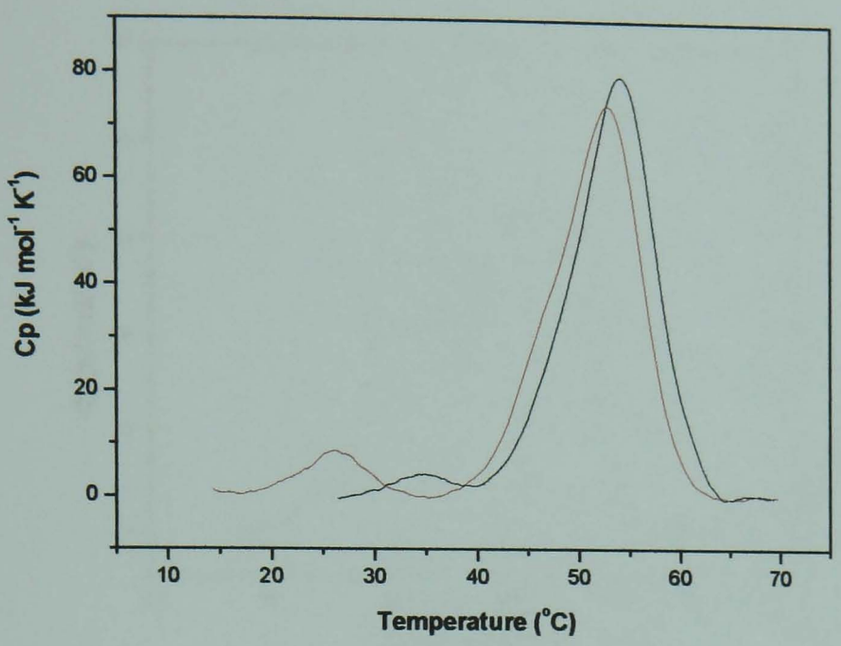

Figure 5.2: DSC melting profile of αα D175N Tm (n3) and αα E180G Tm (n3) in the absence of ME. 20 μM Tm was present in 20 mM Hepes, 100 mM KCl, 2.5 mM $MgCl_2$, pH 7.3. The thermal unfolding of αα D175N (n3) is shown in black. Two separate melting transitions with maxima at 35 °C and 53 °C were observed. The thermal unfolding of αα E180G (n3), shown in red, also showed two melting transitions but with maxima at 25 °C and 52.7 °C. Both mutants showed melting profiles similar to that observed with WT protein (Figure 4.8) except for the appearance of the small low-temperature transitions.

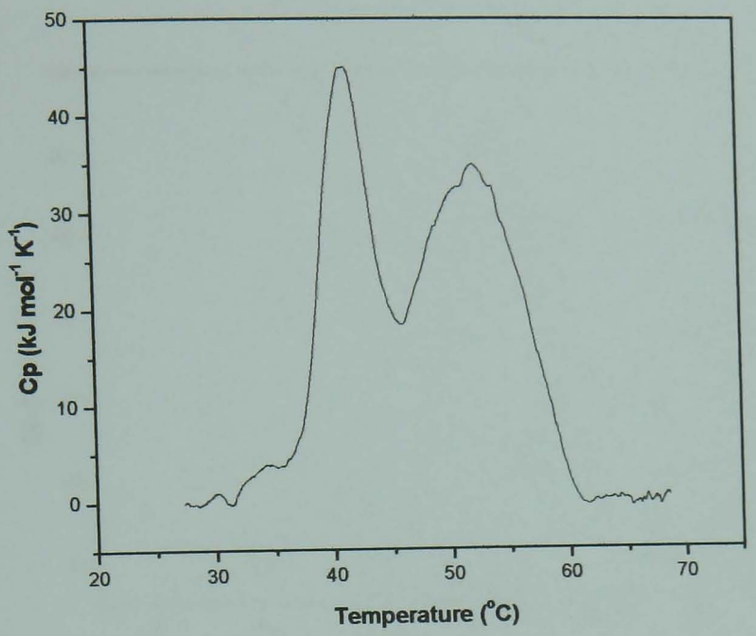

Figure 5.3: DSC melting profile of αα D175N Tm (n3) in the presence of ME. The thermal unfolding of reduced αα D175N (n3) (20 μM) was similar to that of the WT αα Tm (n3) in the presence of ME (Figure 4.9) with transitions at 42 °C and 52 °C. The small transition at 35 °C could also be seen. Buffer conditions were the same as described in Figure 5.2 legend except for the presence of 1 mM ME.

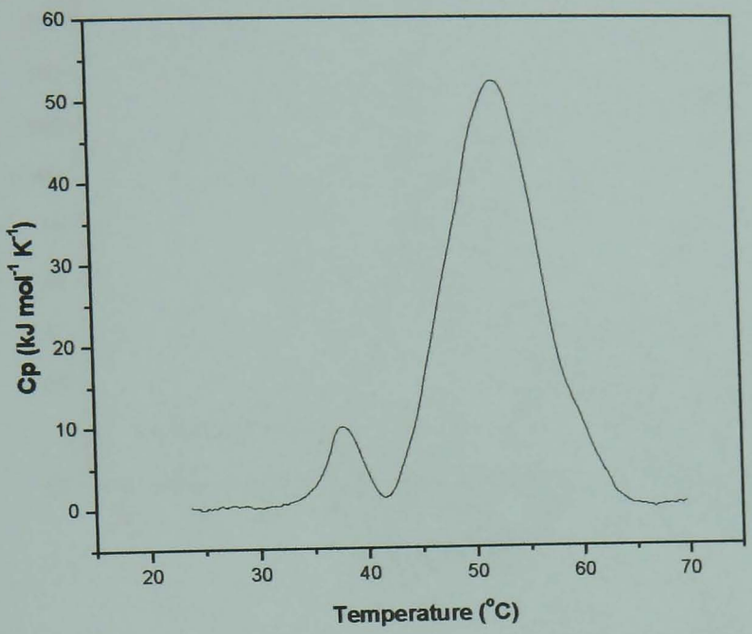

Figure 5.4: DSC melting profile of αα E180G (n3) in the presence of ME. The thermal unfolding of reduced αα E180G (n3) (20 μM) had Two separate melting transitions at 38 °C and 52 °C. Buffer conditions were the same as described in Figure 5.2 legend except for the presence of 1 mM ME.

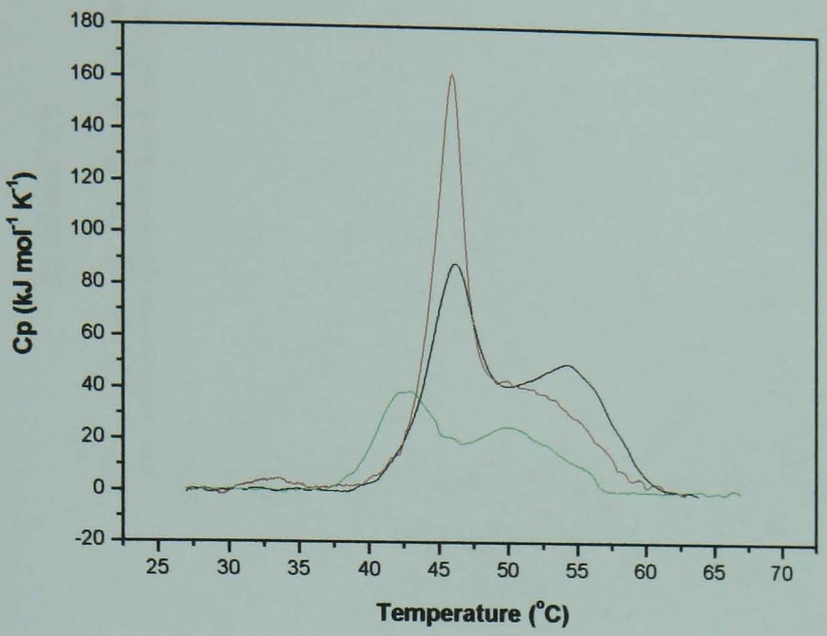

Figure 5.5: DSC melting profile of αα D175N Tm (n3) in complex with F-actin. 7.5 μM αα D175N Tm (n3) was mixed with 46.7 μM phalloidin-stabilised actin. Actin unfolds as a single transition with maximum at 80 °C (not shown). The first heating (black) to 65 °C had two transitions at 47 °C and 54 °C. The second heating to 90 °C (red) displayed the same maximum melting temperatures of the two transitions. The third heating (green) had two peaks at 42 °C and 52 °C. The αα D175N Tm (n3) meting profile in the presence of actin is identical to that of the WT protein (Figure 4.10). Buffer conditions were the same as described in Figure 5.2 except for the presence of 1 mM ME.

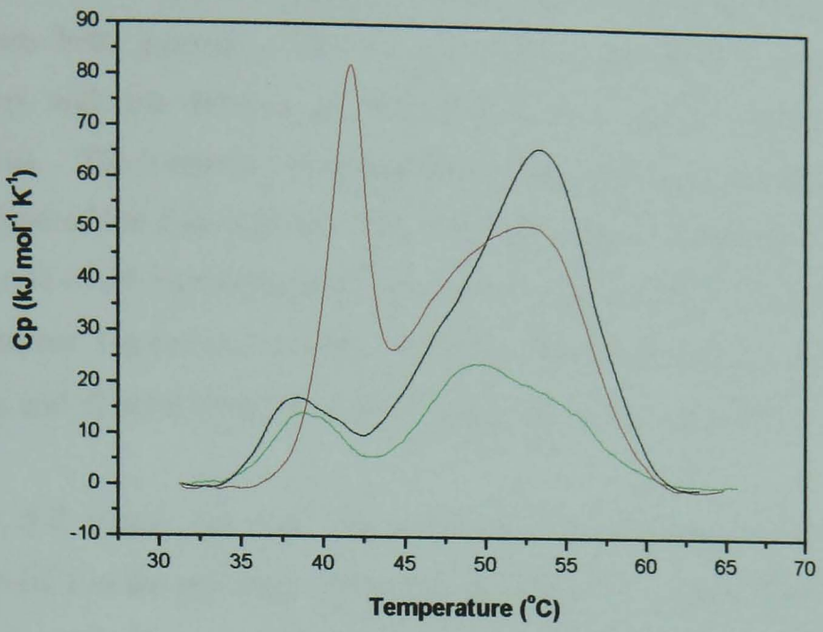

Figure 5.6: DSC melting profile of αα E180G Tm (n3) in complex with F-actin. 7.5 μM of αα E180G Tm (n3) was mixed with 46.7 μM phalloidin-stabilised actin (actin melting transition at 80 °C is not shown). The first heating to 65 °C (black) had two transitions at 38 °C and 52 °C similar to the profile obtained in Figure 5.4. The second heating to 90 °C (red) is characterised by the appearance of a sharp transition at 42 °C and the disappearance of the low-temperature transition. The third heating (green) is that of reduced free Tm. Buffer conditions were the same as described in Figure 5.2 legend except for the presence of 1 mM ME.

2.3 Effect of FHC mutations on the calcium sensitivity of the system

The two FHC mutations D175N and E180G are located in the Tm region which interacts with the TnT2 part of TnT (the TnT region that binds to TnI and TnC proteins). The presence of mutations in this region could affect the Ca^{2+}-mediated regulation of the thin filament. This was investigated by measuring the Ca^{2+} sensitivity of the rate of S1 binding to actin (chapter 3, section 2.4) in the presence of either WT or mutated αα Tm (n3) in complex with Tn. Since the same α-Tm gene is expressed in cardiac and skeletal muscles, both cTn and skTn were examined.

Figure 5.7 shows the Ca^{2+} sensitivity curves obtained for WT and FHC mutant αα Tm (n3) in the presence of phosphorylated cTn. This is shown in comparison with the Ca^{2+} sensitivity measurements obtained with ββ Tm (n3), whose overexpression in the heart was reported to be lethal (Muthuchamy *et al*, 1998). Both D175N and E180G mutations caused a shift in the midpoint of the Ca^{2+} sensitivity curve with a bigger effect reported in the case of E180G mutation. The Ca^{2+} sensitivity curve midpoint shift from 2.69 μM (WT αα Tm (n3)) to 2.18 μM and 1.99 μM in the case of αα D175N Tm (n3) and αα E180G Tm (n3) respectively, is consistent with an increase in the Ca^{2+} sensitivity of the thin filament. In other words, the presence of these two FHC mutations results in the thin filament remaining in the ON state at Ca^{2+} concentrations at which the WT system would normally be turned OFF. A greater shift was observed with ββ Tm (n3) (from 2.69 μM to 1.54 μM). The *h* value in this case is as expected around 1.0 as the cTnC protein has only one functional Ca^{2+}-binding site. The results described above were reproducible when measurements were repeated with proteins from different preparations.

Figure 5.8 shows the Ca^{2+} sensitivity measurements obtained with WT αα Tm (n3) and FHC mutations D175N and E180G in the presence of skTn. A very small increase in the Ca^{2+} sensitivity, which was relatively greater in the case of E180G mutation, was reported. Interestingly, the *h* value did differ between WT and mutant Tms. The cooperativity measured in this case is believed to occur between the Ca^{2+}-binding sites on TnC. In the presence of sk Tn complex, the *h* value is normally around or higher than 1.5, as there are two functional Ca^{2+} binding sites in sk TnC. The *h* value in the

case of the two mutants in the presence of sk Tn is similar to that obtained with cTn (compare values in Figure tables 5.7 and 5.8). This suggests that the presence of either of the two FHC mutations in skeletal muscle does not affect the Ca^{2+} sensitivity of the system to a great extent but does rather affect the cooperativity between the Ca^{2+} sites of TnC.

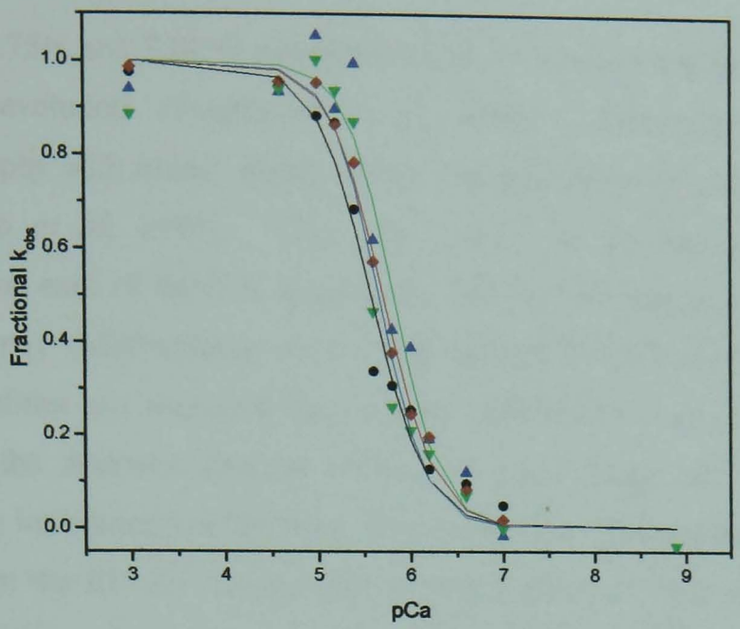

	$h \pm$ SE	$K_{50\%} \pm$ SE	Midpoint [Ca^{2+}] (μM)	Shift in [Ca^{2+}] (μM)
αα Tm (n3)	1.15 ± 0.09	5.57 ± 0.08	2.69	-
αα D175N Tm (n3)	1.21 ± 0.09	5.66 ± 0.07	2.18	0.51
αα E180G Tm (n3)	1.16 ± 0.04	5.70 ± 0.03	1.99	0.70
ββ Tm (n3)	1.20 ± 0.10	5.81 ± 0.07	1.54	1.15

Figure 5.7: Ca^{2+} sensitivity measurements for S1 binding to pyrene-actin in the presence of either WT αα Tm (n3), αα D175N Tm (n3) or αα E180G Tm (n3) in complex with cTn. The Ca^{2+}-sensitivity curves were obtained by plotting the k_{obs} values for S1 binding to pyrene-actin as a function of pCa (Figures 3.6 and 3.7). The curves were fitted to a Hill equation to determine both the midpoint of the curve ($K_{50\%}$) and the Hill coefficient (*h*). Parameters obtained from curve fitting are shown in the table above. The standard error (SE) was obtained from fitting the data shown in this graph. WT αα Tm (n3), αα D175N Tm (n3) and αα E180G Tm (n3) curves are shown in black, blue and red respectively. Both FHC mutants expressed in Tm caused a shift of 0.09 pCa (αα D175N Tm (n3)) and 0.13 pCa (αα E180G Tm (n3)) from the midpoint of the WT protein complex (pCa 5.57). This corresponds to a midpoint Ca^{2+} concentration increase of 0.50 μM and 0.70 μM from the 2.69 μM obtained with αα Tm (n3). Ca^{2+}-sensitivity measurements for S1 binding to pyrene-actin in the presence of ββ Tm (n3) is shown in green. A shift of 1.15 μM in the midpoint Ca^{2+} concentration was observed.

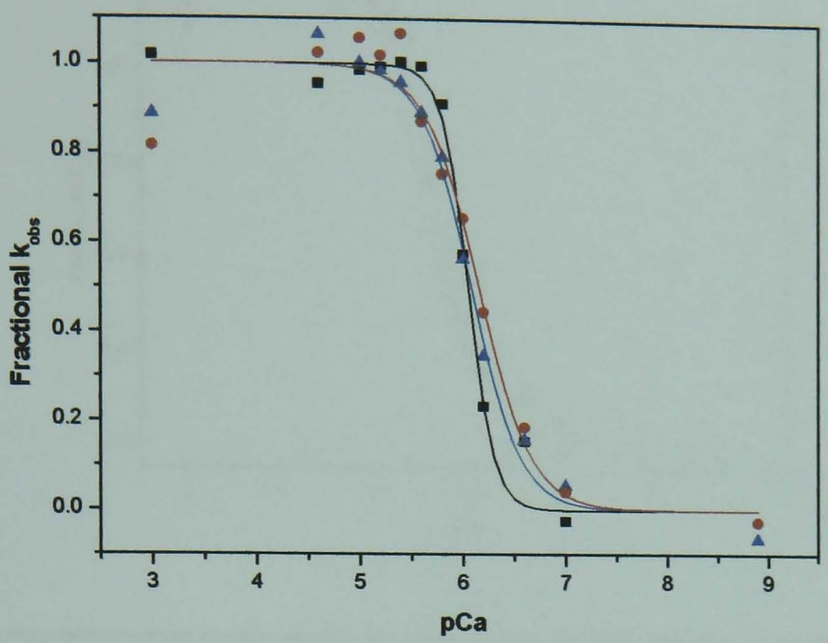

	$h \pm$ SE	$K_{50\%} \pm$ SE	Midpoint [Ca^{2+}] (μM)	Shift in [Ca^{2+}] (μM)
αα Tm (n3)	1.47 ± 0.09	6.05 ± 0.03	0.89	-
αα D175N Tm (n3)	1.22 ± 0.07	6.08 ± 0.04	0.83	0.06
αα E180G Tm (n3)	1.19 ± 0.10	6.15 ± 0.07	0.70	0.19

Figure 5.8: Ca^{2+} sensitivity measurements for S1 binding to pyrene-actin in the presence of either WT αα Tm (n3), αα D175N Tm (n3) or αα E180G Tm (n3) in complex with skTn. The experimental details are outlined in Figure 5.7. The curves for WTαα Tm (n3), αα D175N Tm (n3) and αα E180G Tm (n3) are shown in black, blue and red respectively. The midpoint of the curve ($K_{50\%}$) and the Hill coefficient *h* are shown in the table. The standard error (SE) was obtained from fitting the data shown in this graph.

3 Discussion

Both D175N and E180G mutations occur in residues that have been highly conserved during evolution (Thierfelder *et al*, 1994). However, D175N causes cardiac hypertrophy with milder effects on the life expectancy of patients compared to E180G (Coviello *et al*, 1997). This was verified by producing transgenic mouse lines expressing each of the FHC mutations. The D175N mutation was found to cause mild hypertrophy (Muthuchamy *et al*, 1999) whereas E180G mutation caused severe cardiac abnormalities and ultimately led to death (Prabhakar *et al*, 2001). This is most likely due to the dramatic changes (change in both charge and side chain size) E180G mutation introduces into the helix structure of Tm. The results presented in this chapter show that the E180G mutation has a greater effect on both the overall stability of Tm and its ability to bind actin as compared to D175N and WT Tm.

Tm ends sequences were found to be crucial for its normal binding to actin, (Cho *et al*, 1990; Cho and Hitchcock-DeGregori, 1991, Urbancikova and Hitchcock-DeGregori, 1994). However, single point mutations introduced at a distance from the Tm ends are found to have a major effect on the ability of Tm to bind actin. Both D175N and E180G mutations significantly decrease the affinity of Tm for actin, a bigger effect is observed with E180G (The affinity was reduced by a factor of 2.8 in the case of D175N mutation and by a factor of 3.8 in the case of E180G). These results contrast with those published by Golistina *et al* (1994) who reported a small decrease in the affinity in the presence of D175N and a significant loss of actin affinity in the presence of E180G (2-3 fold decrease). However, those measurements were carried out with bacterially expressed Tm which lacked the N-terminal Ala-Ser extension (see chapter 4, section 1.1). Bing *et al* (1997) also reported a considerable decrease in the E180G Tm affinity for actin as compared with WT but saw no significant change in the affinity of D175N Tm. However, as the salt concentration under which the experiments were performed was low, the binding affinities were very tight and hence not well defined.

The Hill coefficient *m*, which reflects the cooperative nature of Tm binding to actin, is also altered in the presence of the two FHC mutations. In systems where ligand binding to a multi-subunit protein occurs in a cooperative manner, the *m* value reflects the number of protein sites available for ligand binding. However, this rule cannot apply to

the more complex binding of Tm (long filamentous protein) to the multi-subunit actin protein (one Tm binds seven actin monomers). The physical meaning of *m* in this particular case can only be described if the binding of Tm to actin is fitted to a mathematical model that would describe all the possible states of such a complex reaction. For instance, the Tm can either polymerise in solution and then bind actin or undertake the head to tail polymerisation on the surface of actin. It is however likely that an equilibrium between a combination of all these states exists, with distribution between states dependent on experimental conditions.

Although a loss in the affinity of Tm for actin is caused by the two FHC mutations, the affinity between Tm ends should be unaffected. In other words, the mutant Tms should undergo normal head to tail polymerisation but with much weaker binding to actin. The WT Tm which has a high affinity for actin (0.2 μM) is likely to bind actin and polymerise into a long filament concomitantly. In the case of Tm carrying the FHC mutations, the equilibrium for Tm polymerisation could be favoured over the equilibrium for binding actin resulting in Tm binding to actin as a longer filament rather than shorter ones. Alternatively, the presence of a mutation in Tm could introduce a twist in the molecule when bound to actin. This could affect the conformation of Tm ends, preventing the normal head to tail polymerisation process to take place on the surface of actin. In both situations, the *m* values would be inversely proportional to the binding affinity values.

Both D175N and E180G FHC mutations destabilise the local structure of Tm as revealed by the DSC measurements when Tm is oxidised. Yet again a bigger effect is observed in the case of E180G mutation. This is in good agreement with Golistina *et al* (1997) conclusions of partial unwinding of the coiled coil in the region of the mutations as revealed by an increase in ratio of labelling of Cys 190 with pyrene. Even though both D175N and E180G mutations are in the proximity of Cys190, the response to reduction by ME was different. While unfolding of reduced D175N was similar to that of WT Tm, reduced E180G unfolding suggested that this mutation destabilises the C-domain of Tm, which in this case unfolds at 38 °C instead of 42 °C. In the presence of actin, D175N Tm melting profile is indistinguishable from that of WT Tm. The WT Tm has a relatively unstable C-domain as it starts unfolding at about 37 °C, the resting

Missing pages are unavailable

1998). This is also consistent with the fact that FHC is not a severe disease condition as it is lethal only in adulthood.

An increase in Ca^{2+} sensitivity of the heart can be linked to an increase in relaxation time and hence a decrease in the recovery time between two heart beats. The hypertrophy is therefore believed to be a compensatory mechanism for the hypercontractile state of the heart (Bonne *et al*, 1998).

When the mutant Tms were associated with skTn, the Ca^{2+} sensitivity of the system did not appear to be affected as seen with the cTn. However, the Hill coefficient value was lower than expected and similar to that obtained with cTn. The cooperativity measured in this case is thought to be that of the Ca^{2+}-binding sites of TnC as it is around 1.0 in the case of cardiac Tn (one Ca^{2+}-binding site) and less than 2.0 in the case of skeletal Tn (Ca^{2+}-binding sites). The MWC model of cooperativity (see chapter 3, section 3.2.3.1) is defined by three parameters: the equilibrium constant between the low- and the high-affinity state for ligand binding, the equilibrium constant for ligand binding to each state and the ratio between the two binding affinities (Figure 3.9). Alterations in any of these parameters will result in variations in the nature of cooperative system.

CHAPTER 6

STUDY OF FHC MUTATIONS EXPRESSED IN TROPONIN

1 Introduction

A number of FHC-associated mutations in the cardiac Tn complex proteins have been described in the literature. Kimura *et al* (1997) reported the presence of six of these mutations in the cardiac TnI gene interestingly all located at the C-domain of the protein (R145G, R145Q, R162W, S199N, G203S and K206Q). So far, only one mutation (L29E) in the cardiac TnC gene has been associated with the FHC disease (Hoffmann *et al*, 2001). Residue 29 in TnC is located in the surface loop that links the two Ca^{2+}-binding sites of the regulatory domain of TnC (Figure 1.14). Residues 203 and 206 in TnI are located at the C-terminal end of the protein. This is the regulatory domain of TnI which interacts with actin.Tm complex in a Ca^{2+}-dependent manner.

The cardiac TnI protein contains a 31-amino acid extension at the N-terminal part of the protein which does not exist in the skeletal counterparts (Wilkinson and Grand, 1978). In this extension, two adjacent serine residues at position 22 and 23 in the human sequence become phosphorylated by c-AMP dependent protein kinase PKA (Mittmann *et al*, 1990) in response to β-adrenergic stimulation of the heart (England, 1975; Solaro *et al*, 1976). The phosphoserines are dephosphorylated by the action of protein phosphates 2A (PP2A) (Mumby *et al*, 1987; Mittmann *et al*, 1992).

The effect of phosphorylation on the Ca^{2+} sensitivity of the system has been investigated in a number of ways. Ca^{2+}-activated force measurements in skinned muscle (Zhang *et al*, 1995a) as well as myofibrillar Ca^{2+}-activated ATPase activity (Bailin, 1979) showed that phosphorylation of TnI resulted in a decrease in the pCa value at which half-maximal force and ATPase is achieved. This was consistent with results obtained from reconstituting skinned cardiac muscle with human recombinant TnI containing either a Ser-Ala or a Ser-Asp mutation at positions 22 and 23 to mimic the dephosphorylated and bisphosphorylated states of TnI respectively (Dohet *et al*, 1995). Measurements of the Ca^{2+}-dependent binding of S1 to actin carried out with isolated proteins in solution also gave the same results (Reiffert *et al*, 1996). All these results suggest that TnI phosphorylation decreases the Ca^{2+} sensitivity of the system i.e. switching of the filament from the ON to the OFF state occurs at higher Ca^{2+}concentrations. This could be linked to the finding that Tn phosphorylation resulted in reduced Ca^{2+} affinity for TnC (Robertson *et al*, 1982; Zhang *et al*, 1995b).

It was not clear how the phosphorylation of the N-terminal end of TnI influenced the Ca^{2+} binding properties at the N-terminal end of TnC. NMR studies conducted by Jaquet *et al* (1998) suggested that when TnI is monophosphorylated on either Serine residue, the phosphorylation region of TnI does not interact with TnC, TnT or TnI structures. In the bisphosphorylated form, the NMR measurements obtained were used to postulate a likely interaction with the N-domain of TnC explaining the influence on the Ca^{2+} binding properties. Later on, Schmidtmann *et al* (2002) suggested that TnI in the bisphosphorylated form interacted rather with TnT and TnI and not TnC.

Ward and co-workers (2002) put forward another model to explain the molecular mechanisms by which the phosphorylation signal could be transmitted, by identifying the structural regions in the TnI N-domain required for such a process to happen. Their results indicated that deletion of residues 16-29 of the cardiac specific N-terminal extension had the same effect as phosphorylation. They therefore concluded that residues 16-29 when unphosphorylated bind to TnC and stabilise the open state of the protein (the Ca^{2+}-bound state). This action is reversed when the sequence is phosphorylated or deleted.

In this work, the two mutations in TnI (G203S and K206Q) and the mutation in TnC (L29E) have been investigated in terms of their effects on 1) the Ca^{2+} sensitivity of the system 2) the binding properties of S1 to actin and 3) the switching between the three states of the thin filament. Also, the effect of TnI phosphorylation on the Ca^{2+} sensitivity of the system was examined. The results obtained show that all the mutations were indistinguishable from WT except for the K206Q mutation in TnI which was found to affect the Ca^{2+} sensitivity of the system but only when TnI is phosphorylated.

2 Troponin protein preparation

In this study, human cardiac Tn proteins (hcTn) were used. The proteins were cloned, expressed, purified and reconstituted by Anja Schmidtamnn (University of Bochum, Germany). The protein subunits were reconstituted by mixing a 1:1:1 ratio of hcTnI, hcTnC and hcTnT. Phosphorylation of the two Ser residues in the N-terminal arm of TnI was achieved using the recombinant catalytic subunit of Protein Kinase A. TnI bisphosphorylation was checked by Isoelectric Focusing. The details of these preparations are outlined in Lohmann *et al* (2001) and Schmidtamnn *et al* (2002).

Dephosphorylation of TnI was achieved by incubating the 2 μM phosphorylated Tn complex with 2 μM Tm and 5 μM actin in the experimental buffer for 30 min at room temperature to allow the reconstitution of the thin filament complex. Protein Phosphatase 2A (PP2A) was used in the presence of 0.7 mM $MnCl_2$. The solution was then incubated for 5 hours at room temperature. The protein solution was dialysed overnight against the experimental buffer.

3 Results

3.1 Effect of FHC mutations on the calcium sensitivity of the system

Measurements of the Ca^{2+} sensitivity of the system for WT hcTn as well as hcTn expressed with the three different FHC mutations in its components was carried out in order to look at the effect these mutations might have on the Ca^{2+} -dependent regulation of the filament.

Figure 6.1 shows the Ca^{2+}-dependence of the observed rate constant for S1 binding to pyrene-actin. The sigmoid curves were fitted to a Hill equation and both the midpoint of the curve ($K_{50\%}$) and the Hill coefficient (h) were determined and are shown in the table. The results obtained showed that the Ca^{2+} sensitivity properties of the thin filament in the presence of either L29E mutation in TnC or G203S mutation in TnI are indistinguishable from the WT system. However, a 0.28 pCa shift from the 5.80 pCa midpoint obtained with the WT complex was observed in the case of K206E. This corresponds to a shift in the Ca^{2+} concentration midpoint from 1.58 μM to 0.83 μM. This result indicated that K206E caused an increase in the Ca^{2+} sensitivity of the thin filament.

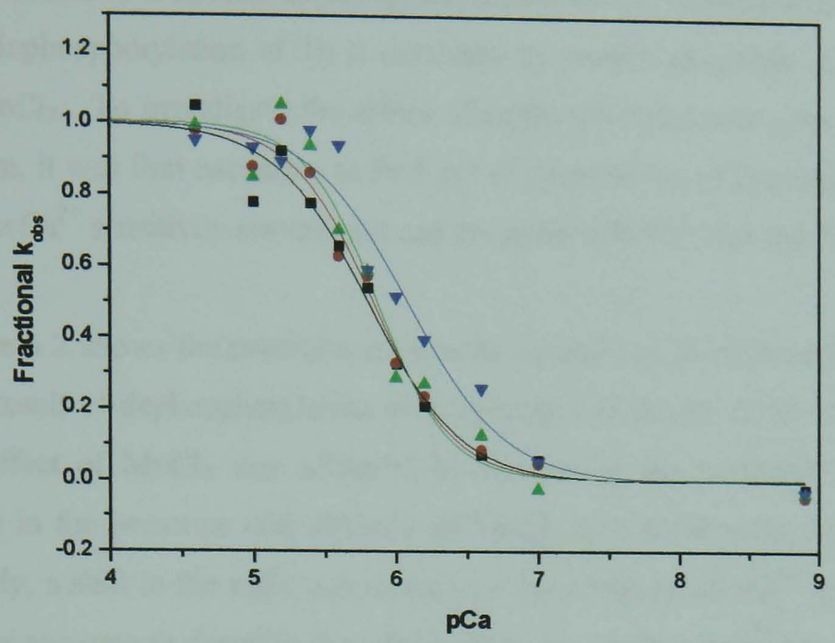

	h ± SE	$K_{50\%}$ ± SE	Midpoint [Ca2+] (μM)	Shift in [Ca2+] (μM)
WT Tn	1.10 ± 0.08	5.80 ± 0.08	1.58	-
TnC L29E	1.16 ± 0.08	5.84 ± 0.06	1.45	0.13
TnI G203S	1.20 ± 0.10	5.86 ± 0.07	1.38	0.20
TnI K206Q	1.08 ± 0.10	6.08 ± 0.10	0.83	0.75

Figure 6.1: Ca^{2+}-sensitivity measurements for S1 binding to pyrene-actin in the presence of phosphorylated human cardiac Tn (hcTn) complex. The binding of S1 (0.25 μM) to pyrene-actin (2.5 μM) was monitored at different pCa values in the presence of skTm (1 μM) and phosphorylated hcTn (1 μM). Three FHC mutations were analysed, L29E in TnC (red), G203S in TnI (green) and K206Q in TnI (blue). The trace for the WT complex is shown in black. The measurements were carried out at 20 °C in 20 mM MOPS, 140 mM KCl, 5 mM $MgCl_2$, 1 mM DTT at pH 7.0. The curves were fitted with a Hill equation. Both the midpoint of the curve ($K_{50\%}$) and the Hill coefficient (*h*) are shown in the table. The standard error (SE) on the data is obtained from fitting the dataset shown in the graph. A 0.28 pCa shift from the 5.80 pCa midpoint obtained with WT protein was observed in the case of K206E mutation expressed in TnI. This corresponds to a 0.75 μM shift in the Ca^{2+} concentration midpoint of the curve from 1.58 μM to 0.83 μM.

3.2 Effect of troponin dephosphorylation on the calcium sensitivity of the system

The dephosphorylation of Tn is catalysed by protein phosphatase PP2A in the presence of $MnCl_2$. To investigate the effect of dephosphorylation on the Ca^{2+} sensitivity of the system, it was first necessary to find out if the presence of the cation Mn^{2+} has any effect on the Ca^{2+} sensitivity curves as it can compete with Ca^{2+} for the TnC binding sites.

Figure 6.2 shows the control experiments carried out in order to test that any effect seen as a result of dephosphorylation is independent of the presence of $MnCl_2$. Investigating the effect of $MnCl_2$ was achieved by comparing the midpoint of the Ca^{2+} sensitivity curve in the presence and absence of $MnCl_2$ (0.7 mM) when hcTn is phosphorylated. Clearly, a shift to the right was caused by the presence of Mn^{2+} ions. However, it might not be accurate to describe this observation as a shift as Mn^{2+} can compete with Ca^{2+} for EGTA, altering the free Ca^{2+} concentration of the pCa solution. It was therefore essential to remove the $MnCl_2$ from the buffer after dephosphorylation by means of dialysis, the efficiency of which was also checked. Figure 6.2 shows that phosphorylated hcTn to which 0.7 mM $MnCl_2$ was added and then removed by dialysis behaved like the untreated phosphorylated hcTn complex. This suggested that dialysis was effective. All the parameters that describe the Ca^{2+} sensitivity curves are shown in the table.

Figure 6.3 shows the effect dephosphorylation has on the Ca^{2+} sensitivity of the system. In order to make the results comparable, the measurements for both phosphorylated and dephosphorylated complexes were carried out at the same time using the same proteins and pCa solutions. Figure 6.3A shows the Ca^{2+} sensitivity measurements for the phosphorylated complexes. The results are comparable to Figure 1 results and as before, only K206E mutation in TnI shows a shift in the midpoint of the Ca^{2+} sensitivity curve. However, the size of the shift is bigger than what was previously found (0.6 pCa shift as compared to 0.28 pCa shift). Figure 6.3B shows the Ca^{2+} sensitivity curves for the dephosphorylated complexes. In this case all the three mutation-containing complexes were indistinguishable from the WT system. These findings are very interesting as they suggest that the effect of an FHC mutation expressed in the C-domain of TnI on the Ca^{2+} sensitivity of the thin filament depends on the phosphorylation state of the TnI N-domain. These results also showed that while WT, L29E mutation in TnC and G203S mutation in TnI caused the expected increase in the Ca^{2+} sensitivity (shift in the curve

midpoint from 5.7 to 5.85), K206E mutation in TnI caused a decrease in Ca^{2+} sensitivity (shift in the curve midpoint from 6.27 to 5.83). As a consequence, dephosphorylated Tn carrying the K206E mutation in TnI has the same Ca^{2+} -sensitivity as the WT protein complex.

3.3 Effect of FHC mutations on the K_B value

K_B defines the equilibrium constant between the blocked and closed states of the thin filament and is defined by the ratio of the observed rate constant for S1 binding to pyrene-actin in the presence and absence of Ca^{2+} (k_{obs} ($+Ca^{2+}$)/k_{obs} ($-Ca^{2+}$) = K_B/1+K_B) (see chapter 3, section 2.4.1). The calculated K_B values for WT system and in the case of each mutation are shown in table 6.2. The K_B, with a value of 0.6, is unchanged in each case and is comparable to previously published values (Reiffert *et al*, 1996). This result suggests that the presence of the FHC mutations under investigation in the Tn complex does not influence the extent by which the filament is switched OFF when Ca^{2+} is removed.

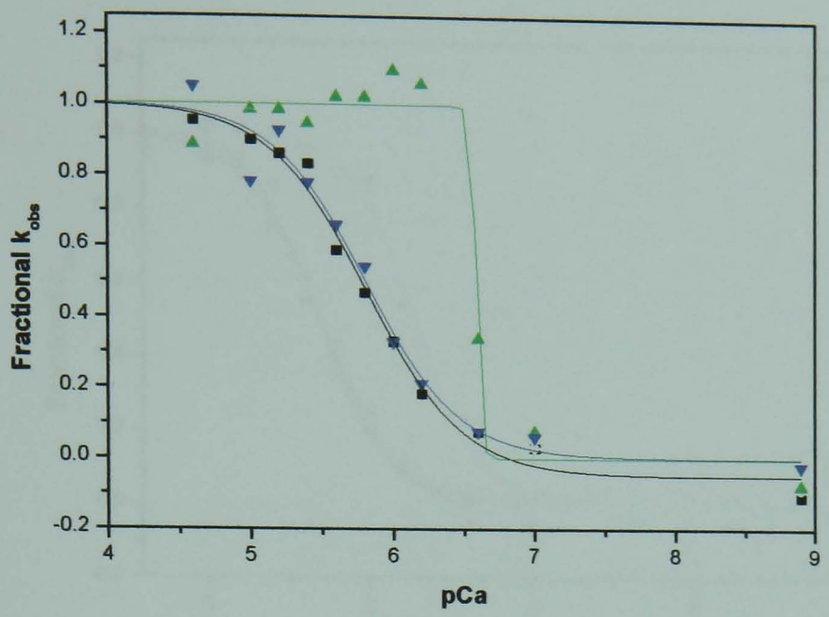

	$K_{50\%}$ ± error	*h*± error
Phosphorylated WT hcTn +$MnCl_2$+dialysis	5.8 ± 0.05	1.13 ± 0.06
Phosphorylated WT hcTn +$MnCl_2$	6.58	2.21
Phosphorylated WT hcTn	5.8 ± 0.08	1.10 ± 0.08

Figure 6.2: Effect of $MnCl_2$ on the Ca^{2+} sensitivity measurements. The experimental conditions and the details of the fitting are described in Figure 6.1 legend. Phosphorylated WT hcTn from which $MnCl_2$ (0.7 mM) was removed by means of dialysis is shown in black. Phosphorylated WT cTn with no added $MnCl_2$ is shown in blue. The effect of $MnCl_2$ on the Ca^{2+} sensitivity curve is shown in green.

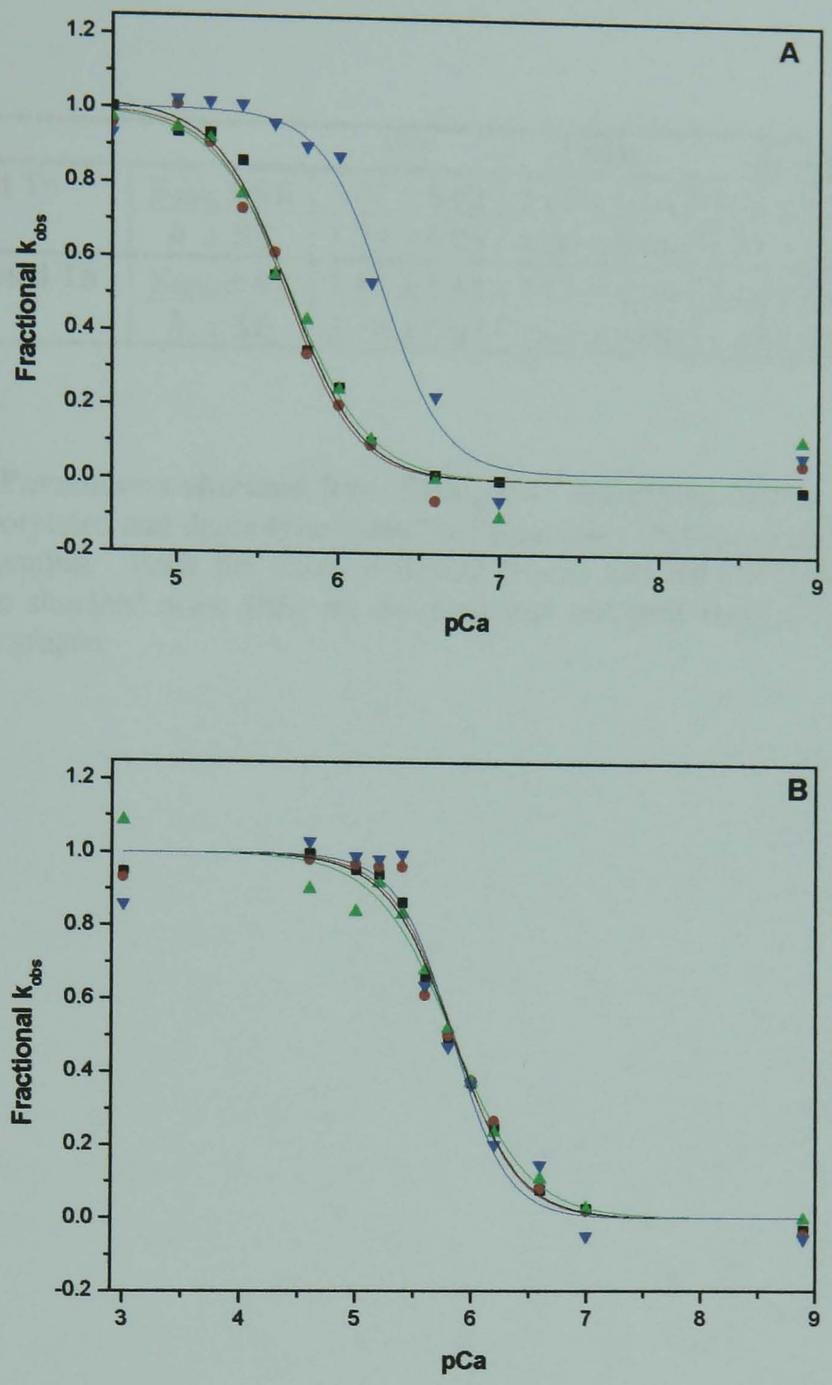

Figure 6.3: Effects of Tn dephosphorylation on the Ca^{2+} sensitivity of the system. The measurement were carried out in the presence of phosphorylated (A) and dephosphorylated (B) hcTn both WT and in the presence of different FHC mutations. Both the experimental conditions and the fitting procedures are detailed in Figure 6.1 legend. In both graphs WT is shown in black, TnC L29E mutation in red, TnI G203S mutation in green and TnI K206Q mutation in blue. The fitting parameters are shown in Table 6.1.

		WT	L29E	G203S	K206Q
Phosphorylated Tn	$K_{50\%} \pm SE$	5.68 ± 0.03	5.67 ± 0.04	5.70 ± 0.05	6.27 ± 0.05
	$h \pm SE$	1.25 ± 0.05	1.26 ± 0.06	1.21 ± 0.08	1.30 ± 0.09
Dephosphorylated Tn	$K_{50\%} \pm SE$	5.84 ± 0.03	5.85 ± 0.06	5.84 ± 0.06	5.83 ± 0.07
	$h \pm SE$	1.15 ± 0.04	1.17 ± 0.08	1.10 ± 0.06	1.22 ± 5.83

Table 6.1: Parameters obtained from fitting Ca^{2+} sensitivity curves. The curves for both phosphorylated and dephosphorylated hcTn complex shown in Figure 6.3 are fitted to a Hill equation. Both the curve midpoint ($K_{50\%}$) and the Hill coefficient (h) are shown. The standard error (SE) on the data was obtained from fitting the datasets shown in the graphs.

3.4 Effect of FHC mutations on S1 binding to actin

Titration of pyrene-actin with S1 in the presence of skTm and hcTn and its mutants both in the presence and absence of Ca^{2+} was used in order to define the three-state model parameters (chapter 1, section3.1).

Figure 6.4 shows the binding curve of S1 to actin in the presence of WT hcTn. As previously reported (Maytum *et al*, 1999; Maytum *et al*, 2003) both binding curves have a sigmoid character, which reflects the cooperative binding of S1 to actin when bound to regulatory proteins. However, the sigmoidicity is more prominent when Ca^{2+} is absent as more S1 is needed to bind actin before the filament is turned into the ON state. Curve fitting of the data gives values for the parameters as shown in table 6.2. As expected, the K_T value shows a 5-fold decrease from 0.11 to 0.022 on Ca^{2+} removal as it has been shown to be Ca^{2+}-dependent (Maytum *et al*, 1999). The value for K_1, which in combination with K_2 (K_1K_2) defines the overall affinity of S1 for actin, is about 80-100 M^{-1}. The K_2 is fixed at the independently determined value of 200 for nucleotide-free S1 (Coates *et al*, 1985). Values for the apparent cooperative unit size (n) are similar in the presence and absence of Ca^{2+}. In both cases, n varies between 7 and 8. This result is inconsistent with the published data of Maytum *et al* (1999, 2003) where n is reported to be around 7 in the absence of Ca^{2+} and larger than 10 in the presence of Ca^{2+}. The K_B equilibrium constant between blocked and closed states is determined with stopped-flow measurements of the rate of S1 binding to actin in the presence and absence of Ca^{2+} as described in section 3.3.

When the experiment was repeated with the Tn complex containing the FHC mutations, there was no noticeable difference with the WT system, suggesting that these FHC mutations do not interfere with the switching between the different regulatory states, or with the binding properties of S1 to actin.

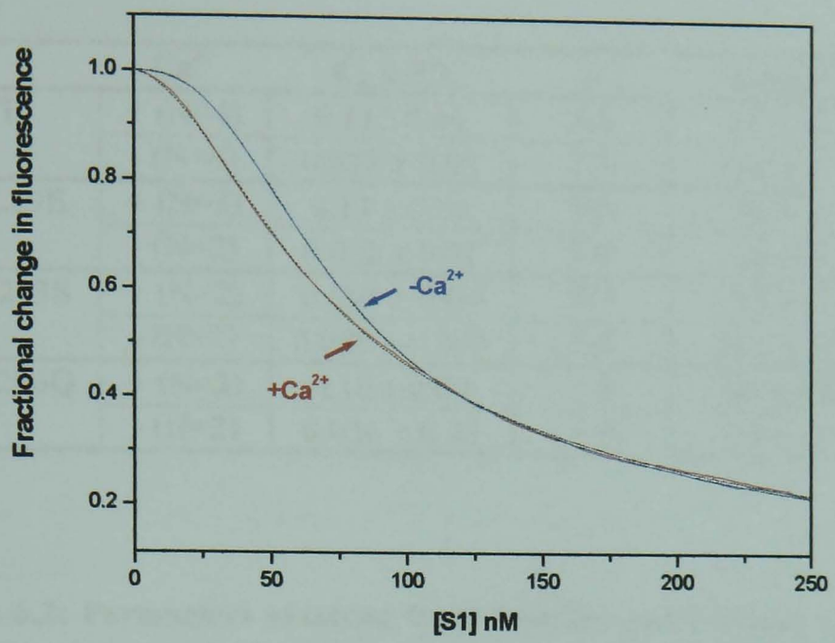

Figure 6.4: Effect of FHC mutations on the binding of S1 to actin. S1 was continuously titrated into a stirred cuvette that contained 50 nM phalloidin- stabilised pyrene-actin and 0.2 μM of both skTm and phosphorylated hcTn in the presence and absence of Ca^{2+}. The curves shown in the graph were obtained with WT hcTn. S1 binding was monitored by fluorescence quenching of the pyrene label. The measurements were carried out at 20 °C and the buffer was 20 mM MOPS, 200 mM KCl, 5 mM $MgCl_2$, 1 mM DTT at pH 7.0. The curves were fitted using the three-state model equation. The raw (continuous) and fitted (dashed) data are superimposed. The parameters that define these curves are shown in Table 6.2.

	Ca^{2+}	$K_T \pm SD$	*n*	$K_1 \pm SD$	K_B
WT	+ (N=4)	0.11± 0.04	7-8	86 ± 13	> 10
	- (N=4)	0.022 ± 0.01	7-8	100 ± 10	0.6
TnC L29E	+ (N=3)	0.13 ± 0.08	7-8	80 ± 7	> 10
	- (N=2)	0.022 ± 0.01	7-8	96 ± 6	0.6
TnI G203S	+ (N=2)	0.095 ± 0.04	7-8	83 ± 4	> 10
	- (N=2)	0.028 ± 0.002	7-8	105 ± 12	0.6
TnI K206Q	+ (N=2)	0.10 ± 0.02	7-8	90 ± 10	> 10
	- (N=2)	0.026 ± 0.03	7-8	93 ± 10	0.6

Table 6.2: Parameters obtained from titration curve fitting of Figure 6.4 data. The three-state model parameters were determined for both the WT and the three FHC mutations expressed in the hcTn components. K_B and K_T are the equilibrium constants between the blocked - closed and closed-open states of the filament respectively. K_1 is the equilibrium constant for the weak binding of S1 to actin and *n* in the cooperative unit size of actin that switches between states. K_B values were obtained independently from stopped-flow experiments. The number of curves analysed is indicated between brackets.

4 Discussion

The C-domain of TnI is where the inhibitory activity of TnI is localised. In the cardiac isoform sequence, residues 150-159 interact with TnC N-domain when Ca^{2+}-saturated. This interaction drives the detachment of two regions of TnI, which in the absence of Ca^{2+} bind to actin and inhibit the acto-myosin ATPase activity. The two FHC mutations expressed in TnI (G203S and K206Q) are located in a region of TnI C-domain that is believed not to have a direct contact with Tn but which can bind actin and relocate along side the inhibitory regions of TnI in a Ca^{2+}-dependent manner (Takeda *et al*, 2003). The two mutations though found in close proximity in TnI were reported to result in slightly different phenotypes. Patients with K206Q developed the characteristic hypertrophy, whereas those with G203S exhibited a hypertrophy only at the apex of the heart (Kimura *et al*, 1997). The result obtained in this study showed that while the Tn complex with G203S mutation in TnI behaved like WT, Tn complex containing K206Q caused an increase in the Ca^{2+}-sensitivity of the thin filament. This result is in agreement with published data by Takahashi-Yanaga *et al* (2001). The authors replaced endogenous TnI with expressed human TnI carrying the FHC mutations into porcine myofibrils and reported a large increase in Ca^{2+} sensitivity with K206Q mutation and not a significant difference between WT and G203S mutation. The FHC mutation expressed in TnC (L29E) also did not have any effect on the Ca^{2+}-sensitivity of the thin filament. The mutated residue is located in the surface loop that joins the Ca^{2+}-binding sites I and II located at the N-domain of TnC.

Assessing the effect of these FHC mutations on the three-state model parameters revealed that the occupancy of the three states is not affected by these mutations as revealed by the unchanged K_B and K_T values. Also the binding affinity of S1 for actin is unaffected both in the presence and absence of Ca^{2+}. The cooperative unit size *n*, which refers to the number of actin monomers that switch between two states at a time, is no bigger than the structural unit size both in the presence and absence of Ca^{2+}. This result contrasts with the previously published values of Maytum *et al* (1999) and Maytum *et al* (2003). In both papers, the *n* value is reported to be around 7 in the absence of Ca^{2+} and larger the 10 in the presence of Ca^{2+}. The published results were similar for skeletal and cardiac Tn. This was explained by the pinning effect of TnI, which binds strongly to every seven actins in the absence of Ca^{2+}. The significant increase of *n* value from 7 to

≥ 10 on Ca^{2+} addition was attributed to the increased stiffness of the Tm overlap region by the TnT1 portion of TnT (Figure 1.19). The K_B, K_T and K_1 values presented in this chapter are very similar to those published by Maytum *et al*, and since the same experimental and fitting procedure was applied, it is possible that the difference in *n* values is due to the use of different Tn isoforms. Maytum *et al* (2003) used bovine cardiac Tn complex and not human cardiac Tn. The explanation put forward by Maytum *et al* could therefore only be true for some TnT isoforms and not others. Over 20 TnT isoforms are produced by alternative splicing, the differences between them arise mainly at the N-terminal hypervariable region (Perry, 1998). The different TnT isoforms most certainly provide different regulatory properties required for the function of the muscle they are associated with.

Overall, both L29E mutation in TnC and G203S mutation in TnI, though reported to cause hypertrophic cardiomyopathy, do not seem to alter the normal function of the system based on our *in vitro* assays. Either the methods used were not sensitive enough for detecting the alterations caused by the mutations (changes could be very subtle and not readily detectable) or the mutations affect other properties of the filament that were not assessed in this study (actin activated myosin ATPase, binding to Tm and actin).

As previously published (Zhang *et al*, 1995a; Zhang *et al*, 1995b; Dohet *et al*, 1995; Reiffert *et al*, 1996), phosphorylation of TnI decreases the Ca^{2+} sensitivity of the thin filament. The results presented in this chapter are consistent with the published work. K206Q mutation in TnI increases the Ca^{2+} sensitivity of the thin filament when TnI is phosphorylated but shows no difference to the WT system on Tn dephosphorylation. In other words, the alteration in the properties of the thin filament caused by this mutation is only detectable when TnI is phosphorylated. In the WT protein residue 206 will carry a positive charge. Though residue 206 is located at the C-domain of TnI and the site of phosphorylation is at the N-domain, the possibility of an interaction between the negatively charged phosphate groups and the positively charged lysine group at position 206 cannot be ruled out. The absence of this interaction might affect the switching between the ON and OFF states of the filament. In other words, the disruption of a possible interaction between the N- and C-domains of TnI by charge change at a single residue position could affect the equilibrium switching between C-TnI attachment and detachment from actin.

K206Q mutation, unlike the WT protein complex, causes a decrease in Ca^{2+} sensitivity upon dephosphorylation. How a single point mutation in the C-domain of TnC reverses the effect of dephosphorylation is not clear. Ward *et al* (2002) proposed that the dephosphorylated N-domain of TnI stabilises the Ca^{2+}-bound state of TnC. Clearly the opposite happens in the presence of K206Q mutation. The results obtained with the K206Q FHC mutation demonstrate that a residue positioned at the C-domain of TnI can influence the nature of interaction between the N-domain of TnI and TnC but also the phosphorylated state of the N-domain of TnI seems to influence the nature of interactions between the C-domain of TnI and actin.

CHAPTER 7

SUMMARY AND GENERAL DISCUSSION

In striated muscle such as skeletal and cardiac, the regulation of the acto.myosin interaction, which ultimately leads to muscle contraction, is primarily dependent on the reversible binding of Ca^{2+} to the thin filament and is mediated by the regulatory protein complex of Tm.Tn. The three-state model of regulation described by McKillop and Geeves (1993) is a widely accepted model of muscle regulation. In this model, the filament is described to be in equilibrium between three myosin-binding states or as shown by structural data between three equilibrium Tm positions on actin (Vibert *et al*, 1997). The position of Tm is influenced by both the allosteric changes triggered as a result of Ca^{2+} binding to TnC and the binding of myosin heads to actin. The three biochemical states are referred to as blocked, closed and open states. In the blocked state, Tm occupies both the weak and strong myosin-binding sites on actin preventing the formation of a stereo-specific acto.myosin complex. In the closed state, Tm position only prevents the strong binding of myosin and a weakly bound acto.myosin complex forms. In the open state, Tm is further displaced to allow the rigor myosin binding and the formation of ATPase active acto.myosin complex. The three-state model of regulation describes the equilibrium constants for the occupancy of the different states of the filament as well as the affinity of myosin head binding to actin. All our results were analysed and discussed in terms of the three-state model of regulation. Both equilibrium and kinetic measurements are required to define the model parameters. The kinetic measurements are carried out with the stopped flow machine and allow the measurements of the rate of S1 biding to thin filaments reconstituted with the desired proteins. These allowed the determination of the equilibrium constant between the blocked and closed states of the filament either in the presence or absence of Ca^{2+} or as a function of pCa ($-\log[Ca^{2+}]$). The equilibrium measurements are obtained by the continuous titration of S1 into a cuvette containing reconstituted thin filaments under varying conditions. Both types of experiments probe the pyrene fluorescence signal as binding of S1 to pyrene-labelled actin causes fluorescence quenching.

The ability to express recombinant Tm in bacteria is a valuable tool as it allows 1) the overexpression of different Tm isoforms and the investigation of their regulatory properties, 2) the production of Tm expressing FHC mutations and the examination of their effect on the regulatory function of Tm. However, the crucial requirement was to

produce recombinant Tm with native-like properties. Bacterially expressed Tm lacks the N-terminal acetyl group, reported to be essential for the normal function of the protein (Heald and Hitchcock-DeGregori, 1988). Expression of Tm with and Ala-Ser extension at the N-terminal was reported to restore the normal function of Tm as revealed by a number of assays (Monteiro *et al*, 1994). We further investigated this claim by applying a wide range of techniques, which included actin-binding assays, stopped-flow and fluorescence titration experiments as well as DSC measurements. In all cases, native tissue-purified and recombinant Tm with the Ala-Ser extension were indistinguishable. Therefore, the Ala-Ser extension expressed at the N-terminus of Tm is a good mimic of the acetyl group.

On this basis, α and β Tm, the two major Tm isoforms in striated muscle were overexpressed in *E.coli* allowing the regulatory properties of each to be characterised. β Tm, which is expressed in very small amount in slow-beating hearts of mammals, causes a significant increase in the Ca^{2+} sensitivity of the thin filament when associated with cardiac Tn proteins. This was reflected by a shift in the Ca^{2+} concentration at which the filament is turned into the OFF state. This finding is consistent with fibre force measurement obtained with transgenic mice where β Tm was overexpressed in the heart (Muthuchamy *et al*, 1998). Determination of the three-state model parameters showed that while the occupancy of the different states is not changed by the type of Tm isoform associated with actin, the affinity of S1 binding to actin is enhanced in the presence of βTm. Finally, DSC measurements clearly indicate that β Tm is thermally less stable than α Tm both in solution and when in complex with actin. A structural domain of β Tm is 50% unfolded at normal body temperature. Though the presence of actin increases its stability by shifting the maximum melting temperature to 42 °C, β Tm will still be susceptible to denaturation in the case of disease. This could explain the low level of β Tm expression in the cardiac muscle and the reason why β Tm is mostly found associated with α Tm as a heterodimer. This also points to the importance of producing the αβ heterodimer as it will provide a better understanding of the *in vivo* system. The heterodimer can be produced by mixing a 1: 1 concentration of the homodimers heated up to 65 °C in the presence of 20 mM DTT. The mixture should be allowed to cool down to 35 °C on a water bath to allow chain exchange.

DTT can then be removed by means of gel filtration and the heterodimer can be oxidised by Cu^{2+}-catalysed $K_3Fe(CN)_6$.

The three state model of regulation was also used as a working model for investigating the effects of FHC mutations expressed in Tm and Tn proteins. The selected mutations in Tm were E180G and D175N, both of which rendered the thin filament more Ca^{2+}-sensitive. A more dramatic effect was seen with E180G mutation previously reported to cause more serious cardiac dysfunction as compared to D175N. This result was consistent with published fibre measurements.

The ability to reproduce *in vivo* results with our *in vitro* assays offers the possibility of studying FHC mutations using a simple system. The use of purified proteins means that the observations could be more easily interpreted as the possibility of an effect from other factors such as the presence of different protein isoforms and different levels of phosphorylation is eliminated. However, not all FHC mutations affect the Ca^{2+} sensitivity of the thin filament and it is important to investigate their potential effect on the stability, binding to the other thin filament proteins as well as the ATPase activity.

Point mutations were also introduced in Tn proteins; these were K206Q, G203S in TnI and L29E in TnC. Only K206Q caused alterations of the Ca^{2+}- dependent regulation of the thin filament. An increase in the Ca^{2+} sensitivity was however observed only when TnI was phosphorylated. Phosphorylation of cardiac TnI modulates the Ca^{2+}-sensitivity of the thin filament by decreasing the affinity of Ca^{2+} for TnC. This was true for WT, G203S and L29E Tn complexes. The opposite effect was observed with K206Q mutation. It was therefore concluded that the phosphorylation state of the N-domain of TnI influences the function of the TnI C-domain, which binds actin in a Ca^{2+}-dependent manner and that the interaction of the N-domain of TnI with TnC C-domain can be disrupted and reversed by a single point mutation in TnI C-domain.

Equilibrium measurements of S1 binding to actin in the presence of phosphorylated Tn complex showed no effect of the FHC mutations expressed in Tn on the three-state model parameters. The measurements were carried out under the conditions where the filament was either fully ON (presence of Ca^{2+}) or fully OFF (absence of Ca^{2+}). However, since the graded response to Ca^{2+} was different from WT in the case of

K206Q mutation, it would be interesting to see if the equilibrium parameters are changed within the range of pCa values where a difference in the Ca^{2+} sensitivity was observed. Also, it will be important to investigate the effect of dephosphorylation on these parameters.

In summary, different FHC mutation expressed in both Tm and Tn as well the β Tm isoform render the thin filament more Ca^{2+} sensitive. The Ca^{2+} sensitivity assays are a measure of the Ca^{2+} dependency of the K_B equilibrium constant between the blocked and closed states. K_B is also the equilibrium for the Ca^{2+}-dependent binding of TnI to either actin or TnC. In the absence of Ca^{2+}, TnI is strongly bound to actin and weakly bound to TnC whereas in the presence of Ca^{2+} TnI is strongly bound to TnC and weakly bound to actin (Grabarek *et al*, 1983).

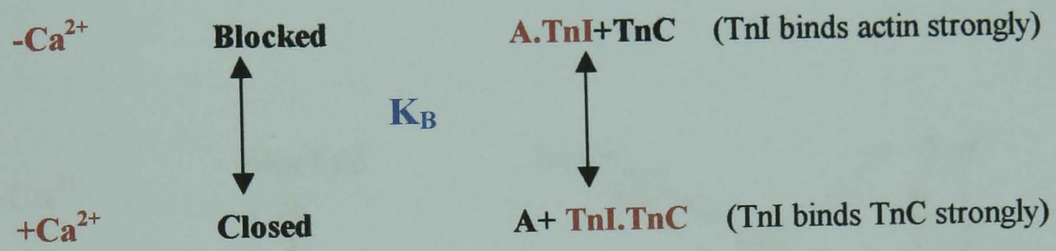

TnC can exist in two states, a low Ca^{2+} affinity state (Kca_{ass} of about $10^6\ M^{-1}$) predominant when TnI is bound to actin, and a high Ca^{2+} affinity state predominant when TnI is bound to TnC (TnC' with $K'ca_{ass}$ of about $10^7\ M^{-1}$) (Potter and Gergely, 1975). An increase in the Ca^{2+} sensitivity is consistent with the stabilisation of the TnC' state.

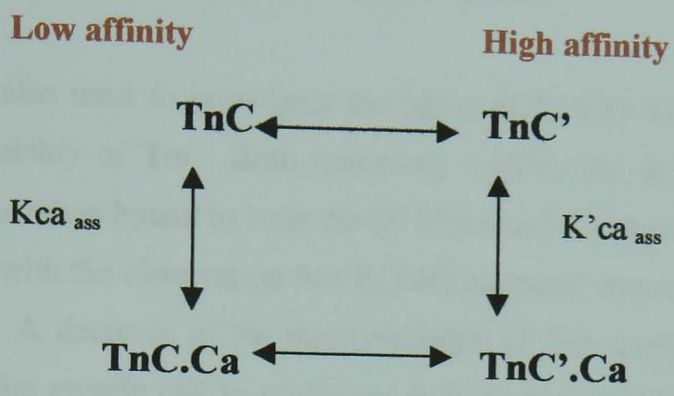

By combining both schemes

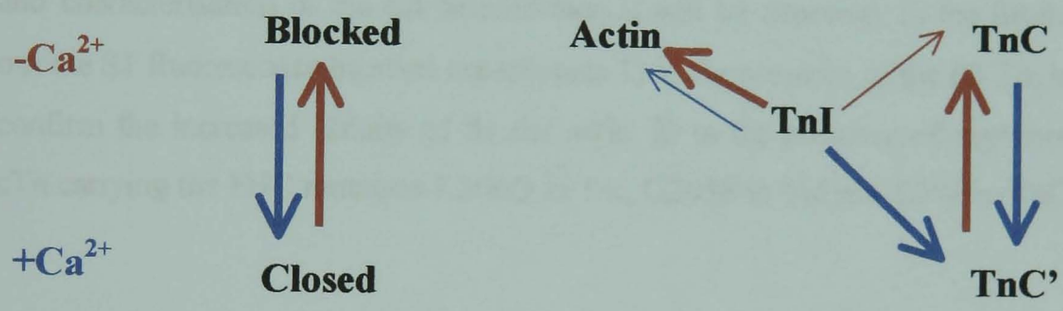

The above model can therefore explain the effect of mutations and isoform being due to an alteration in the equilibrium binding of TnI to actin and the ability of TnI to stabilise the high Ca^{2+} affinity state of TnC explaining the pCa shift.

This model could also account for the differences measured between the cardiac and the skeletal systems, which suggest that the cardiac system is less turned off than the

skeletal one. The TnI.Actin/TnI.TnC equilibrium should be adjusted in order for the cardiac muscle to fulfil its function of constant beating. The structural differences in Tm and Tn proteins between the cardiac and skeletal muscles are specific adaptations which fine-tune the differing needs of each system.

DSC was also used to investigate the effect of E180G and D175N mutations on the thermal stability of Tm. Both mutations significantly destabilised Tm when free in solution but when bound to actin the D175N was indistinguishable from WT. This was consistent with the observation that E180G mutation was more disruptive than D175N mutation. A decrease in the thermostability of Tm could have implications on the ability of the muscle cell to synthesise fully folded and functional Tm molecules but also to maintain the normal assembly of the sarcomere. Such severe consequences are however not expected to arise in the *in vivo* system in view of the late onset of the disease. In future experiments, it will therefore be interesting to examine the effect of Tn proteins on the stability of the mutated Tm.

In order to complete the work presented in this thesis and in addition to the production and characterisation of the αβ heterodimer, it will be necessary in the future to carry out the S1 fluorescence titration experiments 1) in the presence of the ββ Tm in order to confirm the increased affinity of S1 for actin, 2) in the presence of dephosphorylated cTn carrying the FHC mutation K206Q in TnI, G203S in TnI and L29E in TnC.

APPENDIX

1 Equations

1.1 Equations generated using Origin 6.0 Software

1.1.1 Linear equation

Equation
$y = a \times x + b$
Parameter definition
a: slope of the line
b: intercept with y axis

Equation expressed in Origin format
Parameter names: a, b
Indept variable: x
Dept variable: y
Definition: y=a*x+b

1.1.2 Single exponential

Equation
$y=-a \times \exp(-x \times b)+c$
Parameter definition
a: amplitude of the single exponential
b: observed rate constant of the reaction
c: end point of the curve

Equation expressed in Origin format
Parameter names: Amp, k, Vinf
Indept variable: x
Dept variable: y
Definition: y=-Amp*exp(-x*k)+Vinf

1.1.3 Hill equation for fitting Tm binding curves to actin

Equation
$y=(a \times x^c)/(b^c+x^c)$
Parameter definition
a: amplitude
b: the x value corresponding to the midpoint of the curve
c: the Hill coefficient

Equation expressed in Origin format
Parameter names: Amp,k,n
Indept variable: x
Dept variable: y

Definition: y=Amp*x^n/(k^n+x^n)

1.1.4 Hill equation for fitting Ca^{2+}-sensitivity curves

Equation
$y=a-b(10^{cx}/(10^{cd}+10^{cx}))$
Parameter definition
a: maximum value for y
b: the amplitude
c: the Hill coefficient
d: the x value corresponding to the midpoint of the curve

Equation expressed in Origin format
Parameter names: Amp, h, k, Vmax
Indept variable: x
Dept variable: y
Definition: y=Vmax-Amp*((10^x)^h)/((10^k)^h+(10^x)^h)

1.2 Equations generated using Scientist Software

1.2.1 Hyperbolic equation

Equation

$$f = \frac{([S1] + k_d + [A_0]) - \sqrt{([S1] + k_d + [A_0])^2 - 4[A_0][S1]}}{2[A_0]}$$

Equation expressed in Scientist format
Independent Variable(s): s1
Dependent Variable(s): fl
Parameter(s): f0, a0, kd,f1
f=((s1+kd+a0)-((s1+kd+a0)^2-4*s1*a0)^.5)/(2*a0)
f=(f0-fl)/(f0-f1)
Parameter definition
f: fraction of actin with S1 bound
fl: fluorescence value
s1: S1 concentration
f0: starting fluorescence value
a0: starting actin concentration
kd: dissociation constant or S1 value for half the maximum fluorescence value
f1: fluorescence infinity value

1.2.2 Three-state model equation

$$f = \frac{K_1[S1]P^{n-1}\{K_T(1+K_2)^n + 1\}}{(K_TP^n + Qn + 1/K_B)(1+K2)^{n-1}}$$

$P = 1+K_1[S1](1+K_2)$

$Q = 1+K_1[S1]$

Equation expressed in Scientist format

```
IndVars: s1
DepVars:f,fl
Params:k1,k2,kt,n,as,f0,fi,Kb
s=s1-as*(1-f)
P=1+K1*s*(1+k2)
Q=1+K1*S
f=1-(k1*s*p^(n-1)*(Kt*(1+k2)^n+1))/((kt*p^n+Q^n+1/Kb)*(1+k2)^(n-1))
fl=f0-(1-f)*(f0-fi)
0<f<1
0<s1<s
```

1.2.3 Two-state version of the three-state model equation

$$f = \frac{K_1[S1]P^{n-1}\{K_T(1+K_2)^n + 1\}}{(K_TP^n + Qn)(1+K2)^{n-1}}$$

$P = 1+K_1[S1](1+K_2)$

$Q = 1+K_1[S1]$

Equation expressed in Scientist format

```
IndVars: s1
DepVars:f,fl
Params:k1,k2,kt,n,as,f0,fi
s=s1-as*(1-f)
P=1+K1*s*(1+k2)
Q=1+K1*S
f=1-(k1*s*p^(n-1)*(Kt*(1+k2)^n+1))/((kt*p^n+Q^n)*(1+k2)^(n-1))
fl=f0-(1-f)*(f0-fi)
0<f<1
0<s1<s
```

Parameter definition

f: fraction of actin with S1 bound
fl: fluorescence value
k1: equilibrium constant for the weak S1 binding to actin
k2: equilibrium constant for the isomerisation step from weakly to strongly bound acto.S1 complex
Kb: equilibrium for the blocked to closed transition
kt: equilibrium for the closed to open transition
n: the cooperative unit size
as: starting actin concentration
f0: initial fluorescence value
fi: fluorescence infinity value

2 Protein gels

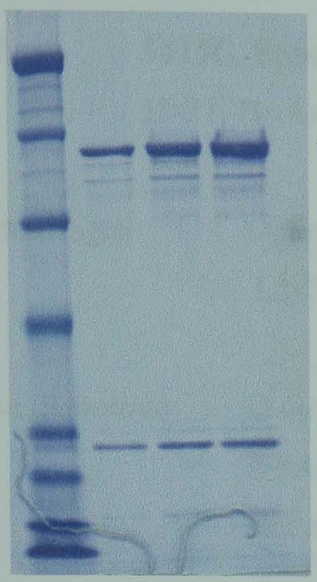

Rabbit S1 preparation run on 15% SDS-gel. From left to right 0.5, 1 and 1.5 µg of S1 were loaded

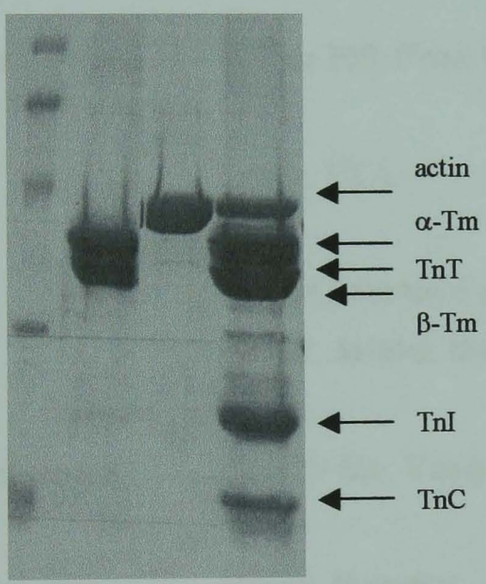

Tm, actin and regulatory protein (Tm, TnT, TnI and TnC) preparations from rabbit skeletal muscle run on a 12% SDS-gel.

3 Hardware

Centrifuges	5415C, Eppendorf, USA
	J2-21, Beckman, USA
Ultracentrifuges	Optima MAX, Beckman, USA
	L8-70M, Beckman, USA
Columns Resource	Q 6ml, Pharmacia
	DEAE-Sephacel
	HiTrap 5 ml Q, Pharmacia product
FPLC	ÄKTA Basic 10, Amersham pharmacia biotech, Sweden
Gel electrophoresis	Mini Protean II, Biorad, USA
pH meter	Hydurs 300, Orion Research, USA
Pipettes	Gilson, USA
Scales	AB104, Mettler, Switzerland
	PB302, Mettler, Switzerland
UV-spectrometer	Cary 50 Bio, Varian, Germany
Quartz cuvettes	Varian, Germany
Rotors	JA 20, Beckman, USA
	JA 10, Beckman, USA
	TLA 110, Beckman, USA.
	TLA 100.1, Beckman, USA
	Ti 60, Beckman, USA

4 Skeletal rat β Tm sequence

```
atggacgccatcaagaagaagatgcagatgctgaaactggacaaggagaatgccatcgac
 M  D  A  I  K  K  K  M  Q  M  L  K  L  D  K  E  N  A  I  D

cgcgcagagcaggccgaagccgacaagaagcaagctgaagaccgatgcaagcagctggag
 R  A  E  Q  A  E  A  D  K  K  Q  A  E  D  R  C  K  Q  L  E

gaagagcagcaggccctccagaagaaactgaaggggacagaggatgaggtggaaaagtat
 E  E  Q  Q  A  L  Q  K  K  L  K  G  T  E  D  E  V  E  K  Y

tccgagtctgtgaaggatgcccaggagaaactggagcaggccgagaagaaggccaccgat
 S  E  S  V  K  D  A  Q  E  K  L  E  Q  A  E  K  K  A  T  D

gctgaagcagatgtggcttctctgaatcgacgcattcagctcgtagaggaggagttggat
 A  E  A  D  V  A  S  L  N  R  R  I  Q  L  V  E  E  E  L  D

cgggcacaggagcgcctggctacagccttgcaaaagctggaggaggctgagaaagccgct
 R  A  Q  E  R  L  A  T  A  L  Q  K  L  E  E  A  E  K  A  A

gatgagagcgagagaggaatgaaggtcattgagaaccgggccatgaaggatgaggagaag
 D  E  S  E  R  G  M  K  V  I  E  N  R  A  M  K  D  E  E  K

atggagctgcaggagatgcagctgaaagaagccaagcacatcgctgaggactcagaccgc
 M  E  L  Q  E  M  Q  L  K  E  A  K  H  I  A  E  D  S  D  R

aaatacgaggaggtggccaggaagctggtgatcctggaaggagagctggagcgctctgaa
 K  Y  E  E  V  A  R  K  L  V  I  L  E  G  E  L  E  R  S  E

gagagagccgaggtggctgagagtaaatgtggggacctagaggaggagctgaaaattgtt
 E  R  A  E  V  A  E  S  K  C  G  D  L  E  E  E  L  K  I  V

accaacaacttgaaatctctggaagcccaagcggacaagtattccaccaaagaggacaaa
 T  N  N  L  K  S  L  E  A  Q  A  D  K  Y  S  T  K  E  D  K

tacgaagaagagatcaaacttctggaggagaagctgaaggaggctgagacccgagcagag
 Y  E  E  E  I  K  L  L  E  E  K  L  K  E  A  E  T  R  A  E

tttgctgaaagatctgtggcaaagttggagaaaaccatcgatgacctggaagatgaagtc
 F  A  E  R  S  V  A  K  L  E  K  T  I  D  D  L  E  D  E  V

tatgcacagaagatgaagtacaaggccatcagcgaggagctggacaacgcgctcaatgac
 Y  A  Q  K  M  K  Y  K  A  I  S  E  E  L  D  N  A  L  N  D

atcacttccctctga
 I  T  S  L
```

5 List of abbreviations, symbols and units

Ala	Alanine
Amp	Ampicillin
APS	Ammonium PerSulphate
ATPase	Adenosine 5' Tripohsphatase
Ca^{2+}	Calcium ions
CP	Control Protein
C-terminal	Carboxyterminal
cTn	Cardiac Tn
D	Aspartic acid
Da	Dalton
DNase	Deoxyribonuclease
DTT	Dithiotreitol
E	Glutamic acid
EDTA	Ethylenediaminetetraacetic acid
EGTA	Ethylene glycol bis (b-aminorthyl ether)- N,N,N',N'-tetraacetate)
ELC	Essential Light Chain
FHC	Familial Hypertrophy Cardiomyopathy
FPLC	Fast Performance Liquid Chromatography
G	Glutimine
Hepes	N'-(2-Hydroxyethyl) piperazine N'(2-ethane sulphonic acid)
HMM	Heavy MeroMysoin
K	Lysine
K	Kelvin
kJ	Kilo Joule
k_{obs}	Observed rate constant
kDa	Kilo Dalton
L	Leucine
LMM	Light MeroMyosin
log	Logarithm
M	Molar
MHC	Myosin Heavy Chain

MOPS	4-morpholinopropanesufonic acid
Mwt	Molecular weight
N	Aspargine
NMR	Nuclear Magnetic Resonance
N-terminal	Aminoterminal
Pi	Inorganic Phospahte
Pyrene	N-(1-pyrenyl)iodoacetamide
Q	Glutamine
RLC	Regulatory Light Chain
RNase	Ribonuclease
S	Serine
Ser	Serine
S1	Myosin Subfragment 1
S2	Myosin Subfragment 2
SDS	Sodium Deodecyl
SkTn	Skeletal Tn
TEMED	N',N',N',N'-tetramethylethylendiamine
Tm	Tropomysoin
Tn	Troponin

BIBLIOGRAPHY

Amphlett, G.W., Syska, H. and Perry, S.V. (1976) The polymorphic forms of tropomyosin and troponin I in developing rabbit skeletal muscle. *FEBS Lett*, **63**, 22-26.

Bailin, G. (1979) Phosphorylation of a bovine cardiac actin complex. *Am J Physiol*, **236**, C41-46.

.Bing, W., Knott, A., Redwood, C., Esposito, G., Purcell, I., Watkins, H. and Marston, S. (2000) Effect of hypertrophic cardiomyopathy mutations in human cardiac muscle alpha -tropomyosin (Asp175Asn and Glu180Gly) on the regulatory properties of human cardiac troponin determined by in vitro motility assay. *J Mol Cell Cardiol*, **32**, 1489-1498.

Bing, W., Redwood, C.S., Purcell, I.F., Esposito, G., Watkins, H. and Marston, S.B. (1997) Effects of two hypertrophic cardiomyopathy mutations in alpha-tropomyosin, Asp175Asn and Glu180Gly, on Ca2+ regulation of thin filament motility. *Biochem Biophys Res Commun*, **236**, 760-764.

Bonne, G., Carrier, L., Bercovici, J., Cruaud, C., Richard, P., Hainque, B., Gautel, M., Labeit, S., James, M., Beckmann, J. and et al. (1995) Cardiac myosin binding protein-C gene splice acceptor site mutation is associated with familial hypertrophic cardiomyopathy. *Nat Genet*, **11**, 438-440.

Bonne, G., Carrier, L., Richard, P., Hainque, B. and Schwartz, K. (1998) Familial hypertrophic cardiomyopathy: from mutations to functional defects. *Circ Res*, **83**, 580-593.

Bottinelli, R., Coviello, D.A., Redwood, C.S., Pellegrino, M.A., Maron, B.J., Spirito, P., Watkins, H. and Reggiani, C. (1998) A mutant tropomyosin that causes hypertrophic cardiomyopathy is expressed in vivo and associated with an increased calcium sensitivity. *Circ Res*, **82**, 106-115.

Brandt, P.W., Cox, R.N. and Kawai, M. (1980) Can the binding of Ca2+ to two regulatory sites on troponin C determine the steep pCa/tension relationship of skeletal muscle? *Proc Natl Acad Sci U S A*, **77**, 4717-4720.

Bronson, D.D. and Schachat, F.H. (1982) Heterogeneity of contractile proteins. Differences in tropomyosin in fast, mixed, and slow skeletal muscles of the rabbit. *J Biol Chem*, **257**, 3937-3944.

Brown, J.H., Kim, K.H., Jun, G., Greenfield, N.J., Dominguez, R., Volkmann, N., Hitchcock-DeGregori, S.E. and Cohen, C. (2001) Deciphering the design of the tropomyosin molecule. *Proc Natl Acad Sci U S A*, **98**, 8496-8501.

Carlier, M.F. (1990) Actin polymerization and ATP hydrolysis. *Adv Biophys*, **26**, 51-73.

Carlier, M.F. (1991) Actin: protein structure and filament dynamics. *J Biol Chem*, **266**, 1-4.

Cassell, M. and Tobacman, L.S. (1996) Opposite effects of myosin subfragment 1 on binding of cardiac troponin and tropomyosin to the thin filament. *J Biol Chem*, **271**, 12867-12872.

Cho, Y.J. and Hitchcock-DeGregori, S.E. (1991) Relationship between alternatively spliced exons and functional domains in tropomyosin. *Proc Natl Acad Sci U S A*, **88**, 10153-10157.

Cho, Y.J., Liu, J. and Hitchcock-DeGregori, S.E. (1990) The amino terminus of muscle tropomyosin is a major determinant for function. *J Biol Chem*, **265**, 538-545.

Coates, J.H., Criddle, A.H. and Geeves, M.A. (1985) Pressure-relaxation studies of pyrene-labelled actin and myosin subfragment 1 from rabbit skeletal muscle. Evidence for two states of acto-subfragment 1. *Biochem J*, **232**, 351-356.

Cooper, J.A. (1987) Effects of cytochalasin and phalloidin on actin. *J Cell Biol*, **105**, 1473-1478.

Coviello, D.A., Maron, B.J., Spirito, P., Watkins, H., Vosberg, H.P., Thierfelder, L., Schoen, F.J., Seidman, J.G. and Seidman, C.E. (1997) Clinical features of hypertrophic cardiomyopathy caused by mutation of a "hot spot" in the alpha-tropomyosin gene. *J Am Coll Cardiol*, **29**, 635-640.

Craig, R. and Lehman, W. (2001) Crossbridge and tropomyosin positions observed in native, interacting thick and thin filaments. *J Mol Biol*, **311**, 1027-1036.

Criddle, A.H., Geeves, M.A. and Jeffries, T. (1985) The use of actin labelled with N-(1-pyrenyl)iodoacetamide to study the interaction of actin with myosin subfragments and troponin/tropomyosin. *Biochem J*, **232**, 343-349.

Cummins, P. and Perry, S.V. (1974) Chemical and immunochemical characteristics of tropomyosins from striated and smooth muscle. *Biochem J*, **141**, 43-49.

Cummins, P. and Perry, S.V. (1973) The subunits and biological activity of polymorphic forms of tropomyosin. *Biochem J*, **133**, 765-777.

Dahiya, R., Butters, C.A. and Tobacman, L.S. (1994) Equilibrium linkage analysis of cardiac thin filament assembly. Implications for the regulation of muscle contraction. *J Biol Chem*, **269**, 29457-29461.

Dohet, C., al-Hillawi, E., Trayer, I.P. and Ruegg, J.C. (1995) Reconstitution of skinned cardiac fibres with human recombinant cardiac troponin-I mutants and troponin-C. *FEBS Lett*, **377**, 131-134.

Dominguez, R., Freyzon, Y., Trybus, K.M. and Cohen, C. (1998) Crystal structure of a vertebrate smooth muscle myosin motor domain and its complex with the essential light chain: visualization of the pre-power stroke state. *Cell*, **94**, 559-571.

Ebashi, S., Endo, M. and Otsuki, I. (1969) Control of muscle contraction. *Q Rev Biophys*, **2**, 351-384.

Eccleston, J.F. (1991) *Spectrometry and Spectrofluorimetry (chapter 8)*. Oxford Press.

Eisenberg, E., Hill, T.L. and Chen, Y. (1980) Cross-bridge model of muscle contraction. Quantitative analysis. *Biophys J*, **29**, 195-227.

England, P.J. (1975) Correlation between contraction and phosphorylation of the inhibitory subunit of troponin in perfused rat heart. *FEBS Lett*, **50**, 57-60.

Flavigny, J., Richard, P., Isnard, R., Carrier, L., Charron, P., Bonne, G., Forissier, J.F., Desnos, M., Dubourg, O., Komajda, M., Schwartz, K. and Hainque, B. (1998) Identification of two novel mutations in the ventricular regulatory myosin light chain gene (MYL2) associated with familial and classical forms of hypertrophic cardiomyopathy. *J Mol Med*, **76**, 208-214.

Flicker, P.F., Milligan, R.A. and Applegate, D. (1991) Cryo-electron microscopy of S1-decorated actin filaments. *Adv Biophys*, **27**, 185-196.

Flicker, P.F., Phillips, G.N., Jr. and Cohen, C. (1982) Troponin and its interactions with tropomyosin. An electron microscope study. *J Mol Biol*, **162**, 495-501.

Freire, E. (1995) Differential scanning calorimetry. *Methods Mol Biol*, **40**, 191-218.

Fujime, S. and Ishiwata, S. (1971) Dynamic study of F-actin by quasielastic scattering of laser light. *J Mol Biol*, **62**, 251-265.

Geeves, M.A. and Holmes, K.C. (1999) Structural mechanism of muscle contraction. *Annu Rev Biochem*, **68**, 687-728.

Geeves, M.A. and Conibear, P.B. (1995) The role of three-state docking of myosin S1 with actin in force generation. *Biophys J*, **68**, 194S-199S; discussion 199S-201S.

Geeves, M.A. and Halsall, D.J. (1987) Two-step ligand binding and cooperativity. A model to describe the cooperative binding of myosin subfragment 1 to regulated actin. *Biophys J*, **52**, 215-220.

Goldmann, W.H. (2000) Binding of tropomyosin-troponin to actin increases filament bending stiffness. *Biochem Biophys Res Commun*, **276**, 1225-1228.

Golitsina, N., An, Y., Greenfield, N.J., Thierfelder, L., Iizuka, K., Seidman, J.G., Seidman, C.E., Lehrer, S.S. and Hitchcock-DeGregori, S.E. (1997) Effects of two familial hypertrophic cardiomyopathy-causing mutations on alpha-tropomyosin structure and function. *Biochemistry*, **36**, 4637-4642. (see correction in *Biochemistry* (199), **38**, 3850.

Goody, R.S. and Holmes, K.C. (1983) Cross-bridges and the mechanism of muscle contraction. *Biochim Biophys Acta*, **726**, 13-39.

Gordon, A.M., Homsher, E. and Regnier, M. (2000) Regulation of contraction in striated muscle. *Physiol Rev*, **80**, 853-924.

Grabarek, Z., Grabarek, J., Leavis, P.C. and Gergely, J. (1983) Cooperative binding to the Ca2+-specific sites of troponin C in regulated actin and actomyosin. *J Biol Chem*, **258**, 14098-14102.

Graceffa, P. and Dominguez, R. (2003) Crystal structure of monomeric actin in the ATP state. Structural basis of nucleotide-dependent actin dynamics. *J Biol Chem*, **278**, 34172-34180.

Greene, L. E. and Eisenberg, E. (1980) The binding of heavy meromyosin to F-actin. *J Biol Chem*, **255**, 549-54

Harrison, S.M. and Bers, D.M. (1987) The effect of temperature and ionic strength on the apparent Ca-affinity of EGTA and the analogous Ca-chelators BAPTA and dibromo-BAPTA. *Biochim Biophys Acta*, **925**, 133-143.

Head, J.G., Ritchie, M.D. and Geeves, M.A. (1995) Characterization of the equilibrium between blocked and closed states of muscle thin filaments. *Eur J Biochem*, **227**, 694-699.

Heald, R.W. and Hitchcock-DeGregori, S.E. (1988) The structure of the amino terminus of tropomyosin is critical for binding to actin in the absence and presence of troponin. *J Biol Chem*, **263**, 5254-5259.

Heeley, D.H., Golosinska, K. and Smillie, L.B. (1987) The effects of troponin T fragments T1 and T2 on the binding of nonpolymerizable tropomyosin to F-actin in the presence and absence of troponin I and troponin C. *J Biol Chem*, **262**, 9971-9978.

Heeley, D.H., Dhoot, G.K., Frearson, N., Perry, S.V. and Vrbova, G. (1983) The effect of cross-innervation on the tropomyosin composition of rabbit skeletal muscle. *FEBS Lett*, **152**, 282-286.

Helfman, D.M. (1994) The generation of protein isoform diversity by alternative RNA splicing. *Soc Gen Physiol Ser*, **49**, 105-115.

Herzberg, O. and James, M.N. (1985) Structure of the calcium regulatory muscle protein troponin-C at 2.8 A resolution. *Nature*, **313**, 653-659.

Hill, L.E., Mehegan, J.P., Butters, C.A. and Tobacman, L.S. (1992) Analysis of troponin-tropomyosin binding to actin. Troponin does not promote interactions between tropomyosin molecules. *J Biol Chem*, **267**, 16106-16113.

Hill, T.L., Eisenberg, E. and Chalovich, J.M. (1981) Theoretical models for cooperative steady-state ATPase activity of myosin subfragment-1 on regulated actin. *Biophys J*, **35**, 99-112.

Hoffmann, B., Schmidt-Traub, H., Perrot, A., Osterziel, K.J. and Gessner, R. (2001) First mutation in cardiac troponin C, L29Q, in a patient with hypertrophic cardiomyopathy. *Hum Mutat*, **17**, 524.

Holmes, K.C. and Geeves, M.A. (2000) The structural basis of muscle contraction. *Philos Trans R Soc Lond B Biol Sci*, **355**, 419-431.

Holmes, K.C. (1997) The swinging lever-arm hypothesis of muscle contraction. *Curr Biol*, 7, R112-118.

Houdusse, A., Love, M.L., Dominguez, R., Grabarek, Z. and Cohen, C. (1997) Structures of four Ca2+-bound troponin C at 2.0 A resolution: further insights into the Ca2+-switch in the calmodulin superfamily. *Structure*, **5**, 1695-1711.

Huxley, A.F. and Niedergerke, R. (1954) Measurement of muscle striations in stretch and contraction. *J Physiol*, 124, 46-47P.

Huxley, H. and Hanson, J. (1954) Changes in the cross-striations of muscle during contraction and stretch and their structural interpretation. Nature, 173, 973-976.

Hwang, C., Sinskey, A.J. and Lodish, H.F. (1992) Oxidized redox state of glutathione in the endoplasmic reticulum. *Science*, **257**, 1496-1502.

Ingraham, R.H. and Swenson, C.A. (1984) Binary interactions of troponin subunits. J Biol Chem, 259, 9544-9548.

Jaquet, K., Lohmann, K., Czisch, M., Holak, T., Gulati, J. and Jaquet, R. (1998) A model for the function of the bisphosphorylated heart-specific troponin-I N-terminus. *J Muscle Res Cell Motil*, **19**, 647-659.

Jancso, A. and Graceffa, P. (1991) Smooth muscle tropomyosin coiled-coil dimers. Subunit composition, assembly, and end-to-end interaction. *J Biol Chem*, **266**, 5891-5897.

Kabsch, W., Mannherz, H.G., Suck, D., Pai, E.F. and Holmes, K.C. (1990) Atomic structure of the actin:DNase I complex. Nature, 347, 37-44.

Kendall, R.L., Yamada, R. and Bradshaw, R.A. (1990) Cotranslational amino-terminal processing. *Methods Enzymol*, **185**, 398-407.

Kimura, A., Harada, H., Park, J.E., Nishi, H., Satoh, M., Takahashi, M., Hiroi, S., Sasaoka, T., Ohbuchi, N., Nakamura, T., Koyanagi, T., Hwang, T.H., Choo, J.A., Chung, K.S., Hasegawa, A., Nagai, R., Okazaki, O., Nakamura, H., Matsuzaki, M., Sakamoto, T., Toshima, H., Koga, Y., Imaizumi, T. and Sasazuki, T. (1997) Mutations in the cardiac troponin I gene associated with hypertrophic cardiomyopathy. Nat Genet, 16, 379-382.

Koshland, D.E., Jr., Nemethy, G. and Filmer, D. (1966) Comparison of experimental binding data and theoretical models in proteins containing subunits. Biochemistry, 5, 365-385.

Kremneva, E.V., Nikolaeva, O.P., Gusev, N.B. and Levitsky, D.I. (2003) Effects of troponin on thermal unfolding of actin-bound tropomyosin. *Biochemistry (Mosc)*, **68**, 802-809.

Kurzawa, S.E. and Geeves, M.A. (1996) A novel stopped-flow method for measuring the affinity of actin for myosin head fragments using microgram quantities of protein. J Muscle Res Cell Motil, 17, 669-676.

Lees-Miller, J.P. and Helfman, D.M. (1991) The molecular basis for tropomyosin isoform diversity. Bioessays, 13, 429-437.

Lehrer, G.a. (2002) Molecular Control mechanisms n Striated Muscle contraction. Kluwer Academic publishers.

Lehrer, S.S. and Geeves, M.A. (1998) The muscle thin filament as a classical cooperative/allosteric regulatory system. J Mol Biol, 277, 1081-1089.

Lehrer, S.S., Golitsina, N.L. and Geeves, M.A. (1997) Actin-tropomyosin activation of myosin subfragment 1 ATPase and thin filament cooperativity. The role of tropomyosin flexibility and end-to-end interactions. Biochemistry, 36, 13449-13454.

Lehrer, S.S. and Qian, Y. (1990) Unfolding/refolding studies of smooth muscle tropomyosin. Evidence for a chain exchange mechanism in the preferential assembly of the native heterodimer. J Biol Chem, 265, 1134-1138.

Lehrer, S.S., Qian, Y.D. and Hvidt, S. (1989) Assembly of the native heterodimer of Rana esculenta tropomyosin by chain exchange. Science, 246, 926-928.

Lewis, W.G. and Smillie, L.B. (1980) The amino acid sequence of rabbit cardiac tropomyosin. *J Biol Chem*, **255**, 6854-6859.

Lodish, h., Berk, A., Zipursky, L.S., Baltimore, D. and Darnell, J. (2000) Molecular Cell Biology. W.H. Freeman.

Lohmann, K., Westerdorf, B., Maytum, R., Geeves, M.A. and Jaquet, K. (2001) Overexpression of human cardiac troponin in Escherichia coli: its purification and characterization. *Protein Expr Purif*, **21**, 49-59.

Lorenz, M., Poole, K.J., Popp, D., Rosenbaum, G. and Holmes, K.C. (1995) An atomic model of the unregulated thin filament obtained by X-ray fiber diffraction on oriented actin-tropomyosin gels. J Mol Biol, 246, 108-119.

Lowey, S., Slayter, H.S., Weeds, A.G. and Baker, H. (1969) Substructure of the myosin molecule. I. Subfragments of myosin by enzymic degradation. J Mol Biol, 42, 1-29.

Lymn, R.W. and Taylor, E.W. (1971) Mechanism of adenosine triphosphate hydrolysis by actomyosin. Biochemistry, 10, 4617-4624.

Mak, A.S., Lewis, W.G. and Smillie, L.B. (1979) Amino acid sequences of rabbit skeletal beta- and cardiac tropomyosins. FEBS Lett, 105, 232-234.

Mak, A.S., Smillie, L.B. and Stewart, G.R. (1980) A comparison of the amino acid sequences of rabbit skeletal muscle alpha- and beta-tropomyosins. J Biol Chem, 255, 3647-3655.

Margossian, S.S. and Lowey, S. (1982) Preparation of myosin and its subfragments from rabbit skeletal muscle. Methods Enzymol, 85 Pt B, 55-71.

Marian, A.J. and Roberts, R. (2001) The molecular genetic basis for hypertrophic cardiomyopathy. J Mol Cell Cardiol, 33, 655-670.

Maron, B.J., Pelliccia, A. and Spirito, P. (1995) Cardiac disease in young trained athletes. Insights into methods for distinguishing athlete's heart from structural heart disease, with particular emphasis on hypertrophic cardiomyopathy. Circulation, 91, 1596-1601.

Mathews, C.K., Van Holde, K.E. and Ahern, K.G. (2000) Biochemistry. Addison Wesley Longman, San Fransisco.

Maytum, R., Westerdorf, B., Jaquet, K. and Geeves, M.A. (2003) Differential regulation of the actomyosin interaction by skeletal and cardiac troponin isoforms. *J Biol Chem*, **278**, 6696-6701.

Maytum, R., Konrad, M., Lehrer, S.S. and Geeves, M.A. (2001) Regulatory properties of tropomyosin effects of length, isoform, and N-terminal sequence. Biochemistry, 40, 7334-7341.

Maytum, R., Lehrer, S.S. and Geeves, M.A. (1999) Cooperativity and switching within the three-state model of muscle regulation. Biochemistry, 38, 1102-1110.

McKillop, D.F. and Geeves, M.A. (1993) Regulation of the interaction between actin and myosin subfragment 1: evidence for three states of the thin filament. Biophys J, 65, 693-701.

McKillop, D.F. and Geeves, M.A. (1991) Regulation of the acto.myosin subfragment 1 interaction by troponin/tropomyosin. Evidence for control of a specific isomerization between two acto.myosin subfragment 1 states. *Biochem J*, **279 (Pt 3)**, 711-718.

McLachlan, A.D. and Stewart, M. (1975) Tropomyosin coiled-coil interactions: evidence for an unstaggered structure. *J Mol Biol*, **98**, 293-304.

McLaughlin, P.J., Gooch, J.T., Mannherz, H.G. and Weeds, A.G. (1993) Structure of gelsolin segment 1-actin complex and the mechanism of filament severing. *Nature*, **364**, 685-692.

Mittmann, K., Jaquet, K. and Heilmeyer, L.M., Jr. (1992) Ordered phosphorylation of a duplicated minimal recognition motif for cAMP-dependent protein kinase present in cardiac troponin I. *FEBS Lett*, **302**, 133-137.

Mittmann, K., Jaquet, K. and Heilmeyer, L.M., Jr. (1990) A common motif of two adjacent phosphoserines in bovine, rabbit and human cardiac troponin I. *FEBS Lett*, **273**, 41-45.

Mogensen, J., Klausen, I.C., Pedersen, A.K., Egeblad, H., Bross, P., Kruse, T.A., Gregersen, N., Hansen, P.S., Baandrup, U. and Borglum, A.D. (1999) Alpha-cardiac actin is a novel disease gene in familial hypertrophic cardiomyopathy. *J Clin Invest*, **103**, R39-43.

Monod, J., Wyman, J. and Changeux, J.P. (1965) On the Nature of Allosteric Transitions: A Plausible Model. *J Mol Biol*, **12**, 88-118.

Monteiro, P.B., Lataro, R.C., Ferro, J.A. and Reinach Fde, C. (1994) Functional alpha-tropomyosin produced in Escherichia coli. A dipeptide extension can substitute the amino-terminal acetyl group. *J Biol Chem*, **269**, 10461-10466.

Mumby, M.C., Russell, K.L., Garrard, L.J. and Green, D.D. (1987) Cardiac contractile protein phosphatases. Purification of two enzyme forms and their characterization with subunit-specific antibodies. *J Biol Chem*, **262**, 6257-6265.

Muthuchamy, M., Pieples, K., Rethinasamy, P., Hoit, B., Grupp, I.L., Boivin, G.P., Wolska, B., Evans, C., Solaro, R.J. and Wieczorek, D.F. (1999) Mouse model of a familial hypertrophic cardiomyopathy mutation in alpha-tropomyosin manifests cardiac dysfunction. *Circ Res*, **85**, 47-56.

Muthuchamy, M., Boivin, G.P., Grupp, I.L. and Wieczorek, D.F. (1998) Beta-tropomyosin overexpression induces severe cardiac abnormalities. *J Mol Cell Cardiol*, **30**, 1545-1557.

Muthuchamy, M., Grupp, I.L., Grupp, G., O'Toole, B.A., Kier, A.B., Boivin, G.P., Neumann, J. and Wieczorek, D.F. (1995) Molecular and physiological effects of overexpressing striated muscle beta-tropomyosin in the adult murine heart. *J Biol Chem*, **270**, 30593-30603.

Muthuchamy, M., Pajak, L., Howles, P., Doetschman, T. and Wieczorek, D.F. (1993) Developmental analysis of tropomyosin gene expression in embryonic stem cells and mouse embryos. *Mol Cell Biol*, **13**, 3311-3323.

Nakajima-Taniguchi, C., Matsui, H., Nagata, S., Kishimoto, T. and Yamauchi-Takihara, K. (1995) Novel missense mutation in alpha-tropomyosin gene found in Japanese patients with hypertrophic cardiomyopathy. *J Mol Cell Cardiol*, **27**, 2053-2058.

Narita, A., Yasunaga, T., Ishikawa, T., Mayanagi, K. and Wakabayashi, T. (2001) Ca(2+)-induced switching of troponin and tropomyosin on actin filaments as revealed by electron cryo-microscopy. *J Mol Biol*, **308**, 241-261.

Nishimura, A., Morita, M., Nishimura, Y. and Sugino, Y. (1990) A rapid and highly efficient method for preparation of competent Escherichia coli cells. *Nucleic Acids Res*, **18**, 6169.

Palmiter, K.A., Kitada, Y., Muthuchamy, M., Wieczorek, D.F. and Solaro, R.J. (1996) Exchange of beta- for alpha-tropomyosin in hearts of transgenic mice induces changes in thin filament response to Ca2+, strong cross-bridge binding, and protein phosphorylation. *J Biol Chem*, **271**, 11611-11614.

Parry, D.A. and Squire, J.M. (1973) Structural role of tropomyosin in muscle regulation: analysis of the x-ray diffraction patterns from relaxed and contracting muscles. *J Mol Biol*, **75**, 33-55.

Pearlstone, J.R. and Smillie, L.B. (1982) Binding of troponin-T fragments to several types of tropomyosin. Sensitivity to Ca2+ in the presence of troponin-C. *J Biol Chem*, **257**, 10587-10592.

Perry, S.V. (2001) Vertebrate tropomyosin: distribution, properties and function. *J Muscle Res Cell Motil*, **22**, 5-49.

Perry, S.V. (1999) Troponin I: inhibitor or facilitator. *Mol Cell Biochem*, **190**, 9-32.

Perry, S.V. (1998) Troponin T: genetics, properties and function. *J Muscle Res Cell Motil*, **19**, 575-602.

Phillips, G.N., Jr., Fillers, J.P. and Cohen, C. (1986) Tropomyosin crystal structure and muscle regulation. *J Mol Biol*, **192**, 111-131.

Polevoda, B. and Sherman, F. (2000) Nalpha -terminal acetylation of eukaryotic proteins. *J Biol Chem*, **275**, 36479-36482.

Potter, J.D., Sheng, Z., Pan, B.S. and Zhao, J. (1995) A direct regulatory role for troponin T and a dual role for troponin C in the Ca2+ regulation of muscle contraction. *J Biol Chem*, **270**, 2557-2562.

Potter, J.D. and Gergely, J. (1975) The calcium and magnesium binding sites on troponin and their role in the regulation of myofibrillar adenosine triphosphatase. *J Biol Chem*, **250**, 4628-4633.

Potter, J. D., and J. Gergely. (1974) Troponin, tropomyosin, and actin interactions in the Ca2+ regulation of muscle contraction. *Biochemistry* **13**: 2697-703.

Prabhakar, R., Boivin, G.P., Grupp, I.L., Hoit, B., Arteaga, G., Solaro, J.R. and Wieczorek, D.F. (2001) A familial hypertrophic cardiomyopathy alpha-tropomyosin mutation causes severe cardiac hypertrophy and death in mice. *J Mol Cell Cardiol*, **33**, 1815-1828.

Privalov, G.P. and Privalov, P.L. (2000) Problems and prospects in microcalorimetry of biological macromolecules. *Methods Enzymol*, **323**, 31-62.

Rayment, I., Holden, H.M., Whittaker, M., Yohn, C.B., Lorenz, M., Holmes, K.C. and Milligan, R.A. (1993a) Structure of the actin-myosin complex and its implications for muscle contraction. *Science*, **261**, 58-65.

Rayment, I., Rypniewski, W.R., Schmidt-Base, K., Smith, R., Tomchick, D.R., Benning, M.M., Winkelmann, D.A., Wesenberg, G. and Holden, H.M. (1993b) Three-dimensional structure of myosin subfragment-1: a molecular motor. *Science*, **261**, 50-58.

Reiffert, S., Maytum, R., Geeves, M., Lohmann, K., Greis, T., Bluggel, M., Meyer, H.E., Heilmeyer, L.M. and Jaquet, K. (1999) Characterization of the cardiac holotroponin complex reconstituted from native cardiac troponin T and recombinant I and C. *Eur J Biochem*, **261**, 40-47.

Reiffert, S.U., Jaquet, K., Heilmeyer, L.M., Jr., Ritchie, M.D. and Geeves, M.A. (1996) Bisphosphorylation of cardiac troponin I modulates the Ca(2+)-dependent binding of myosin subfragment S1 to reconstituted thin filaments. *FEBS Lett*, **384**, 43-47.

Redwood, C.S., Moolman-Smook, J.C. and Watkins, H. (1999) Properties of mutant contractile proteins that cause hypertrophic cardiomyopathy. *Cardiovasc Res*, **44**, 20-36.

Robertson, S.P., Johnson, J.D., Holroyde, M.J., Kranias, E.G., Potter, J.D. and Solaro, R.J. (1982) The effect of troponin I phosphorylation on the Ca2+-binding properties of the Ca2+-regulatory site of bovine cardiac troponin. *J Biol Chem*, **257**, 260-263.

Rosenberg, A.H., Lade, B.N., Chui, D.S., Lin, S.W., Dunn, J.J. and Studier, F.W. (1987) Vectors for selective expression of cloned DNAs by T7 RNA polymerase. *Gene*, **56**, 125-135.

Rosenfeld, S.S. and Taylor, E.W. (1985) Kinetic studies of calcium binding to regulatory complexes from skeletal muscle. *J Biol Chem*, **260**, 252-261.

Schaertl, S., Lehrer, S.S. and Geeves, M.A. (1995) Separation and characterization of the two functional regions of troponin involved in muscle thin filament regulation. *Biochemistry*, **34**, 15890-15894.

Schiaffino, S. and Reggiani, C. (1996) Molecular diversity of myofibrillar proteins: gene regulation and functional significance. *Physiol Rev*, **76**, 371-423.

Schmidtmann, A., Lohmann, K. and Jaquet, K. (2002) The interaction of the bisphosphorylated N-terminal arm of cardiac troponin I-A 31P-NMR study. *FEBS Lett*, **513**, 289-293.

Schroder, R.R., Manstein, D.J., Jahn, W., Holden, H., Rayment, I., Holmes, K.C. and Spudich, J.A. (1993) Three-dimensional atomic model of F-actin decorated with Dictyostelium myosin S1. *Nature*, **364**, 171-174.

Schutt, C.E., Myslik, J.C., Rozycki, M.D., Goonesekere, N.C. and Lindberg, U. (1993) The structure of crystalline profilin-beta-actin. *Nature*, **365**, 810-816.

Sellers, J.R. (2000) Myosins: a diverse superfamily. *Biochim Biophys Acta*, **1496**, 3-22.

Sheterline, P., Clayton, J. and Sparrow, J.C. (1995) *Protein Profile: Actin.* Oxford University Press.

Sia, S.K., Li, M.X., Spyracopoulos, L., Gagne, S.M., Liu, W., Putkey, J.A. and Sykes, B.D. (1997) Structure of cardiac muscle troponin C unexpectedly reveals a closed regulatory domain. *J Biol Chem*, **272**, 18216-18221.

Smillie, L.B. (1982) Preparation and identification of alpha- and beta-tropomyosins. *Methods Enzymol*, **85 Pt B**, 234-241.

Smith, C.A. and Rayment, I. (1996) Active site comparisons highlight structural similarities between myosin and other P-loop proteins. *Biophys J*, **70**, 1590-1602.

Solaro, R.J., Moir, A.J. and Perry, S.V. (1976) Phosphorylation of troponin I and the inotropic effect of adrenaline in the perfused rabbit heart. *Nature*, **262**, 615-617.

Spudich, J.A. and Watt, S. (1971) The regulation of rabbit skeletal muscle contraction. I. Biochemical studies of the interaction of the tropomyosin-troponin complex with actin and the proteolytic fragments of myosin. *J Biol Chem*, **246**, 4866-4871.

Squire, J.M. (1997) Architecture and function in the muscle sarcomere. *Curr Opin Struct Biol*, 7, 247-257.

Studier, F.W., Rosenberg, A.H., Dunn, J.J. and Dubendorff, J.W. (1990) Use of T7 RNA polymerase to direct expression of cloned genes. *Methods Enzymol*, **185**, 60-89.

Studier, F.W. and Moffatt, B.A. (1986) Use of bacteriophage T7 RNA polymerase to direct selective high-level expression of cloned genes. *J Mol Biol*, **189**, 113-130.

Stryer, L. (1996) *Biochemistry.* W.H. Freeman.

Syska, H., Wilkinson, J.M., Grand, R.J. and Perry, S.V. (1976) The relationship between biological activity and primary structure of troponin I from white skeletal muscle of the rabbit. *Biochem J*, **153**, 375-387

Syska, H., Perry, S.V. and Trayer, I.P. (1974) A new method of preparation of troponin I (inhibitory protein) using affinity chromatography. Evidence for three different forms of troponin I in striated muscle. *FEBS Lett*, **40**, 253-257.

Takahashi-Yanaga, F., Morimoto, S., Harada, K., Minakami, R., Shiraishi, F., Ohta, M., Lu, Q.W., Sasaguri, T. and Ohtsuki, I. (2001) Functional consequences of the mutations in human cardiac troponin I gene found in familial hypertrophic cardiomyopathy. *J Mol Cell Cardiol*, **33**, 2095-2107.

Takeda, S., Yamashita, A., Maeda, K. and Maeda, Y. (2003) Structure of the core domain of human cardiac troponin in the Ca(2+)-saturated form. *Nature*, **424**, 35-41.

Thierfelder, L., Watkins, H., MacRae, C., Lamas, R., McKenna, W., Vosberg, H.P., Seidman, J.G. and Seidman, C.E. (1994) Alpha-tropomyosin and cardiac troponin T mutations cause familial hypertrophic cardiomyopathy: a disease of the sarcomere. *Cell*, **77**, 701-712.

Tobacman, L.S. and Butters, C.A. (2000) A new model of cooperative myosin-thin filament binding. *J Biol Chem*, **275**, 27587-27593.

Tobacman, L.S. (1996) Thin filament-mediated regulation of cardiac contraction. *Annu Rev Physiol*, **58**, 447-481.

Tripet, B., Van Eyk, J.E. and Hodges, R.S. (1997) Mapping of a second actin-tropomyosin and a second troponin C binding site within the C terminus of troponin I, and their importance in the Ca2+-dependent regulation of muscle contraction. *J Mol Biol*, **271**, 728-750.

Urbancikova, M. and Hitchcock-DeGregori, S.E. (1994) Requirement of amino-terminal modification for striated muscle alpha-tropomyosin function. *J Biol Chem*, **269**, 24310-24315.

Van Eerd, J.P. and Takahshi, K. (1976) Determination of the complete amino acid sequence of bovine cardiac troponin C. *Biochemistry*, **15**, 1171-1180.

Vassylyev, D.G., Takeda, S., Wakatsuki, S., Maeda, K. and Maeda, Y. (1998) The crystal structure of troponin C in complex with N-terminal fragment of troponin I. The mechanism of how the inhibitory action of troponin I is released by Ca(2+)-binding to troponin C. *Adv Exp Med Biol*, **453**, 157-167.

Vibert, P., Craig, R. and Lehman, W. (1997) Steric-model for activation of muscle thin filaments. *J Mol Biol*, **266**, 8-14.

Wakabayashi, T., Huxley, H.E., Amos, L.A. and Klug, A. (1975) Three-dimensional image reconstruction of actin-tropomyosin complex and actin-tropomyosin-troponin T-troponin I complex. *J Mol Biol*, **93**, 477-497.

Ward, D.G., Cornes, M.P. and Trayer, I.P. (2002) Structural consequences of cardiac troponin I phosphorylation. *J Biol Chem*, **277**, 41795-41801.

Watkins, H., McKenna, W.J., Thierfelder, L., Suk, H.J., Anan, R., O'Donoghue, A., Spirito, P., Matsumori, A., Moravec, C.S., Seidman, J.G. and et al. (1995) Mutations in the genes for cardiac troponin T and alpha-tropomyosin in hypertrophic cardiomyopathy. *N Engl J Med*, **332**, 1058-1064.

Watkins, H., Thierfelder, L., Anan, R., Jarcho, J., Matsumori, A., McKenna, W., Seidman, J.G. and Seidman, C.E. (1993) Independent origin of identical beta cardiac myosin heavy-chain mutations in hypertrophic cardiomyopathy. *Am J Hum Genet*, **53**, 1180-1185.

Wegner, A. (1982) Kinetic analysis of actin assembly suggests that tropomyosin inhibits spontaneous fragmentation of actin filaments. *J Mol Biol*, **161**, 217-227.

Wegner, A. and Walsh, T.P. (1981) Interaction of tropomyosin-troponin with actin filaments. *Biochemistry*, **20**, 5633-5642.

Weiss, A., Schiaffino, S. and Leinwand, L.A. (1999) Comparative sequence analysis of the complete human sarcomeric myosin heavy chain family: implications for functional diversity. *J Mol Biol*, **290**, 61-75.

Wilkinson, J.M. and Grand, R.J. (1978) Comparison of amino acid sequence of troponin I from different striated muscles. *Nature*, **271**, 31-35.

Williams, D.L., Jr. and Greene, L.E. (1983) Comparison of the effects of tropomyosin and troponin-tropomyosin on the binding of myosin subfragment 1 to actin. *Biochemistry*, **22**, 2770-2774.

Williams, D.L., Jr. and Swenson, C.A. (1981) Tropomyosin stability: assignment of thermally induced conformational transitions to separate regions of the molecule. *Biochemistry*, **20**, 3856-3864.

Winegrad, S. (1999) Cardiac myosin binding protein C. *Circ Res*, **84**, 1117-1126.

Zhang, R., Zhao, J., Mandveno, A. and Potter, J.D. (1995a) Cardiac troponin I phosphorylation increases the rate of cardiac muscle relaxation. *Circ Res*, **76**, 1028-1035.

Zhang, R., Zhao, J. and Potter, J.D. (1995b) Phosphorylation of both serine residues in cardiac troponin I is required to decrease the Ca2+ affinity of cardiac troponin C. *J Biol Chem*, **270**, 30773-30780.

Zot, H. G., and J. D. Potter. (1982) A structural role for the Ca2+-Mg2+ sites on troponin C in the regulation of muscle contraction. Preparation and properties of troponin C depleted myofibrils. *J Biol Chem*, **257**: 7678-83